Cubesat Power System Design for High Precision Solar Observation

A Project Presented to
The Faculty of the Department of Aerospace Engineering
San José State University

In Partial Fulfillment of the Requirements for the Degree
Master of Science in Aerospace Engineering

By

Daniel Hernandez

December 2015

The Designated Project Committee Approves the Project Titled

CUBESAT POWER SYSTEM DESIGN FOR HIGH PRECISION SOLAR OBSERVATION

by

Daniel Hernandez

APPROVED FOR THE DEPARTMENT OF AEROSPACE ENGINEERING
SAN JOSÉ STATE UNIVERSITY
December 2015

Marcus J. Murbach 12-15-15

Marcus Murbach
Department of Aerospace Engineering

Date

Abstract

There is much need for improvement upon the current mechanisms of space weather study and monitoring of solar activity. It is proposed that a constellation of nano-satellites would provide as an invaluable source for space weather study. The focus of this paper is on the power subsystem design and analysis of a low cost, 3U demonstrator cubesat, which will have 3-axis stability within a 10^{th} of a degree. Design choices are made based on current state of the art technology, relative cost and flight heritage. The orbital environment is modeled under the assumption that the cubesat will be launched from the International Space Station. System level analysis is performed to determine feasibility of the cubesat's power generation, storage and structural design to support a mission requiring solar pointing in LEO. The presented design can adequately power the proposed demonstrator satellite throughout a 1-year mission lifespan. Future design steps are suggested in order to provide adequate methods of testing the rigidity of the subsystem to support the functionality of the final bus design in a higher orbit.

Table of Contents

Nomenclature

P_{sa} = Total power required from solar array
P_e = Required power during eclipse
P_d = Required power during daylight
T_d = Period spacecraft is in daylight
T_e = Period spacecraft is in eclipse
X_e = Efficiency of solar cells in eclipse
X_d = Efficiency of solar cells in daylight
P_{BOL} = Beginning of life power
P_{out} = Solar cell output power
η_{cell} = Efficiency of solar cell
P_{in} = Input power to solar cell
I_D = Inherent degradation
θ = Incidence angle
L_D = Life degradation
D = Degradation of solar cell
L = Lifetime of mission
P_{EOL} = End of life power
A_{SA} = Area of solar arrays
e = Deviation from a circular orbit
a = Half the distance between closest and furthest point of approach
I = Tilt of orbital plane with respect to Equatorial plane
Ω = Angle from origin of longitude to direction of ascending node
ν = Angle between satellite and perigee
ρ = Apparent size of the Earth from the spacecraft.
r_p = Point of closest approach
r_a = Point of furthest approach
J_2 = Coefficient to account for bulge of the Earth
q_{solar} = Direct solar flux
q_{albedo} = Heat flux from albedo
q_{IR} = Earth emitted infrared radiation
q_{EIR} = Earth emitted blackbody infrared radiation
q_{Sc} = Power converted to electricity
ε_S = Emissivity of solar cells
ε_{BS} = Emissivity of back side of solar cells
G_s = Solar Constant
α_s = Absorptivity of solar cells
a = Earth's albedo
σ = Stefan-Boltzmann constant
T = Temperature of surface in subject
I_{PV} = Photovoltaic current
I_D = Diode current
I_0 = Reverse bias saturation current
A = Ideality factor

V_T = Thermal voltage
N_S = Number of cells
k = Boltzmann constant
T = P-n junction temperature
q = Charge of electron
R_S = Series resistance
R_{SH} = Parallel resistance
P_{BOL} = Beginning of life power
P_{out} = Solar cell output power
η_{cell} = Efficiency of solar cell
P_{in} = Input power to solar cell
U = Potential energy
κ = Torsion spring constant
θ = Torsion spring rotation angle
M = Moment
d = Diameter of spring wire
T = Deflection or revolutions of the spring
E = Modulus of elasticity
N_t = Number of coils
D = Mean coil diameter
S = Bending stress
L_t = Spring body length in deflected position
l = Stretched body length
K_i = Stress concentration factor
C = Spring index
I = Mass moment of inertia
t = Time for spring deployment
ω = Frequency
k_a = Angular spring rate
P_r = Receiver power density
P_t = Transmitter power density
G_t = Transmitter gain
G_r = Receiver gain
λ = Wavelength
L_{PATH} = Path loss

I. Introduction

The basis for this project was influenced by Dr. Nagi Mansour, who is a helio-physicist at NASA Ames. There is a need to improve upon our current methods of space weather study and monitoring of solar activity. Society as a whole is more dependent and reliant on modern technology and interconnected systems. Space weather events are a systematic risk to society as they can cause big disturbances in transport, power and aviation sectors [1]. The sun is frequented with eruptions and extreme activities. Coronal Mass Ejections (CMEs) are of particular interest as they are the biggest scale solar phenomenon to occur. It has been observed that earth directed Coronal Mass ejections correlate to and are the main cause of disruptions of the geomagnetic field. CMEs can cause induced currents within long distance power transmission lines, transformers, pipelines and result in damaged electrical networks, transformer meltdowns and overall economic loss [9].

Cubesats and small satellites alike have continued to become more attractive as a method for scientific study in space. Their small size and improving functionality opens up more opportunities for cost effective mission design. It is proposed that a constellation of cubesats would provide as an invaluable source of space weather study. They can provide a method of in-situ solar wind measurements at distances within 1AU as well as improve upon current CME and overall solar modeling [6].

While at this point in time, a full design, build and launch of a constellation of satellites is years away and out of scope for our project, we will focus on launching a cubesat within LEO with the capability of continuously monitoring the sun with high precision (less than a tenth of a degree of error). The scientific analysis is the

responsibility of the customer. This mission will not require propulsion and the final structure will ultimately depend upon the scientific instrumentation. This review will focus on system design of cubesats and small satellite missions designed for space weather study or high precision pointing.

A. Cubesat Subsystems

1. General

A 1U cubesat with a 10x10x10 cm cube weighs 1 kg at most and is a large picot-sat by definition and a 3U cubesat (30x10x10 cm) is a Nano-sat by definition. Historically, 20% of all satellites launched are small satellites [16]. Small satellites are simpler than large satellites, but have limited capability. Basic objectives of small satellites missions are typically simple and less complex. However, as technology has developed, the capabilities of small satellites have increased, while still maintaining a low cost. Typical funding for small satellites require design and build to be accomplished within 1-3 years [16].

2. Power

The power subsystem is responsible for providing, storing, distributing and controlling spacecraft's electrical power. Photovoltaic arrays are commonly found on spacecraft, mounted on its external structure for energy generation.

Table 1. Power system design drivers and impacts.

Major Design Drivers	Driven By	Impact
Power Consumption	Payload Requirements	Solar array, battery
Power Distribution	Spacecraft Design	Power electronics, wiring
Eclipse Duration	Orbit	Battery
Bus Voltage	Spacecraft Design	Power electronics, wiring
Payload Duty Cycle	Operations Concept	Solar array, battery

The main design drivers of the electrical power system of a spacecraft include power consumption, power distribution, eclipse duration and payload duty cycle. Table 1 displays the system drivers, what they're driven by and their impacts. Power consumption will be driven by payload requirements and will affect the solar array sizing and battery choices. Power distribution will be driven by spacecraft design and will affect the electronic power board design. Eclipse duration will be driven by the spacecraft's orbit and will affect the battery choice.

3. Controls

The attitude control system of a spacecraft is responsible for orienting the spacecraft with respect to an inertial reference frame by adjusting the pitch, roll and yaw of the spacecraft. Attitude determination and command is essential, as solar panels need to be directed towards sunlight, antennas oriented towards Earth for communications, and proper orientation of scientific instruments. Attitude measurement is achieved through the use of sensors and gyroscopes. Attitude correction is achieved through the use of thrusters, actuators and torques. Control is implemented through embedded software.

Before choosing an adequate attitude control and demand system, system requirements such as payload requirements, pointing accuracy, maneuvering rates and frequencies, control system type, disturbance torques, size of hardware, attitude determination method, and control law must first be defined. Usage of an active or passive control method must also be determined. Passive attitude control systems, while the most economical, cannot achieve a high enough accuracy for our mission. Passive systems usually involve a hysteresis material and magnet being mounted on the cubesats, which orient the cubesats with earth's magnetic field.

The most common control systems are spin stabilized systems, 3 axis stabilized, momentum bias, and gravity gradient. For the purpose of our mission, high pointing accuracy is required for adequate imaging of the sun. We need accuracy within a tenth of a degree [5]. Out of the most common systems, 3 axis-stabilized systems are the most accurate. Typical hardware includes precision gyroscopes, horizon sensors, sun sensors and star trackers. The advantages of 3 axis stabilized systems include having high accuracy, no payload limitations, can adapt to mission changes and is applicable for large power requirements [6]. However, this system is usually the most expensive and requires the heaviest weight.

4. Thermal Control

The purpose of the thermal control subsystem is to ensure that all the spacecraft components remain in their designed operational temperature limits throughout the duration of the mission. It normally accounts for two to five percent of the spacecraft's weight and cost [6]. In orbit, the spacecraft is exposed to heat from the sun, the earth and heat dissipation from its electrical components. The power system is more coupled with

thermal control than any other system as a result of dissipating electrical energy [6]. Spacecraft structures commonly have large temperature limits, however those limits ultimately depend on the spacecraft's instruments. For our mission, which requires a high-resolution camera and is dependent upon a control system with less than a tenth of a degree of accuracy, the thermal control system will require a lot of attention to avoid error from thermal expansion of the optics.

5. Communications

The communications system provides interaction between the ground station and the spacecraft where the mission payload data and spacecraft status are transmitted. The communication system design is dependent on the mission requirements. Common cubesat communication systems are either RF or optical based. The systems differ in order of magnitude of the signal wavelengths and size of the required antennas. While RF based systems cover larger ranges, optical systems have no restrictions of frequency and bandwidths are not vulnerable to jamming. Deciding on the type of communication system will be based on trade studies dependent on the link range between the ground station and spacecraft orbital position and data rate [7].

II. Literature Review

A. Current State of the Art Technology

A critical aspect of our design is the attitude demand and control system. As of now, the best means to achieve our required pointing accuracy is through use of a sun senor and gyroscope. For small spacecraft, there are coarse sun sensors and fine or medium

precision sensors. Fine sun sensors assess analog current from solar cells in order to identify the direction of the sun. Coarse sun sensors incorporate a photo diode and solar cell. As of 2014, The SS-411 digital is the most advanced sun sensor for small spacecraft on the market, which can be seen in Table 2 along with the Micro Digital Sun Sensor. The most precise gyroscopes are mechanical and ring laser gyroscopes. After that is fiber optical gyroscopes and micro electric and mechanical systems gyroscopes are the least precise. Fiber optical gyroscopes are more commonly used in small spacecraft. A list of the most commonly used gyroscopes can also be seen in Table 2. Table 3, Table 4 and Table 5 display different state of the art solar cells and materials that are commonly used for solar cells.

Table 2. State of the art small spacecraft sun sensors and high precision gyroscopes [8].

Tech. Name	Description	Developer	TRL Status
Sun Sensors			
SS-411 Digital Sun Sensor	World's best seller micro DSS (Accuracy= .1 degrees)	Sinclair Interplanetary (Canada)	9
Micro-DSS	2-D APS (Active Pixel Sensor) Detector Array DSS (Accuracy =.1 degrees)	TNO (Netherlands)	7
Gyroscopes			
Micro-FORCE-1	Single axis fiber optical gyro for mini satellites (BI=1deg/h)	Northrop Grumman LITEF GmbH (USA/Germany)	9
VSGA	3-axis MEMS gyro using CRS09 for micro satellites (BI =3deg/h)	AES (Japan)	7
ADIS16405BLM	Triazial inertial sensor with magnetometer for nano and pico satellites (BI=25.2deg/h)	Analog Devices (USA)	8

Table 3. State of the art cubesat solar cells [8].

Tech Type	Description	Developer	Efficiency	TRL Status
Solar Cell	Improved Triple Junction TASC	SpectroLab (USA)	27%	9 (On Orbit)
Solar Cell	Next Triple Junction (XTJ)	SpectroLab (USA)	29.50%	9 (On Orbit)
Solar Cell	BTJ/ZTJ Space Solar Cell	Emcore (USA)	27 – 29%	9 (On Orbit)
Solar Cell	Triple Junction Solar Cell 2G28 / 3G30	AzurSpace Solar (Germany)	28 – 30%	9 (On Orbit)

Table 4. Solar Cell specifications [8].

Cells	Description	Area (cm^2)	Isc(mA)	Voc(V)	Pmax(W)
TASC	Triangular Advanced Solar Cells	2.77	0.031	2.52	0.07479
XTJ	29.5% Next Triple Junction(XTJ) Solar cells	26.62	0.4727712	2.633	1.24480657
UTJ	28.3% Ultra Triple Junction	32	0.5140575	2.66	1.2066075
BTJ/ZTJ	Space Solar Cell	26	0.4524	2.762	1.03389
3G28C	28% Solar Cell	30.18	0.506	2.667	1.154677

Table 5. Solar cell materials [16].

Cell	Silicon (Si)	Gallium Arsenide (GaAS)	Triple Junction GaAS
Theoretical efficiency	29%	23.50%	40+%
Achieved efficiency (Best Lab)	25%	21.80%	33.80%

B. Relevant Missions

After an extensive search through online databases, there are a handful of missions with similar objectives and requirements to ours, and of those, even fewer have hardware

specifications published online. The MinXSS is a 3U Cubesat designed to measure the energy distribution in solar flare activity by the University of Colorado at Boulder [9]. The MinXSS uses XACT from Blue Canyon Technologies, which is a 3-axis, high precision control system. The system integrates a star tracker with momentum torque rods and a reaction wheel to achieve accuracy with .007 degrees [9]. However, their technology has not been flight proven. While our mission does need high precision, it does not need a star tracker. This technology is too costly and unnecessary for locating the sun. Our mission requires more precision than coarse sensors offer, yet not as much precision as the top sensors provide. Developing or finding a sun sensor half the cost and half the precision is ideal for our mission. Specifications for the MinXSS mission can be seen in the following table.

Table 6. MinXSS specifications [9].

Orbital Parameter	Requirement	Reference Orbit
Altitude	<700 km (Cubesat)	450 km x 600 km
Inclination	>35 degrees	50 degrees
Period	N/A	95.1 minutes
Eclipse	N/A	34.9 minutes
Spacecraft Size	3U	3U
Orbit Average Power	>10W	12.5

Passerone et al. discusses design solutions for a nano-satellite developed at the Politecnico di Torino. This paper discussed the cost and reliability constraints using commercial off the shelf technology for a nano-satellite. The satellite contained 5 solar panels, 6 battery packs, 3 cameras with different focal lengths, 5 processors on full redundancy, and 2 communication modules with different antennas.

The spacecraft must generate its own power throughout the duration of the mission. In Sunlight, at 3 sides of the satellite will be exposed to sunlight and generating

power. When in eclipse, the satellite will completely rely on stored power from the batteries. To meet power constraints, they implemented a low power consumption design. Initially, the goal was to use low power commercial technology. When the desired technology was not available, they designed a system to keep systems in idle state or completely turned off when not in use.

Table 7. Power budget for Politecnico di Torino satellite [10].

Device	Duty Cycle	Peak Power	Avg. Power
PowerMgmt.	100%	20mW	20mW
Proc A&B	6%	200mW	12mW
Payload	0.50%	3.84W	21m!
TxRx	2.60%	17.2W	443mW
Total			496mW

The main power sources were triple junction GaAs solar panels, with each having MPPT based on a switching converter, which are not vulnerable to latch-up events. Six battery packs were used to drive the two independent buses. The power switches regulated voltage, selected the proper batteries, scheduled power ups and tracked latch-up events. Proc-A uses a Microchip PIC. Chain B uses a TI MSP430.

A power budget can be seen in the table 6, which displays the peak power percentage, average power, and duty cycle of on-board systems. The solar panels chosen provide around .8 W to give a margin of around .3 W based on the average power, which is around .5 W.

Viscio et al. discusses a proposed mission design for the purpose of in-situ solar observation and space weather measurements at the L1 Lagrange point. The design was based on creating a low cost bus for the cubesat, which will efficiently achieve its

mission. The cubesat has a 6U design, where 2U is devoted for solar sails, 2U for scientific instrumentation, and 2U for the other subsystems such as telecommunications, power, attitude determination and control, etc. The scientific instruments include a magnetometer and plasma spectrometer for plasma environment measurements, ion and neutral mass spectrometer for sampling low mass and ionized particles in the spacecraft Ram direction [7], radiation micro dosimeters to investigate space environment, and a NanoCam C1U to image the Sun. A link budget of the scientific instruments and payload was made and can be seen in Table 8.

Table 8. Cubesat system budget [7].

S/S	Mass [g]	Power [W]
Structure	1500	0
EPS	500	1
TCS	300	0
CDHS	150	0.5
AODCS	500	3
Comms	250	3
P/L	1000	3
Solar sail	860	0
Total	5060	10.5

Our mission however requires no propulsion and no use of solar sails. While, it was useful to observe the process at which they conducted their trade study, they did not provide specifics on power system design. At this time, we cannot truly create such a trade study since the final payload and scientific instrument is not yet known.

C. TechEdSat Heritage

The TechEdSat (Technological and Educational Nanosatellite) satellites are a series of nano-satellites developed by students of San Jose State University, NASA Ames and AAC Microtech for future Earth and planetary missions. The TechEdSat-1 was a 1U cubesat, which one of the first cubesats deployed from the International Space Station in

2012 and was functional for 7 months. The TechEdSat-3P is a 3U satellite, which posses its own passive deorbiting system. The 3P implements an Exo-Brake, which creates drag for an accelerated deorbit and re-entry. Rather than starting from scratch, the proposed cubesat, HELIOS, will be heavily influenced by design choices of the TechEdSat cubesats. Modifications will need to be made to accommodate for continuous pointing at the sun and 3-axis stabilization, but preliminary design choices for structures, C&DH, power generation, power storage, and communications will be based off of TechEdSat flight heritage.

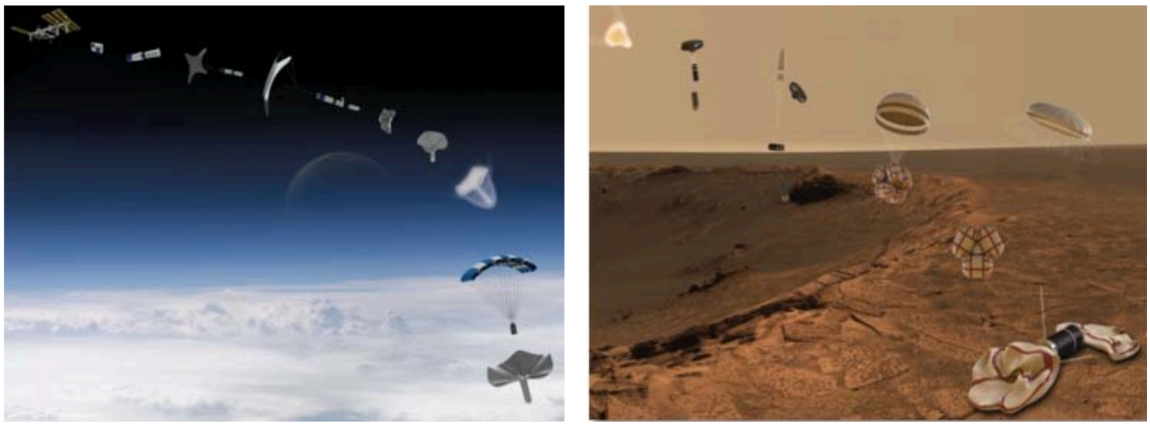

Figure 1. Concept of ISS small payload quick Return (left). Mars Companion Mission (right) [11].

III. Preliminary Design and Approach

A. Mission Objectives

Three objectives have been defined for this mission. The primary objective is to develop a flight system ready for hardware delivery, that is minimal and able to achieve the maximum success level. The secondary objective is to demonstrate the attitude determination and control of the spacecraft and evaluate the TRL from 6-7. The third

objective of this mission is to investigate iridium satellite-to-satellite communication as a method of eliminating the need for a physical ground station.

B. Success Criteria

Three levels of success have been defined for this mission as well. The minimum, medium and maximum success levels define realistic goals that can be accomplished pending any set backs due to constrains such as cost, scheduling, constraints, etc. The minimum success level is to demonstrate one axis of control over the spacecraft. The medium success level is to achieve full attitude control over the spacecraft. This will consist of successfully de-tumbling the spacecraft and allowing for 2 to 3 axis of control. The maximum success level is to achieve sun pointing and download an image of the sun. When 3-axis control is obtained and optics are facing the sun, a picture will be taken and downloaded via a series of compressed data packets, which will be uncompressed on ground.

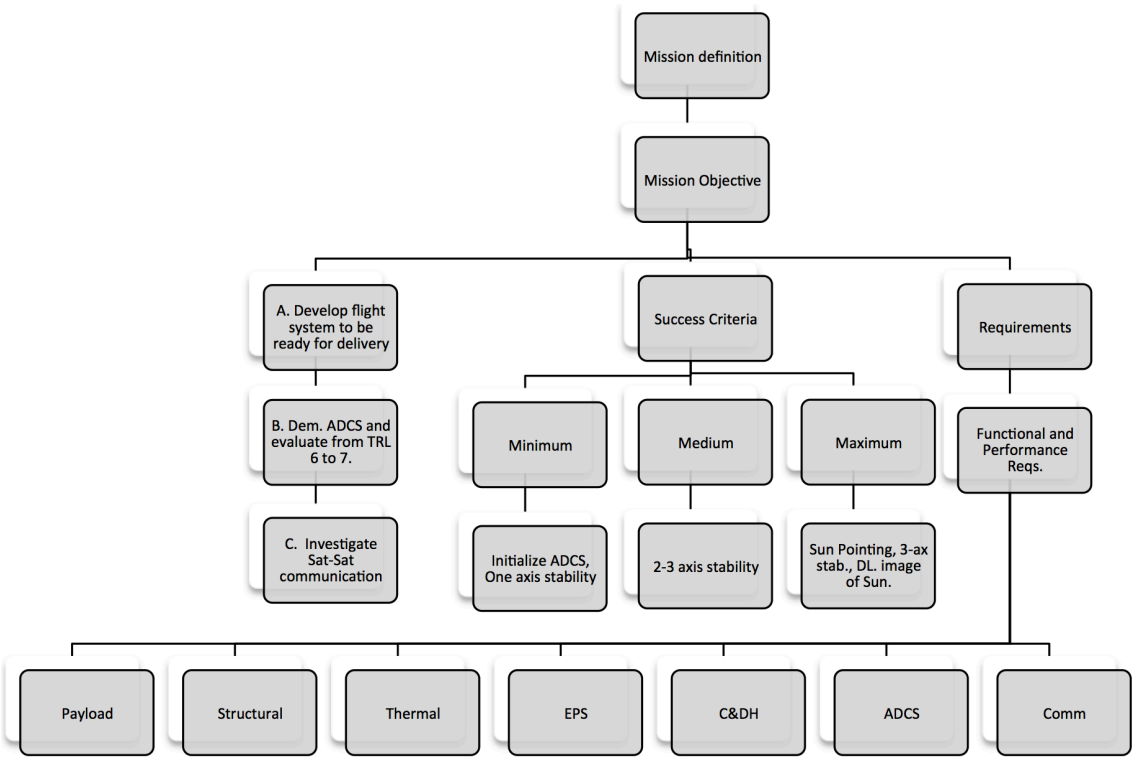

Figure 2. Mission Objectives and Requirements flowchart

Figure 2 displays a mission objectives and requirements flowchart. The first level of the flowchart is mission definition. The second level is mission objectives. The third level contains mission objectives, success criteria and requirements. The needed subsystems are defined by the system requirements. The next level would define each subsystem's particular components as needed. The main driving subsystems to be considered are: Structures, Thermal, Power, Command and Data Handling, Attitude Determination and Control, Communications and Payload.

C. Power

As the power subsystem is the focus of this paper, the following results, analysis and discussion will be focused around it. The figure below displays a flow chart of the power subsystem.

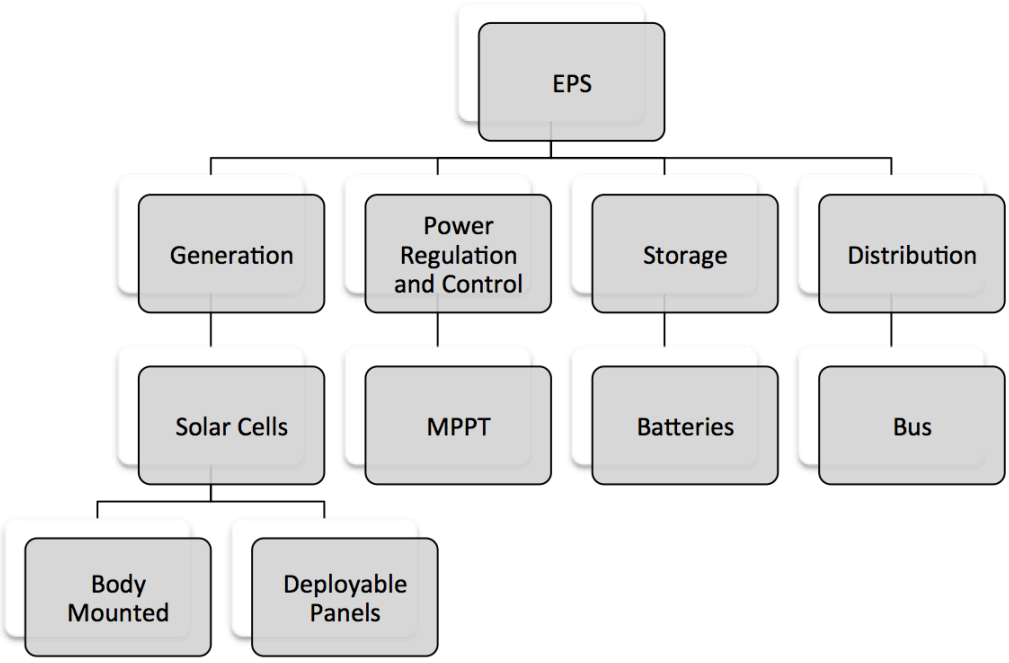

Figure 3. Power subsystem Flow chart

The Electrical power system can be broken down into four main components. The first is power generation. The second is Power regulation and control. The third is energy storage. The Fourth is power distribution. Power generation is dependent upon energy absorbed by photovoltaic cells, which will be mounted on the body of the spacecraft and in this case, will also be mounted on deployable panels, which will be designed in house. Power regulation and control will be guided by a maximum power point system. Lithium ion battery cells will be implemented for energy storage. Power distribution will allow for functionality for the rest of the battery bus. Each one of these topics will be touched up further in the report.

Figure 4 displays an N2 diagram, which provides for a visual representation between systems and their dependency on another. The basic components of the power system include are the spacecraft's structure, the PCB panel, photovoltaic (or Solar) cells, the electrical power system board, and the battery. The connections between components

are shown as well as, which components will be connected mechanically, electrically, or both. The structure will have mechanical connections between the PCB Panels and the electrical power system board. The PCB panel will have a mechanical connection to the solar cells. The Solar cells will have an electrical connection with the electrical power system board. Finally, the electrical power system board will have both mechanical and electrical connections with the battery.

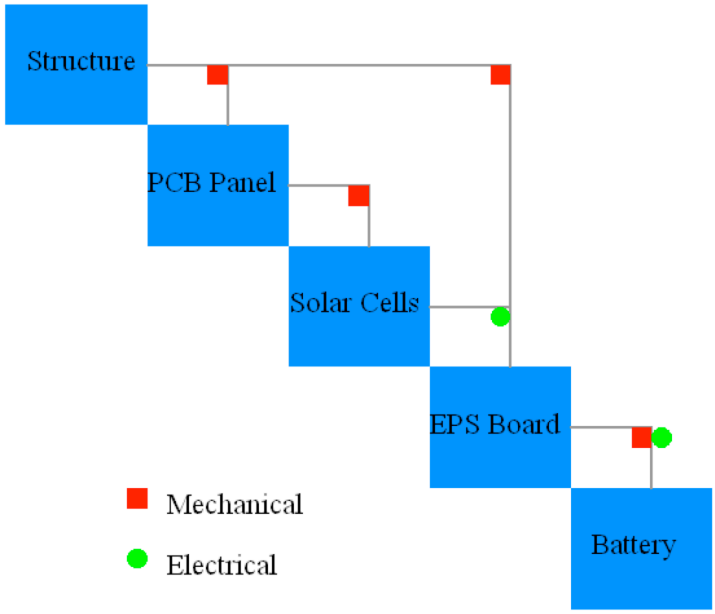

Figure 4. Power system N2 diagram.

IV. Orbital Mechanics

A. Background

In order to properly describe or design the orbit of a spacecraft, it is required to use the classical orbital elements described in Table 9.

Table 9. Classical orbital elements [12].

Element	Symbol	Description
Eccentricity	e	Deviation from a circular orbit
Semi-major axis	a	Half the distance between closest and furthest point of approach
Inclination	i	Tilt of orbital plane with respect to equatorial plane
Right ascension of ascending node	Ω	Angle from origin of longitude to direction of ascending node
Argument of perigee	ω	Angle between ascending node and position vector
True anomaly	ν	Angle between satellite and perigee

The period of the orbit can be defined by the equation:

$$P_o = 2\pi\sqrt{\frac{a^3}{\mu}} \tag{1}$$

Where μ is the standard gravitational parameter between the Sun and Earth and equal to about $3.986 * 10^5 \frac{km^3}{s^2}$ [12].

The Earth centered inertial frame (ECI) is the non-rotating of reference XYZ, the center of the earth as its center where the Z-axis of the ECI points toward the geographical North Pole [12].

$$\begin{bmatrix} x \\ y \\ z \end{bmatrix} = r \cdot \begin{bmatrix} c(\nu+\omega)c(\omega) - s(\nu+\omega)s(\Omega)c(i) \\ c(\nu+\omega)\,s(\Omega) + s(\nu+\omega)c(\Omega)c(i) \\ s(\nu+\omega)\,c(i) \end{bmatrix} \tag{2}$$

Where,

$$r = \frac{a(1+e^2)}{1+ecos\nu} \tag{3}$$

The angular radius of the earth describes the apparent size of the earth from the spacecraft and is seen in equation 4:

$$\rho = \sin^{-1}\left(\frac{r_e}{a}\right) \tag{4}$$

The angular radius is dependent upon the altitude of the spacecraft. As can bee seen in Figure 5, the radius is indirectly proportional to the altitude.

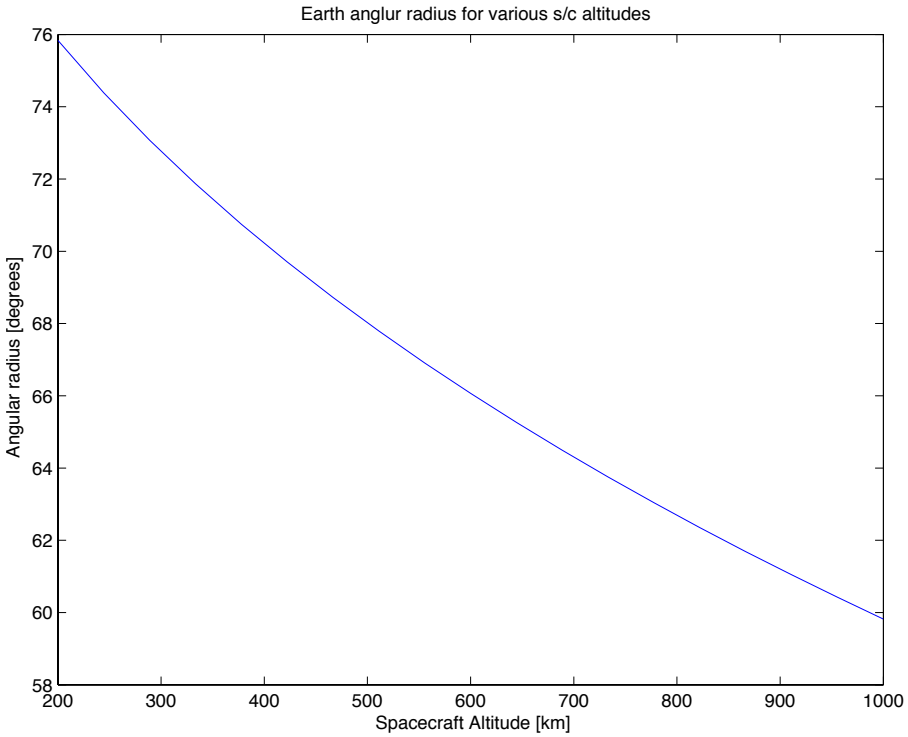

Figure 5. Angular radius of earth vs. altitude via equation (4).

The time of eclipse is dependent upon the satellites period and angular radius. The relation between eclipse time and orbital period can be seen in Figure 6.

$$TE = P_o * \frac{2\rho}{2\pi} \tag{5}$$

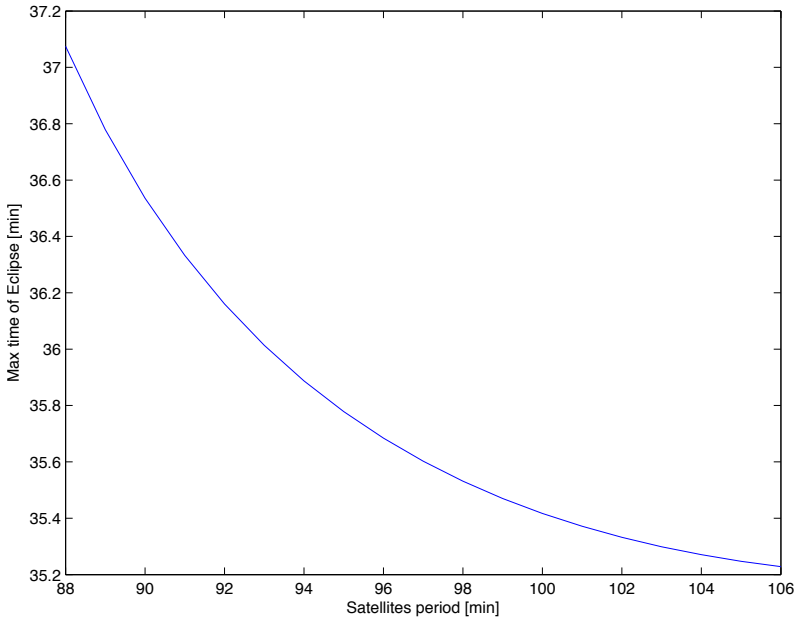

Figure 6. Max time of eclipse vs. orbital period via equation (5).

Earth has an equatorial bulge and is not in fact a sphere. The radius of earth is around 22km larger at the bulge (or along the equator) than at the poles. However, a spherical model is adequate enough for our calculations. The elevation of the sun varies throughout the year. On the first day of spring, elevation is 0°. The elevation varies between $\pm 23°$throughout the remainder of the year. The elevation can be seen through the equation:

$$\epsilon_S = \frac{23\pi}{180} \sin\left(\frac{T_s}{365} 2\pi\right) \tag{6}$$

A correlation between the elevation of the sun and time of the year can be seen in Figure 7. The elevation varies sinusoidally, as the azimuth is dependent on time.

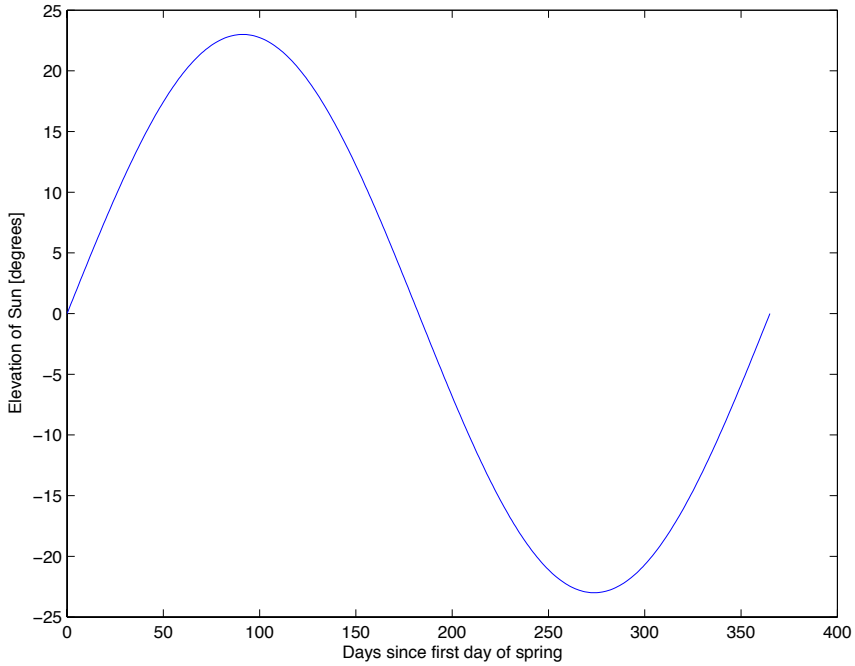

Figure 7. Sun elevation vs days since spring via equation (6).

The fundamental equation of relative two-body motion is given by:

$$\ddot{\boldsymbol{r}} = -\frac{\mu}{r^3}\boldsymbol{r} \tag{7}$$

This is a non-linear second order differential equation, which governs motion of two point masses [12]. However, in reality a number of additional forces will affect our satellite so we will need to introduce another parameter $\boldsymbol{k_s}$, which is the perturbing vector.

$$\ddot{\boldsymbol{r}} = -\frac{\mu}{r^3}\boldsymbol{r} + \boldsymbol{k_S} \tag{8}$$

Where $\boldsymbol{k_S}$ represents perturbing forces from the Earth, Sun, Moon, atmospheric drag, oceanic tides and Earth reflected solar radiation pressure.

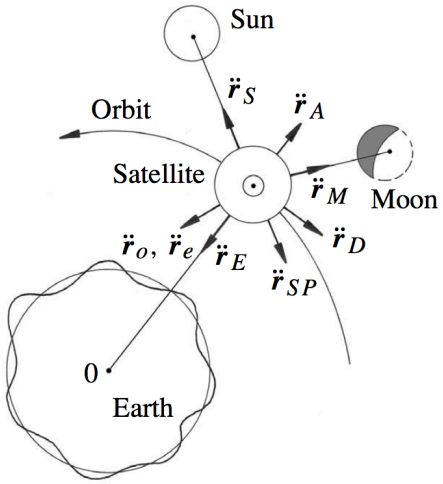

Figure 8. Perturbing forces on a satellite [13].

After atmospheric drag, the next most dominant cause of perturbation is due to the oblateness of the Earth. As the Earth is not perfectly spherical, a force of gravity on a body isn't directed towards the center of the earth [12]. The dimensionless parameter, which quantifies the variation in latitude due to the oblateness of the Earth, is referred to as J_2. For Earth $J_2 = 1.08263 \times 10^{-3}$

The bulge affects the right ascension of ascending node and the argument of perigee by the factors:

$$\dot{\Omega} = -\frac{\frac{3}{2}\sqrt{\mu}J_2R^2}{(1-e^2)^2a^{\frac{7}{2}}}\cos(i) \tag{9}$$

$$\dot{\omega} = -\frac{\frac{3}{2}\sqrt{\mu}J_2R^2}{(1-e^2)^2a^{\frac{7}{2}}}\left(\frac{5}{2}sin^2(i) - 2\right) \tag{10}$$

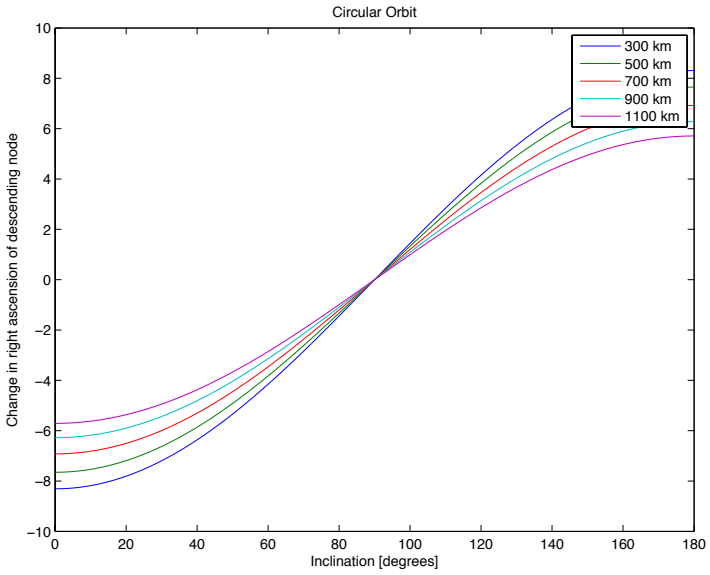

Figure 9. Change in nodal regression with respect to inclination via equation (9)

From Figure 9, it can be seen that inclination of 90 degrees results in zero nodal regression. Inclination choices can compensate for the earth's motion around the sun and prevent the satellite from going into eclipse. It can also be seen that higher altitude orbits are less affected by the earth's bulge.

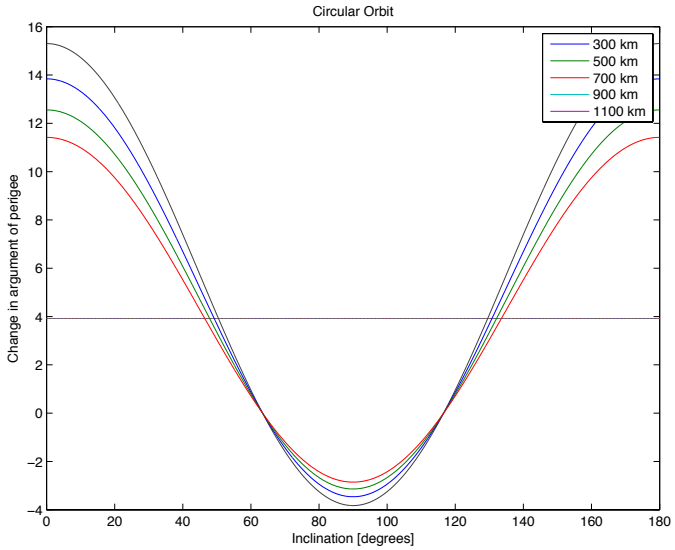

Figure 10. Change inargument of perigee with respect to inclination via equation (10).

It can be seen form Figure 9 and Figure 10 that the effect of oblateness is increasing as inclination drifts from 90 degrees, where the satellite is closest to the equatorial bulge. Negative numbers for the rate of change in right ascension of ascending node correlate to westward movement and positive numbers refer to eastward movement.

Sun Synchronous Orbits

A sun synchronous orbit makes a constant angle α with radial from the Sun to the Earth. It requires that orbital plane rotate in inertial space with angular velocity of the earth in its orbit around the sun [12]. In other words, it requires a nodal regression of:

$$\dot{\Omega} = .9856° \, per \, day$$

At this rate, the satellites motion will compensate for eastward processing at inclinations larger than 90 degrees. . A satellite in a sun synchronous orbit has a constant view of the sun.

With proper choices of eccentricity, altitude, and inclination, a sun synchronous orbit can be achieved. Sun synchronous orbits provide optimal solar exposure for satellites, which maximizes energy production and minimizes need for energy storage.

The eccentricity of an orbit describes the shape of the orbit and its deviation from a circular orbit. Eccentricity is zero for a circular orbit. An elliptical orbit has an eccentricity between zero and one. A parabolic orbit has an eccentricity of one and a hyperbolic orbit has an eccentricity, which is greater than one. The eccentricity can be found by dividing the difference of the perigee and apogee radius by their sum

$$e = \frac{r_a - r_p}{r_a + r_p} \tag{11}$$

Table 10. Eccentricity values for different type of orbits.

Orbit	Value
Circular	0
Elliptical	<1
Parabolic	1
Hyperbolic	>1

The semi-major axis of an orbit can be described as half the distance between the furthest and closes point of approach of an orbit [12]. The semi-major axis of an orbit can be shown through the relationship:

$$a = \frac{r_p + r_a}{2} \tag{12}$$

B. Orbital Environment Calculations

The assumption is that the initial launch will be from the International Space Station (ISS). Therefore, our cubesat will have the same orbital parameters as the ISS. This includes the apogee altitude, perigee altitude and inclination. The values of the ISS orbit can be seen in the following table. It can be seen that the perigee altitude and apogee altitude are very close leading to an almost circular orbit.

Table 11. ISS orbital values.

ISS	
Perigee	409 km
Apogee	416 km
Inclination	51.65 degrees

We can then take these values, and use the above equations to calculate the parameters of our cubesat's orbit. In the following table, the calculated values for semi-major axis, eccentricity, period, angular radius and time in eclipse.

Table 12. Calculated orbit values based off of ISS parameters.

Parameter	Calculated Value
Semi-major axis	6783.5 km
Eccentricity	0.0005
Orbital Period	5564.4 seconds (92.74 min)
Angular radius	69.92 degrees
Time in eclipse	2161.3 seconds (36 min, 38% of orbit)

C. STK Data

By defining the orbital elements found in section III, we can create a 3D representation of our orbit using STK (Systems Tool Kit), which is a physics-based software used for various engineering applications. Figure 11 displays the change radius in the x, y and z-axis throughout the orbit. In Figure 12, roughly 4.3 orbits are plotted in red, which corresponds to 6.7 hours. From Figure 12, we can see the change in position of the spacecraft relative to the earth's surface due to the gravitational perturbations. Each passage, there will be a slight change in each orbital element. The x, y and z-axis correspond to the altitudes in those directions.

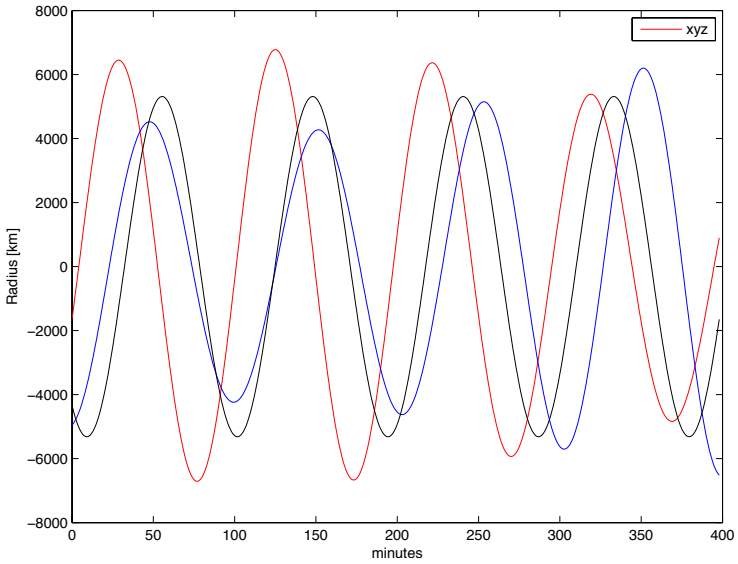

Figure 11. Change in radius over time with respect to the center of the Earth.

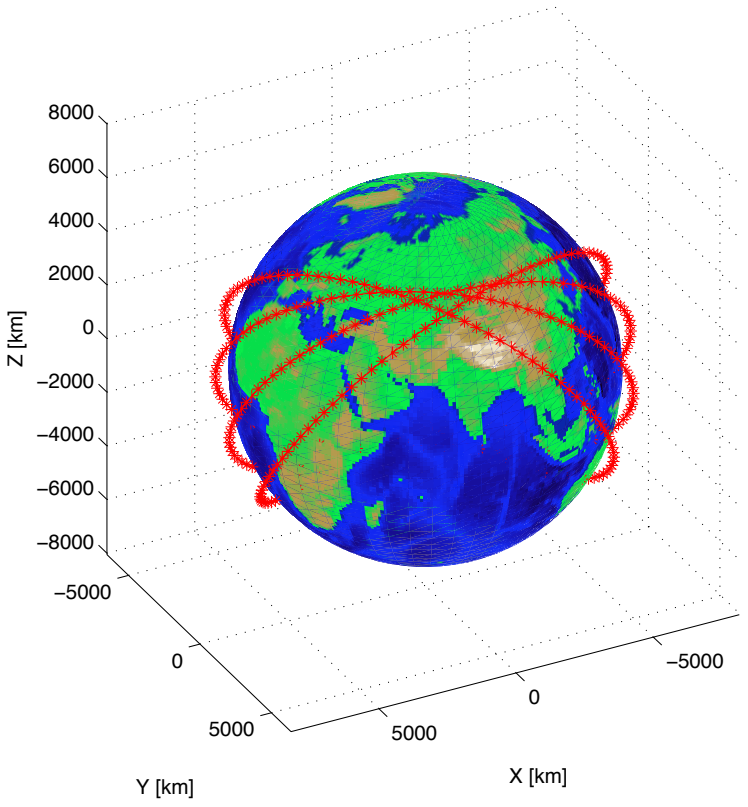

Figure 12. 3D model of HELIOS orbit over Earth surface.

From the STK data, we can also extract the periods of sunlight exposure and eclipse. Figure 13 displays roughly nine orbits corresponding to around 890 minutes

based on our average orbital period. The x-axis displays time in minutes in reference to UTCG (or universal time code generator). This is a default time setting based on the time of simulation. The y-axis displays solar intensity on a scale from 0-100 with 100 denoting full solar exposure at 1368W/m^2. Times in full eclipse are denoted by 0-solar intensity and times in between denote penumbra conditions. Times in full sunlight exposure are essential to the mission since that is when the spacecraft will be generating all of its power. It will need to generate enough power to store in the batteries for use during eclipse times such that the battery does not discharge below allotted levels.

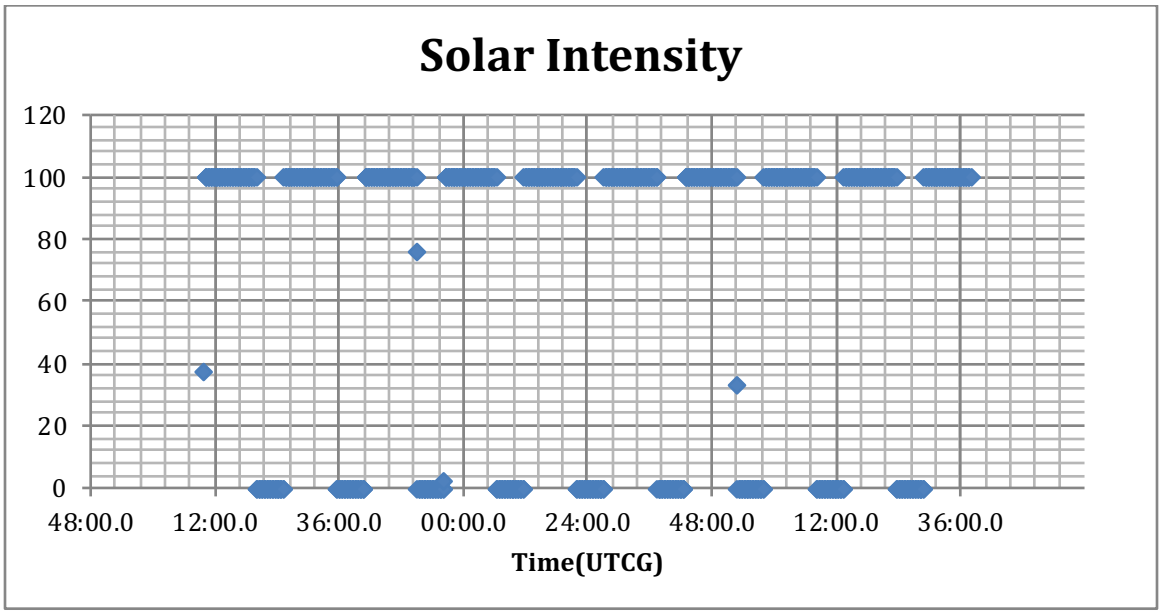

Figure 13. Solar Intensity plot of HELIOS orbit.

From Figure 13, we can tabulate the data in order to determine the frequency of each orbit condition. The following table displays the counted minuets of each condition and percentage of data, which that condition represented. From the sample data, total eclipse accounted for 38.89% of the data while sunlight accounted for 60.62%. All other

conditions accounted for .07% percent of the data. The eclipse time closely resembles the calculated value of in the Orbital mechanics section.

Table 13. Orbit condition frequency

Value	Count	Percent
0	547	38.89
2.26754	1	.07
3.32801	1	.07
33.3893	1	.07
33.5372	1	.07
37.4295	1	.07
76.6119	1	.07
86.1189	1	.07
100	887	60.62

V. Orbital Temperatures

When the solar panels are deployed, it is important to account for incoming heat from solar flux, albedo and Earth's infrared radiation. The incoming solar flux, q_{solar}, can be calculated through equation 13, which takes into account the solar constant G_s, the absorptivity of the solar cells α_s, and the power converted to electricity q_{Sc}:

$$q_{solar} = G_s \alpha_s - q_{Sc} \tag{13}$$

Where G_s is $1368\ W/m^2$ and α_s is .9 [16]. The incoming heat from albedo and the Earth's infrared radiation can be calculated through the equations:

$$q_{albedo} = G_s\ \alpha_s\ a\ \sin^2 \rho \tag{14}$$

$$q_{IR} = q_{EIR} \varepsilon_S \sin^2 \rho \tag{15}$$

Where, a is the Earth's albedo, q_{EIR} is the Earth's emitted black body infrared radiation, and ε_S is the emissivity of the solar cells. Earths albedo is .52 and the emitted black body

radiation is $257 W/m^2$ [16]. The total incoming heat, q_{in}, can be calculated by summing the three previous parameters:

$$q_{in} = q_{solar} + q_{albedo} + q_{IR} \tag{16}$$

The emitted heat from the satellite can be calculated through the following equation where ε_{BS} is the emissivity of the back of the solar cells, σ is the Stefan-Boltzmann constant, and temperature T:

$$q_{out} = (\varepsilon_s + \varepsilon_{BS})\sigma T^4 \tag{17}$$

The temperature can be calculated through the following equation with thermal equilibrium conditions:

$$T = \left(\frac{q_{in}}{(\varepsilon_s + \varepsilon_{BS})\sigma}\right)^{\frac{1}{4}} \tag{18}$$

Table 14. Results from orbital temperature calculations (13) through (18).

Parameter	Worst Case	Zero Incidence	% Difference
q_{solar} [w/m^2]	969.4	946.79	2.38806916
q_{albedo} [w/m^2]	619.06	619.06	0
q_{IR} [w/m^2]	192.6998	192.6998	0
q_{in} [w/m^2]	1.78E+03	1.76E+03	1.290872903
T_{HOT} [K]	369.2396	368.0622	0.319891584
T_{COLD} [K]	211.7644	211.7644	0

Table 14 displays the results found from using the heat flux and temperature equations. Two temperature calculations are made for a hot and cold case. The hot case uses the total incoming heat where the cold case neglects albedo and solar flux [14]. This gives us two extremes for the orbital temperature the solar panels will experience. Two different scenarios were accounted for. The first is a worst-case scenario referring to a solar incidence angle of 23 degrees. The second scenario uses a zero incidence angle.

These scenarios are explained further in the following sections. Three of six parameters are not affected by the incidence angle. Whereas the solar flux, total flux and hot case are affected. These temperatures will ultimately affect the performance of the solar cells.

VI. Sizing and Configuration

A. Battery

1. Background

Battery selection is an essential part of spacecraft design as spacecraft as energy storage must be sufficient to meet load demands during daylight and eclipse. Batteries are made of individual electromechanical cells, which area connected in a series-parallel circuit. A typical configuration of a battery cell can be seen in Figure 14. There are typically 1 positive and 1 negative terminal. A chemical electrolyte is placed between two electrode plates. Each cell voltage is more dependent upon the chemistry and makeup of the cell rather than the size. The capacity of the cells is defined in amp-hours (Ah), which can be delivered at room temperature. The voltage of the battery defines the average deliverable voltage. The product of the Ah rating and voltage gives watt-hour energy rating (Wh). This defines the rate that energy can be discharged from the battery to the spacecraft load when fully charged.

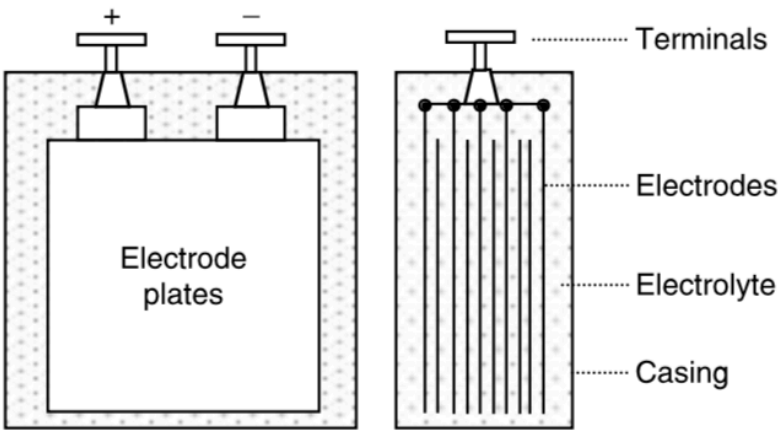

Figure 14. Typical configuration of a battery cell [15].

A battery can be modeled as a voltage source with an internal resistance [15]. Figure 15 displays the electrical circuit of a battery where R_i is the internal resistance, E_i is the internal electromechanical voltage, R_L is the load resistance and V is the voltage across the load. E_i is varies inversely with Ah discharge while R_i increases with Ah discharge. Therefore, when a battery is fully charged, it will have a higher electromechanical voltage and lower internal resistance compared to a partially charged battery.

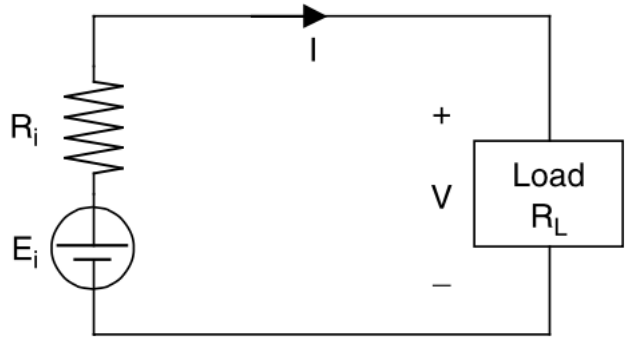

Figure 15. Electrical circuit model of a battery [15].

The selection criteria for batteries depend on four primary figures of merit, which include specific energy, energy density, specific power and power density, and cycle life. Specific energy defines the energy stored per unit mass. Energy density defines the

energy stored per unit volume. Specific power defines the deliverable power of the battery. Cycle life defines the charge and discharge cycles the battery can sustain while operating without excess degradation [15]. There are many different types of batteries. Table 15 and Table 16 display characteristics and descriptions of various batteries used on small spacecraft today.

Table 15. Small spacecraft battery characteristics [8].

Chemistry	Mission	Specific Energy (Wh/kg)	Energy Density (Wh/l)	Operating Temp Range, C	Cycle Life	Mission Life (yrs)	Issues
Ag-Zn, Li-SO2, Li-SOC12	Launch vehicles, Cassini MER lander, Sojoumer Rover	90-250	130-500	-20 to 60	1	1-9	Limited temp range & voltage decay
Ni-Cd, Ni-H2	ToPex, HST, Space Station	24-35	10-80	-5 to 30	>50,000 @25% DOD	>10	Heavy/ bulky, temp range
Li-Ion, Li-Polymer	MER rovers, Cubesat	100	250	-20 to 30	>400 @50% DOD	>2	Cycle life

Table 16. Small spacecraft battery types [8].

Name	Description	Developer	TRL level
Primary battery	Ag-Zn, SZHR 50, .76 kg, 1.5V, 50 Ah	Eagle Picher	6
Primary battery	Ag-Zn, Silvercels, 1.5 V, .1-20k, Ah	Yardney	6
Rechargeable battery	Ni-H2, SAR10097, 28kg, 10V, 75 Ahr	Eagle Picher	6
Advanced battery	Li-Ion, custom from space qualified COTS	ABSL Space products	6
Advanced battery	Li-Polymer, 8.2V, 1.24 Ahr	Clyde Space Ltd.	6
Advanced battery	Li-Ion VEL/VL, 2.6V, 4.5-50 Ahr	Saft SA	6
Advanced battery	Li-Ion #18650HC raw, #19670 protected Sony	Sony	6
Advanced battery	Li-Ion, Lithion 3.6V 7-350 Ahr	Yardney	6

Nickel Cadmium has been primarily used in the space industry before the 1980s [15]. Nickel Hydrogen batteries provided for larger discharge and became a commonly used successor. The industry has swayed towards using Lithium batteries for their specific-energy to energy-density ratio. Nickel Metal Hydride cells improve specific energy and energy density. They are also less vulnerable to temperature. Lithium-Ion battery cells are a relatively newer technology for the space industry. These cells can be commonly found in personal devices such as computers and cameras. While these cells do have a shorter life span, they are more resistant to corrosion in comparison to other cell technologies and have a high specific-energy to energy-density ratio. Lithium-Ion cells are also common choices for spacecraft operating in LEO for their tolerable temperature range. Lithium-Polymer and Lithium-Phosphate are also other cell technologies with high specific energy ratings [15]. Figure 16 displays comparisons of battery cell technology used in the space industry and small spacecraft.

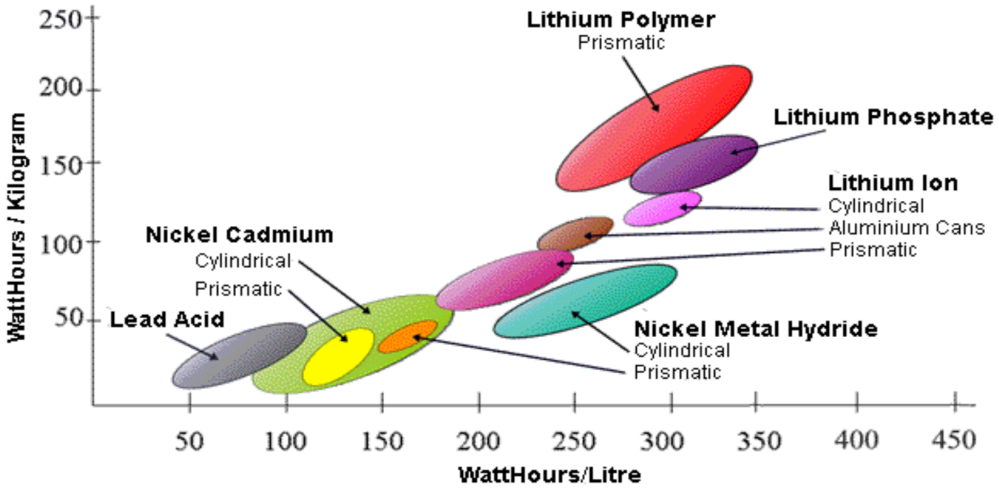

Figure 16. Plot of battery cell technologies performance [8].

Nickel and lithium based batteries are optimal choices for small devices. Their relative high cost and small lifespan provide for impractical choices for larger applications. They have high energy density, relative low self-discharge and require low maintenance. This particular mission requires a rechargeable battery. Space is limited and the spacecraft will be constantly cycling through sun and eclipse periods allowing for charging. The Battery University provides comparisons of more characteristics of battery cell technology.

2. SMAD Calculations

Following the Space Mission analysis and Design model, we can make preliminary estimates for battery sizing. From the estimated period of the orbit, eclipse time, mission duration and required power during eclipse, we can make simple calculations to find the minimum required battery capacity and mass of the batteries. Based on the power required and orbit time, dimensional analysis was used to calculate a minimum battery capacity of 8.5Wh, .7Ah and mass of .2kg.

Table 17. SMAD battery sizing 1.

Orbit period	*92.7*	**92.7**	**min**
Maximum eclipse time	*36.0*	**36.0**	**min**
Mission duration	*1.000*	**1.000**	**years**
Required power during eclipse	*8.0*	**8.0**	**W**

Table 18. SMAD battery sizing 2.

Battery capacity	**8.5**	**W-hr**
Battery capacity	**0.7**	**A-hr**
Mass of batteries	**0.2**	**kg**

Table 19. 18650 battery cell calculations.

Cell 18650	
Nominal Voltage (V)	3.7
Nominal Capacity (Ah)	2.2
Battery Pack (4 cells)	
Volume (m^3)	0.000980734
Voltage (V)	12
Capacity (Ah)	34
Cubesat Fitting	
Battery Packs per U	1
Number of U's used	2
Total Power (Wh/24 hr)	**34**

Table 19 displays specifications of and sizing calculations for the 18650 lithium-ion battery cell. The cell has a voltage of 3.7V and 2.2Ah. Inside one battery pack would contain 4 cells. The total deliverable power over a 24-hour period of a 4-cell battery pack using 18650 cells would be 34W.

3. Selection

The BP-930 battery was chosen for the energy storage device of the HELIOS cubesat. The BP-930 uses 18650S lithium-ion rechargeable cells. Two strings of series cells are connected in parallel. The material safety data sheet along with the manufacturing data sheet can be found in the appendix. This battery was chosen for its flight heritage on the Tech Ed Sat series, its temperature range, specific energy rating, and life cycle.

B. Power Regulation

Due to the dynamic environment in LEO, the temperature is constantly changing. For a self-sustaining spacecraft, the efficiency of the solar cells vary with temperature. There are shifts in the maximum power point of solar cells. In order to account for these variations due to temperature, a specific topology must be implemented into the electrical power system. In 2006, Clyde Space Ltd. presented a report covering the three commonly used power systems implemented on cubesats; direct energy transfer with battery bus, direct energy transfer with regulated bus, and maximum point tracker with battery bus.

Direct energy transfer with battery bus is the most simple of the three and requires the smallest mass. However, the design requires larger solar arrays resulting in a larger spacecraft mass as it lacks in operational efficiency. While this design requires less mass and volume for the actual bus, it requires more mass and volume of the overall spacecraft. A design flaw in coupling the solar array and battery restricts its optimum performance. The maximum power point of the solar array's current and voltage asynchronously increase and decrease with temperature, which results in the maximum power output occurring when the battery is completely charged [16].

Direct energy transfer with regulated bus is commonly found on European spacecraft. The design introduces a subsequent bus regulator, which regulates bus voltage during sunlight and is best suited for a spacecraft that experiences extended periods of sunlight and eclipse. This design again suffers from inefficiencies in LEO, as it doesn't operate at optimum potential unless at max temperature and at its end-of-life. However, this design has proved to be efficient in GTO or GEO [16].

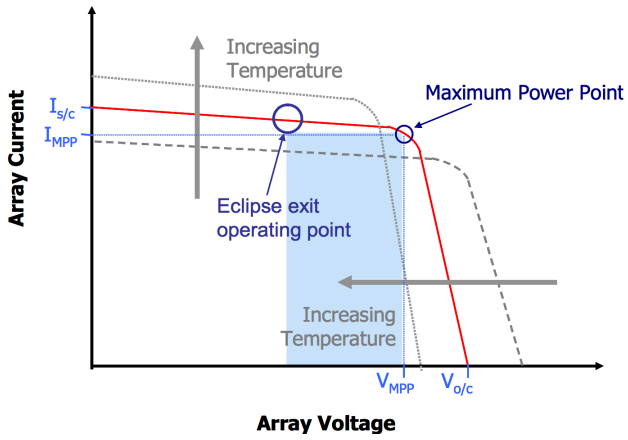

Figure 17. Temperature effects on solar cell I-V curve [16].

The maximum power point tracker with battery steps down the solar array voltage to bus voltage using a control loop. The tracker observes the max power point of the solar array and charges the battery at maximum power conditions. When fully charged, the current from the battery discharges and limits the voltage supply from the array. The power of the array is maximized in this topography, yet it suffers from a five to ten percent loss of power [16]. This design is most effective with applications that experience significant changes in maximum power point as in LEO, yet are insufficient in GEO applications.

C. Solar Cells

1. TASC Solar cells

Spectrolab TASC (Triangular Advanced Solar Cells) were chosen as the solar cells to be used for power generation of our cubesat. TASC solar cells are low cost, efficient and provide four times higher voltage compared to silicon solar cells. In fact, one of the multi-junction solar cells can generate the voltage of five silicon solar cells in series. They are also twice as efficient and can produce twice the power for the same area. A big part of the selection process for the TASC solar cells involved flight heritage. TASC solar cells were flown on other university cubesats including the TechEdSat cubesats. The datasheet for the TASC solar cells can be found in Appendix A.

2. Theory

Solar cells are composed of semiconductor materials, that when excited by a particle of sufficient energy, covalent electrons within the cell's material detach, begin to flow and generate current. An ideal solar cell can be modeled by the highlighted red box in Figure 18. It is composed of a current source, diode and resistance in parallel [17].

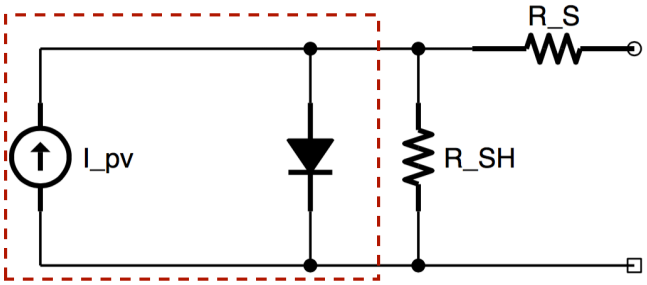

Figure 18. Practical PV circuit model with highlighted ideal circuit

The output current of the ideal solar cell can be expressed by the following equation:

$$I = I_{PV} - I_D \tag{19}$$

Where

$$I_D = I_0\left[e^{\frac{V}{AV_T}} - 1\right] \quad , \qquad V_T = \frac{N_S KT}{q} \tag{20), (21}$$

I_{PV} is the incoming current generated by the light source. I_D is the current across the diode and I_0 is the reverse bias saturation current. A is the ideality factor. V_T is the thermal voltage of the photovoltaic module, which is composed of the number of cells N_S, Boltzmann constant K $(1.3807 * 10^{-19})$, temperature of the p-n junction T, and the charge of an electron q $(1.60218 * 10^{-19})$. The max current produced (or open circuit current) occurs when the voltage is zero, which is equal to the incoming light current I_{PV}.

With the inclusion of the series resistance R_S and parallel resistance R_{SH}, the more accurate model can be represented by

$$I = I_{pv} - I_0\left[e^{\frac{V+IR_S}{AV_T}-1}\right] - (\frac{V+TR_S}{R_{SH}}) \tag{22}$$

There are more complicated models, however for the purpose of this application, the above equation provides for a good compromise between accuracy and simplicity [17].

3. Solar Cell Model

Using MATLAB, we were able to recreate the IV curve and power plots of the TASC solar cells in order to observe the characteristics of the cells based on the *Simple Solar Cell Panel Model.* The relationship between current and voltage as well as power and voltage can be seen in Figure 19. The TASC solar cell IV curve can be seen in the datasheet in the appendix. The datasheet specifies a maximum power current and max power voltage of $28mA$ and $2.19V$. This would lead to a maximum power of $.0613W$.

We could then extract the maximum point of the power vs. voltage curve. The modeled maximum power found was $.0621W$. The error between the two was 1.27%.

Table 20. Solar Cell Model vs Specification.

I_{MP}	$.028\ mA$
V_{MP}	$2.19\ V$
P_{max}	$.0613\ W$
P_{model}	$.0621\ W$
$Error$	1.2712 %

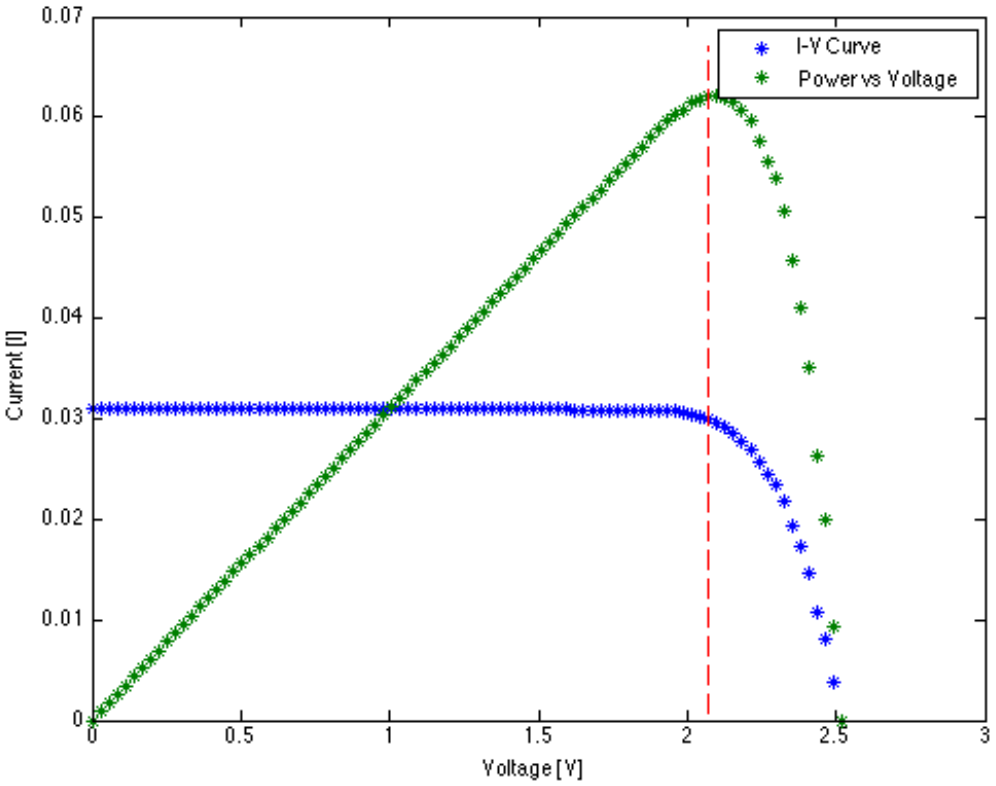

Figure 19. TASC Solar Cell IV and Power vs. Voltage curves via equations (19) through (22). Maximum power point indicated.

From the orbital temperature section, we were able to calculate a hot and cold case representing the theoretical extremes of the environment. The following curves in Figure 20 were modeled for the TASC solar cells to display the possible effects of the solar cells heating and cooling. As can be seen in the IV curve, both the short circuit

current and the open circuit voltage shift with changes in temperature. This in turns changes the maximum power output and affects the performance of the solar cells. The open circuit voltage and short circuit current change on average by roughly 20% and 5%, while the max power changes on average over 50% As this is only a model, physical testing of the solar cells will allow for accurate results and analysis. This can be done through the use of a ceramic heater, applying a thermo-couple to the solar cells and taking current and voltage measurements.

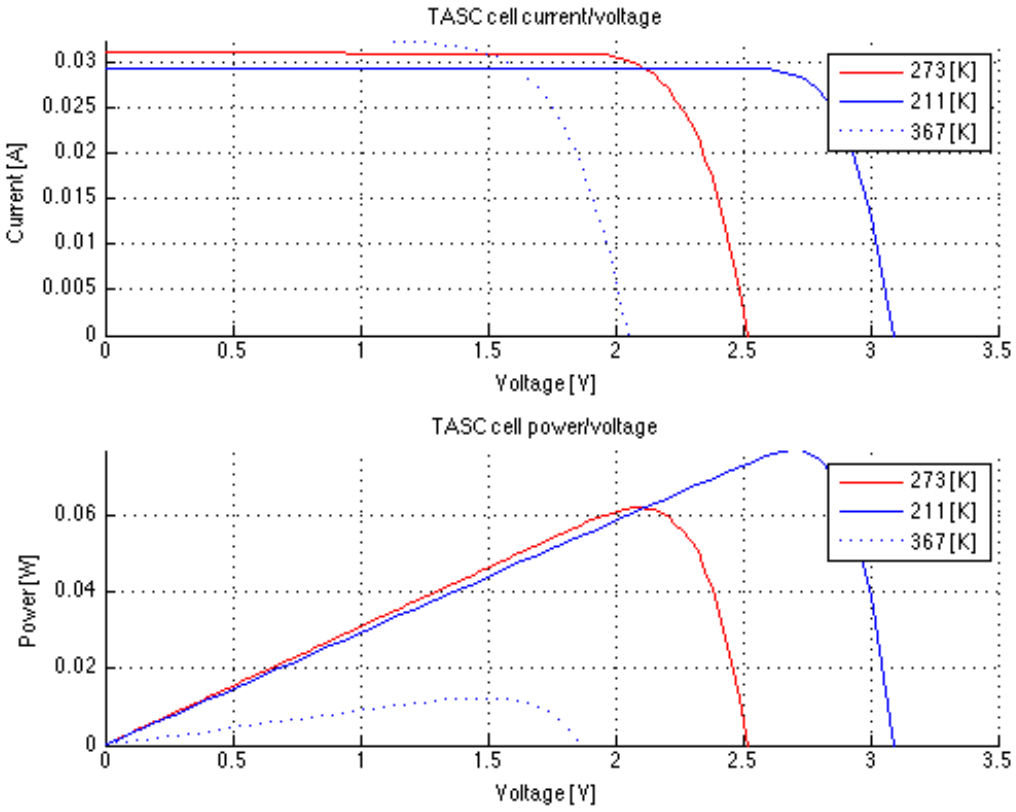

Figure 20. TASC solar cell modeled power and current curves with changes in temperature via equations (19) through (22).

Table 21. Model results temperature effect on solar cell performance.

Temp	V_oc	I_sc [A]	P_max [W]
273 [K]	2.52	0.031	0.0621
Hot Case, 367 [K]	2.046	0.0323	0.0123
Cold Case, 211 [K]	3.069	0.02936	0.0771
Ave. Error	0.5115	0.00147	0.0324
Error %	20.29761905	4.741935484	52.17391304

D. Solar Panel Sizing

1. Cubesat Design Specifications

The cubesat standard was defined by Cal Poly, San Luis Obispo and Stanford University to assist universities in designing and building low cost nano-satellites. These standards enforce restrictions on weight, size, and operations. There are P-Pod rails used to hold the cubesat during launch, which restrict the area on the faces of the cubesat. On four longitudinal faces of the cubesat, the area is restricted to 8.3 cm by 10 cm per 1U panel. This allows for $0.0083\ m^2$ per 1U panel.

2. Panel Design

After selecting the TASC solar cells, the panels need to be sized. With fully deployed solar panels, there is an available area of nine 1U panels, which would be facing the sun the entire time the cubesat is in sunlight. Designating 1U for the payload of the cubesat leaves 8Us available for solar cell placement. Taking into account the area of each solar cell and design choices from universities who have used TASC solar cells, it was found that 10 pairs of solar cells (or 20 cells) could be fitted per 1U panel. This allows for 160 cells for available 8Us or 80 pairs of solar cells.

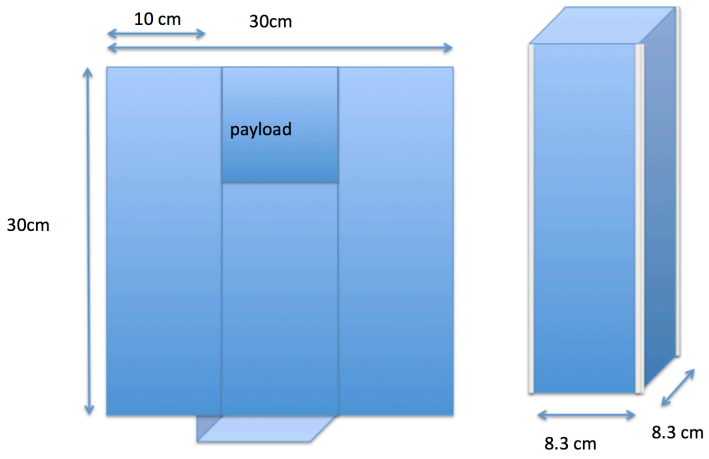

Figure 21. Rough design of 3U cubesat and opened solar panels

3. Cell Configuration

The next step after determining the number of cells is to determine the configuration that the cells will be connected. This will be based off the input voltage and current limits by power storage system. The BP-930 battery input voltage is 7.2V and the input current is 3.7A. The datasheet can be found in Appendix C.

Every pair of cells connected in series is considered a string. The voltage of a string cannot exceed the battery voltage. The highest potential voltage, which a single solar cell can reach, is its open circuit voltage or V_{oc}. The max power voltage of a TASC cells is 2.19V. The max current from a TASC cells is 31 mA. With two cells connected in series, the voltages are added to get the battery input. Based on the data sheet specifications, the input voltage will be around 5.04V using the max voltage. This is below the battery input voltage. The max current each string will produce is 31mA. For 10 strings on 8 1U panels, the total input current to one battery is 2480mA, which is below the battery input current requirement for one battery pack. Therefore, the configuration displayed in Figure 22 is adequate to not exceed the power storage requirements.

Figure 22. Solar cell string configuration.

VII. Power Production

A. SMAD Model

1. Theory

Following the Space Mission analysis and Design model, we can correctly size our power generation system to determine if the allotted area is adequate to supply power for the cubesat bus. We can calculate the total power required of a cubesat solar panel using the equation:

$$P_{SA} = \frac{\left(\frac{P_e T_e}{X_e} + \frac{P_d T_d}{X_d}\right)}{T_d} \tag{23}$$

Where P_e is the required power during eclipse and P_d is the required power during daylight. T_e and T_d are the periods in which the spacecraft is in daylight or eclipse. X_e and X_d represent the efficiency of the solar array during daylight and eclipse. The values of the two depend on the method of power regulation. Efficiency in peak power tracking is lost through converters.

Table 22. Solar cell eclipse and daylight efficiency [16].

	DET	PPT
X_e	0.65	0.6
X_d	0.85	0.8

The input power for a solar cell is $1368\,W/m^2$ [16]. This is the amount of energy received atop the earth's atmosphere for a surface, which is directed normal to the sun. The output power of a solar cell can be calculated using:

$$P_{out} = \eta_{cell} * P_{in} \tag{24}$$

At BOL, the power per unit area of the solar cell can be calculated through the equation:

$$P_{BOL} = P_{out} I_D \cos(\theta) \tag{25}$$

Where I_D is the inherent degradation, or efficiency lost due to manufacturing. A typical value for inherent degradation is 77%. θ is the incidence angle between the solar intensity vector and the spacecraft surface normal vector. This angle will vary throughout the orbit and different panels can have different incidence angles. A more standard power output can be calculated through the following equation:

$$P = I_0 A \eta \tag{26}$$

Where I_0 is the intensity of solar radiation, A is the effective area of the solar cells and η is the efficiency of the solar cells. Area is a function of the angle of incidence.

$$A = A_o \cos(\theta) \tag{27}$$

A_0 is the area of solar cells on one side of the satellite. At zero degrees of incidence, the sunlight reaches the highest potential effective area. As the angle of incidence increases away from the perpendicular, a smaller effective area is available.

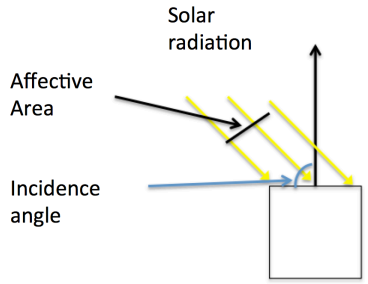

Figure 23. Solar radiation, incidence angle and effective area.

Figure 23 displays the relationship between the effective area of solar cells on one face of the cubesat and the incidence angle at which the sunlight strikes the surface. The effective area of the cubesat was chosen to be $0.036\ m^2$. It can be seen that the effective area is indirectly proportional to the incidence angle. A higher incidence angle results in a lower amount of effective area.

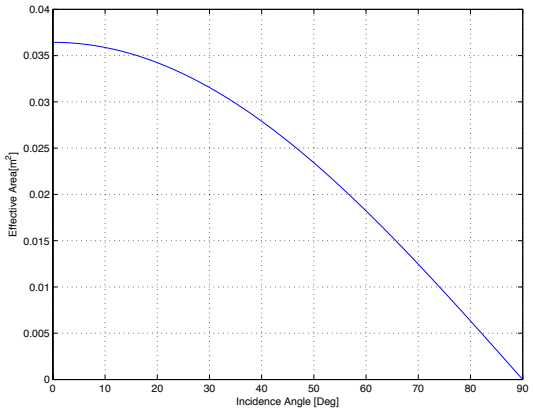

Figure 24. Effective area vs. Incidence angle via equation (27).

Using the efficiency of the TASC solar cells, the total available solar cell area calculated in the solar panel sizing section, and the solar radiation intensity provided by SMAD, we can see the relationship between energy produced, incidence angle and

effective area. It can be seen that energy production is directly proportional to the effective area and indirectly proportional to the incidence angle.

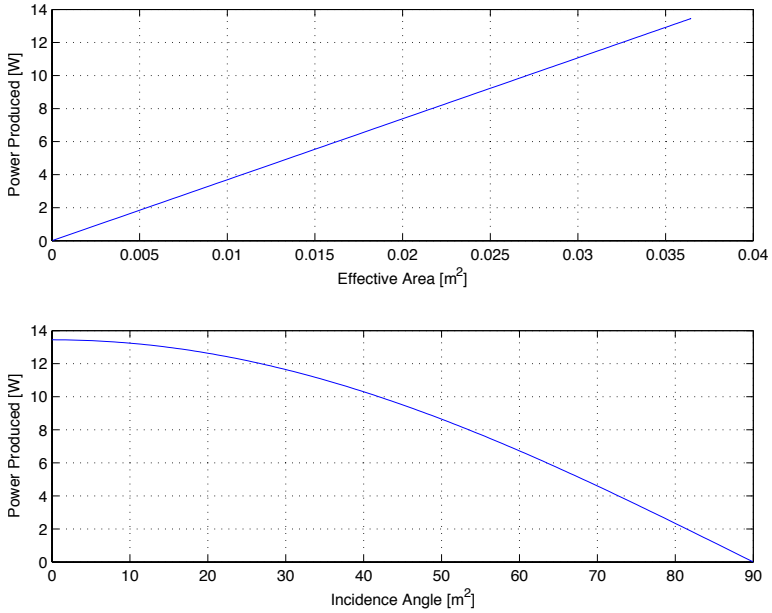

Figure 25. Power production vs. Effective area and incidence angle via equations (26) and (27).

The efficiency of the solar cell, η, is a nominal value given by manufacturers in data sheets. However, this efficiency is also a function of incidence angle as well, $\eta\ (\theta)$. For preliminary calculations, it is adequate to assume a nominal efficiency for solar cells. The maximum output power at zero incidence and the maximum effective area was calculated to be 13.45W. However, life degradation needs to be included for more accurate calculations.

Whether it is from radiation or from photons trapped in the earth's magnetic field, solar cells face degradation over time. For a gallium arsenide solar cell, degradation is about 2.75% per year in LEO. The life degradation of a solar cell can be shown through the equation:

$$L_d = (1 - D)^L \tag{28}$$

Where D is the degradation of the solar cell and L is the lifetime of the mission. The end of life power of a solar cell can be found by multiplying the beginning of life power by the life degradation.

$$P_{EOL} = P_{BOL} * L_D \tag{29}$$

Dividing the total power required of the cubesat solar panel by the end of life power, we can obtain the total solar array area needed to supply to the cubesat with power for the duration of the mission:

$$A_{SA} = \frac{P_{SA}}{P_{EOL}} \tag{30}$$

Since we have not yet decided on every component of the cubesat's different subsystems, we cannot yet obtain an official amount of power needed from the cubesat during daylight or eclipse, nor can we properly determine if our current configuration is adequate. A model was provided to us by the authors of the SMAD textbook, which entails an intricate spreadsheet based on the above equations, amongst others, to adequately size the solar generation unit of the power system. A screenshot of the model can be seen in the Appendix D.

2. Preliminary Calculations

In order to make preliminary calculations, assumptions had to be made for cell efficiency, inherent degradation, degradation and incidence angles. Two different values of incidence angle were used. The first was at zero incidence and the second was to see the effects using a worst-case scenario of twenty-three degrees. The assumption values can be seen in Table 23. The values for efficiency were taken from the data sheet of the TASC solar cells in Appendix A. The input power was taken from the Space Mission

Analysis and Design handbook. Inherent degradation and degradation were both taken from the SMAD handbook as well.

Table 23. Assumptions for Preliminary sizing calculations

Assumptions	Worst Case	Zero incidence
Cell efficiency	27%	27%
Input power [w/m^2]	1368	1368
Inherent degradation	0.77	0.77
Degradation	2.75%	2.75%
Incidence angle [deg]	23	0

The following table displays the results of those calculations using the SMAD model. The power output density, beginning of life power density, life degradation and end of life power density was calculated for both incidence angles. Between both angles, there is only an eight percent difference between the beginning of life and the end of life power at zero and worst-case incidence angles.

Table 24. Results for preliminary sizing calculations

Results	Worst Case	Zero incidence	Difference
Pout [w/m^2]	369.36	369.36	0
PBOL [w/m^2]	261.8	284.41	7.95%
LD	0.975	0.975	0
PEOL [w/m^2]	254.6	276.6	7.95%
Area [m^2]	N/A	N/A	

However, at this point in time, the most important parameter is the required area of the solar cell and it cannot be officially determined. As it was pointed out in the previous section, the total output power of the solar array and required area is dependent upon the required power draw during eclipse and daylight. In order for this information to be determined, the final list of components and power budget needs to be decided upon. The required power is heavily dependent upon the design of the ADCS subsystem. As a

final design has not been made, and therefore a power requirement has not been made, official calculations for the rest of the design cannot be made as well.

B. Design of Experiment (DOE)

In order to find the required solar cell area, a Design of Experiment (DOE) was performed. A DOE is a systematic way to sample the design space, study the effects that multiple changing variables have on a system, and study the effects that multiple input variables have on the output of a system. It is a technique commonly used to identify key drivers for a potential design and key design variable ranges. The design space of the power draw and the required solar cell area was not determined. However, the approximated solar panel area can be used as a reference to determine if the initial design is accurate. From the Sizing and Configuration section, 8Us of available solar panel area allowed for 160 solar cells. This approximated to $.036432m^2$.

1. Parametric study

A parametric study was performed in order to observe the effects that multiple values of eclipse and sunlight power (P_e, P_d), would have on the solar array area (A_{SA}). The main functions of subject can be found in the SMAD Model section for total power required by a cube-sat solar panel, P_{SA}, through A_{SA}. T_e, T_d, X_e, X_d and P_{sa} were all held constant through these preliminary calculations. Zero-incidence was also assumed. The next steps were to determine potential values for each variable. For a wide scope, P_e and P_d were varied from $0w - 8w$. The values for each variable can be seen in Table 25.

Table 25. Parametric Study Values

Pe	Pd	Te(s)	Td(s)	Xe	Xd	Peol
0:20	0:20	2192.3	3372.1	0.6	0.8	276.6

The next step was to determine the amount of experiments to be performed. This can be determined using the following formula, where n is the amount of factors or changing variables and l is the amount of levels or different values for each factor:

$$Experiment\ \# = l^n \tag{31}$$

This gave 400 experiments. In order to then complete the study, Area was calculated for different combinations of P_e and P_d. First, P_e was held constant at its first value, while P_d was varied. Using the design value of $.036432m^2$, an "if" statement at the end of each experiment determined if the design area was sufficient to satisfy the day and eclipse power requirements. A sufficient value is indicated by "Suff.", while a value, which exceeds the design value is labeled as "EXC." 25 of the calculations can be seen in Table 26.

Table 26. Parametric Study Results.

P_total	Pe	Pd	Te(s)	Td(s)	Xe	Xd	Peol	P_SA	Asa	
2	1	1	2192.3	3372.1	0.6	0.8	276.6	2.333548333	0.008436545	Suff.
3	1	2	2193.3	3371.1	0.6	0.8	276.6	3.584364154	0.012958656	Suff.
4	1	3	2194.3	3370.1	0.6	0.8	276.6	4.83518046	0.017480768	Suff.
5	1	4	2195.3	3369.1	0.6	0.8	276.6	6.08599725	0.022002882	Suff.
6	1	5	2196.3	3368.1	0.6	0.8	276.6	7.336814525	0.026524998	Suff.
7	1	6	2197.3	3367.1	0.6	0.8	276.6	8.587632285	0.031047116	Suff.
8	1	7	2198.3	3366.1	0.6	0.8	276.6	9.838450531	0.035569235	Suff.
9	1	8	2199.3	3365.1	0.6	0.8	276.6	11.08926926	0.040091357	EXC
10	1	9	2200.3	3364.1	0.6	0.8	276.6	12.34008848	0.04461348	EXC
11	1	10	2201.3	3363.1	0.6	0.8	276.6	13.59090819	0.049135604	EXC
12	1	11	2202.3	3362.1	0.6	0.8	276.6	14.84172838	0.053657731	EXC
13	1	12	2203.3	3361.1	0.6	0.8	276.6	16.09254907	0.058179859	EXC
14	1	13	2204.3	3360.1	0.6	0.8	276.6	17.34337024	0.062701989	EXC
15	1	14	2205.3	3359.1	0.6	0.8	276.6	18.5941919	0.067224121	EXC
16	1	15	2206.3	3358.1	0.6	0.8	276.6	19.84501405	0.071746255	EXC
17	1	16	2207.3	3357.1	0.6	0.8	276.6	21.09583668	0.07626839	EXC
18	1	17	2208.3	3356.1	0.6	0.8	276.6	22.34665981	0.080790527	EXC
19	1	18	2209.3	3355.1	0.6	0.8	276.6	23.59748343	0.085312666	EXC
20	1	19	2210.3	3354.1	0.6	0.8	276.6	24.84830754	0.089834807	EXC
21	1	20	2211.3	3353.1	0.6	0.8	276.6	26.09913215	0.094356949	EXC
22	2	1	2212.3	3352.1	0.6	0.8	276.6	3.449914481	0.012472576	Suff.
23	2	2	2213.3	3351.1	0.6	0.8	276.6	4.701565655	0.016997707	Suff.
24	2	3	2214.3	3350.1	0.6	0.8	276.6	5.953217814	0.021522841	Suff.

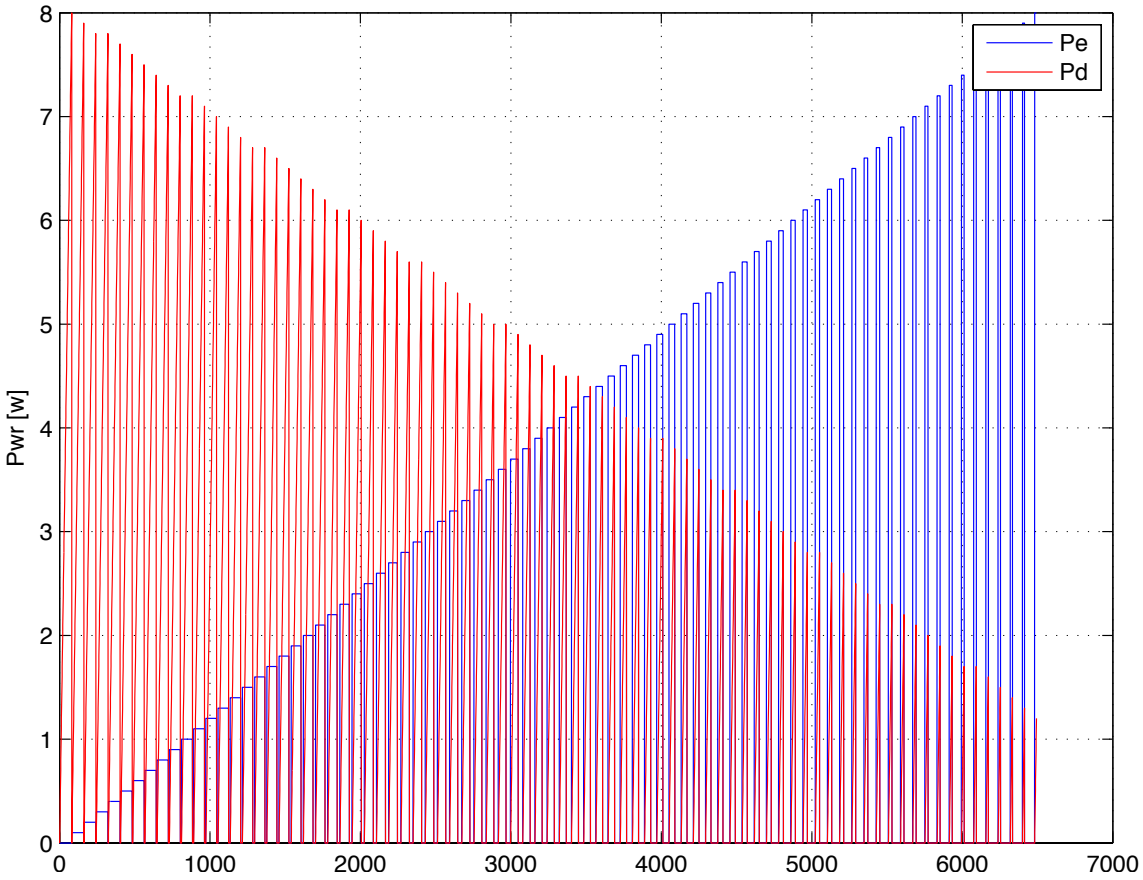

Figure 26. Sufficient power ranges for solar array design space per equation (23).

The values form the parametric study were then extracted and imported into Figure 26. Using the "if" statement, the pairs of values for both eclipse power draw and sunlight power draw were extracted and plotted in Figure 26. From the data used to plot Figure 26, it was determined that a combined sum of 8w, would allow the current design to sufficiently power the spacecraft. Figure 26 displays the relationship between different values P_e and P_d. As expected the two values are indirectly proportional to one another. As the power draw during sunlight increases, the amount of power draw during eclipse needs to decrease for sufficient power generation. As the power draw during eclipse increases, the power draw during sunlight needs to decrease.

2. Interactions

The values found from the parametric study were then used to create an interaction plot. The variables from the parametric study were held constant besides P_e and P_d. All other variables besides incidence angle are held constant and are a result of initial design choice. However, power draw is heavily dependent upon incidence angle and incidence angle is a function of performance more so than design choice. While sunlight and eclipse period may vary throughout the mission lifetime, we can assume a constant value for preliminary calculation purposes. Incidence angle is a function of the performance of the ADCS subsystem. The power generation subsystem is designed more or less for precise 3-axis stability. If the spacecraft is not accurately stabilized and able to point at the sun, the power generation will be greatly affected.

Interaction plots provide a visual representation between possible interactions of multiple variables. The main variables in subject are power during eclipse (X1), daylight (X2) and incidence angle (X3). With three variables in subject, there are 6 total plots representing each interaction. Plots on the same columns share the same x-axis. Each y-axis represents the solar array area, which is the main result under observation. In the first column in the left hand side, the x-axis is represented by the range of values for X1 (Pe), so it varies from 0-8w. In the second column, the x-axis represents the range of values for X2 (Pd), which also varies from 0-8w. For the column on the right hand side, the x-axis represents the range of values for X3 (θ), which varies from 0-45 degrees in steps of 6 degrees. A worst-case scenario of 23 degrees is assumed in earlier calculations, but the range was increased to view interactions for a larger array of values.

In each graph, we can see how variables interact with each other and how that relationship relates to the solar array area.

Parallel lines in each plot indicate that there are no interactions. This can be seen in the middle plot on the left most column as well as on the top plot in the middle column. However, larger differences in slopes between lines correlate to larger degrees of interaction. The bottom two graphs in the middle and left most columns represent the interactions between X1 (Pe) and X3 (θ) as well as X2 (Pd) and X3 (θ). Since, the Pe and Pd have the same range, the plots will be the same. We can see that for smaller values of the theta, the lines remain parallel to each other and there isn't much interaction. However, as theta increases, the slopes of the lines become less and less parallel indicating that there is larger interactions between theta and power draw at higher values of theta. This is also seen in top and middle plots on the right most column where theta is the x-axis. The interaction degree between incidence angle and power draw increase for higher values of theta and power draw. These three factors are fully coupled and dependent on one another. It is also worth noting that the solar array area needed significantly increases with higher incidence angles. The largest solar array area shown nearly doubles the design value of $.036432m^2$. As long as incidence angle is maintained, a total power draw around 8 watts will allow for the current design to sufficiently power the spacecraft.

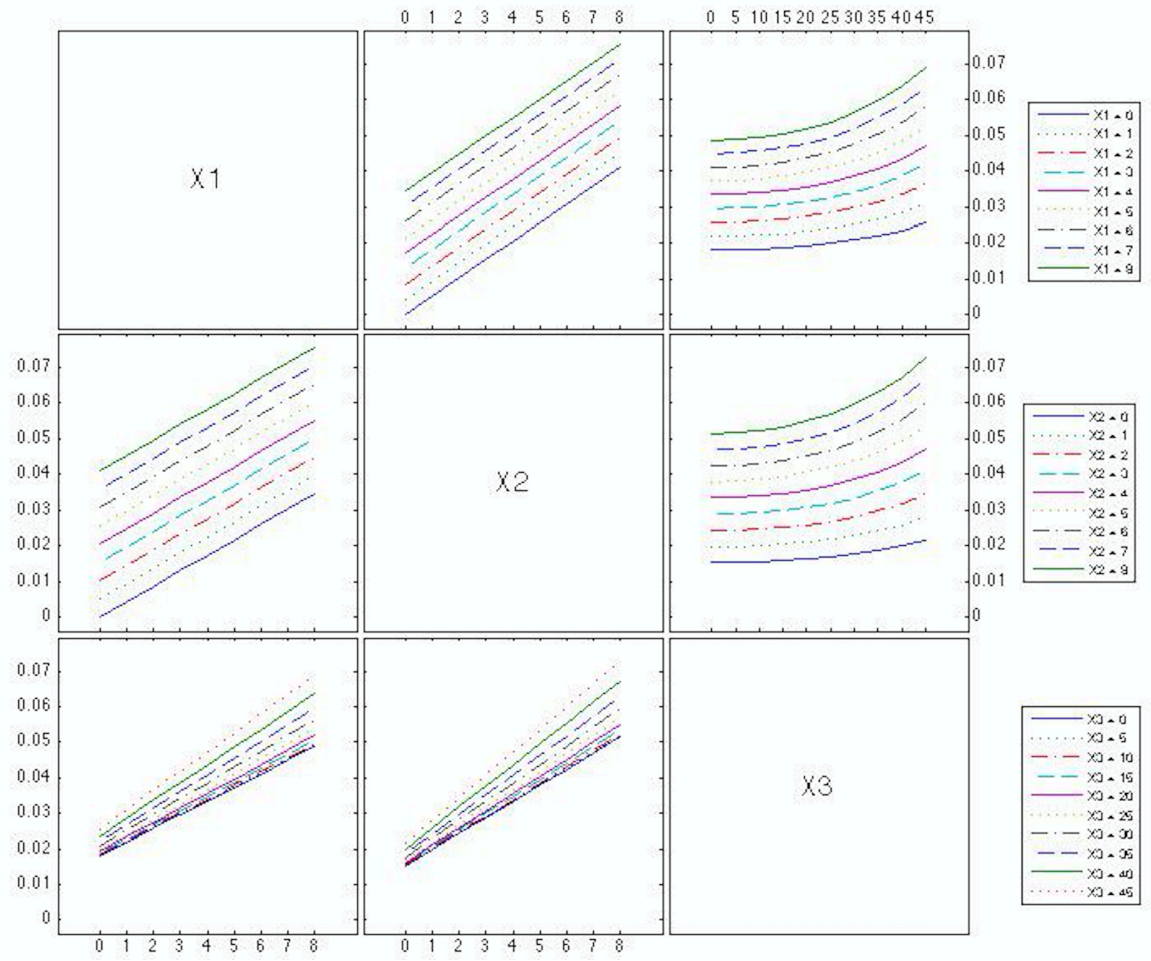

Figure 27. Interaction plot between power draw and incidence angle.

3. Main effects

Main effects are the difference between factor averages and grand mean (average of all results). Effect sizes describe which factors have more significant impact on the results. The y-axis is the same for each plot. There are three plots correlating to each of the three factors in subject. Factors with steeper slopes have greater effects and impacts on the results.

In order obtain the main effects of the incidence angle variations; an average of each result is taken for all the cases when theta is zero degrees. The average is then taken for results of each individual level of theta. Those averages of those results are then plotted

against the levels of theta. For this study, theta ranged from 0 to 45 degrees. The same process was repeated for power draw during eclipse and daylight. All the results for the first level of eclipse power draw were averaged. Each result of the remaining levels were averaged. All the means were then plotted against each level of eclipse power draw. This process was again repeated for daylight power draw.

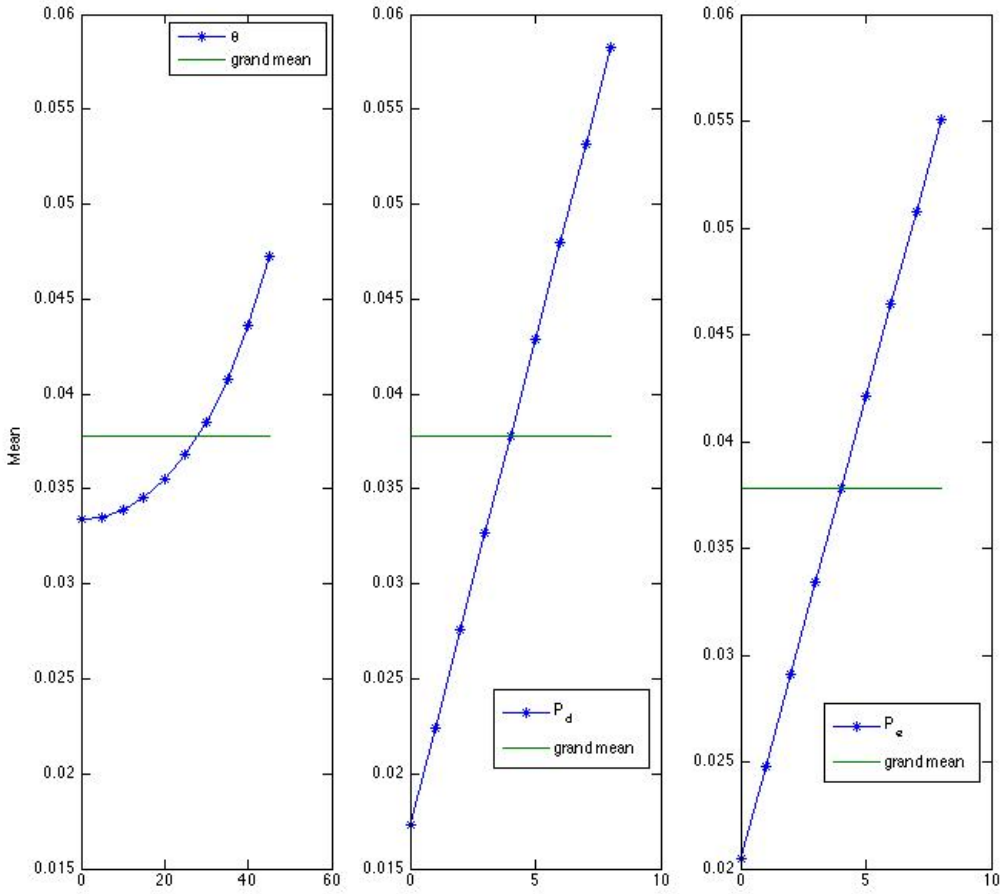

Figure 28. Main effects plots.

The left most plot describes the main effect of the theta, the middle plot describes the main effect of daylight power draw and the rightmost plot describes the main effect of

eclipse power draw. It can be observed that daylight power draw has the greatest main effect on the system as it deviates the furthest from the grand mean. Daylight power draw also has the steepest slope of .0051. The highest slope at any time of the main effect of theta is 7.3e-4. Also, the slope of the main effect of eclipse power draw is .0043.

4. Multi-variable chart

Multi-variable charts present analysis of varying data. It provides for a visual representation of varying factors and overall look at the main effects of a system. All plots within the multivariable chart, Figure 29, possess the same y-axis and x-axis. The y-axis is the solar array area, while the x-axis represents the range of eclipse power draw levels. From left to right, each plot correlates to one level of incidence angle theta. Each line corresponds to a different level of daylight power draw. For each level of incidence angle, there is a linear relationship between eclipse and daylight power draw. However, as incidence angle increases, the distribution of solar array area increases. This leaves little power draw available during sunlight and eclipse under the design solar array size. For an incidence of zero degrees, an equal power draw of 4w each from eclipse and daylight leaves the solar array design sufficient as it is less than .036m^2. For a total power draw of 16w (8w daylight, 8w eclipse), an area of at least .06 m^2 is needed. On the other extreme, if designing for an incidence angle of 45 degrees and 16w eclipse power draw, an area of .09m^2+ is needed for sufficient power generation.

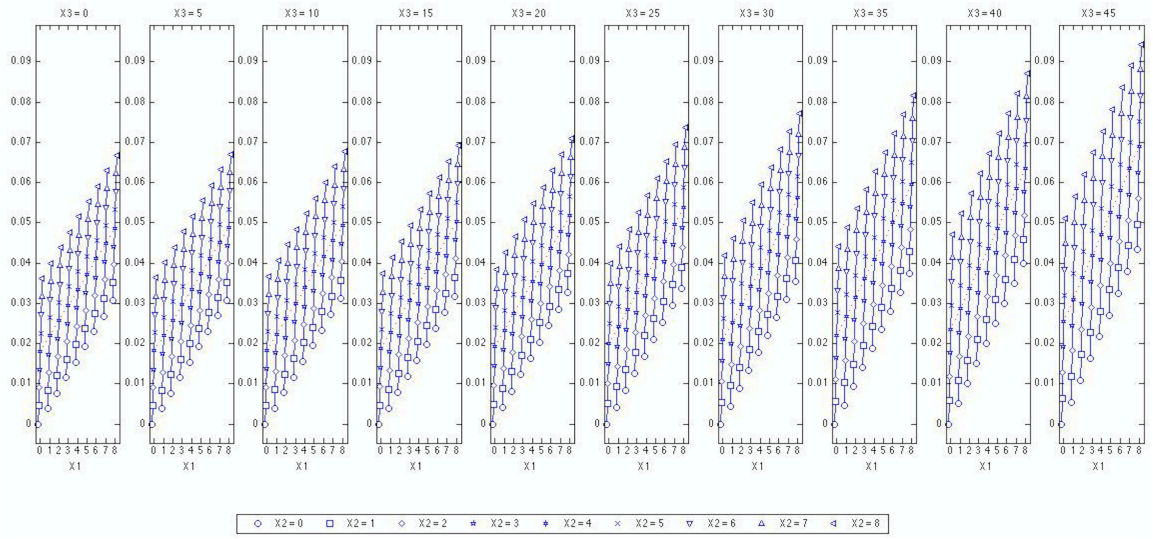

Figure 29. Multi-variable chart.

VIII. Power Budget

A. Components List

The first step in creating a power budget for the mission is creating a list of components and corresponding subsystems needs to be made. Table 27 and Table 28 below display the full list of components and each subsystem, which they are designated for. This includes the main payload of the spacecraft, attitude determination and control, command and data handling, power, structures and telecommunication subsystems. Table 28 displays the quantity of each component used in the spacecraft and the mass. Also listed are the average power, peak power and standby power in watts used by each component, which can be found in their respective datasheets.

Table 27. Components List

Subsystem	Name	Type	Model
Payload	X-123	Instruments.Sensors	X-123
ADACS	MAI-101	Actuators.Wheels	Maryland Aerospace MAI-101
ADACS	IMU	Sensors.IMUs	EPSON M-G350/S4E5AOAOA1
ADACS	Sun Sensor	Sensors.Sun	STAR Fine Sun Sensor
ADACS	Magnetorquers	Actuators.Torquers	NASA ARC torque Coil for Nano-sats (conceptual Design)
C&DH	ADCS Computer	Computers	Beagle Bone Processor
C&DH	Main OBC	Computers	Arduino Mega
Power	Battery	Batteries	Canon BP 930 (TechEdSat
Power	Solar Panels	SolarArrays	Spectrolab TASC
Structures	3U Structure	Other	CubeSatKit 3U Solid Wall Structure (p/n: 703-00245
Structures			Cabling Mass
Structures			Secondary Structure
Structures			Primary Structure
Telecomm	Iridium	Transponders	Iridium 9602-I

Table 28. Components List continued

Subsystem	Quantity	Unit (mass/kg)	Unit Power/W (avg)	Unit Power/W (peak)	Unit Power/W (Standby)
Payload	1	0.18	2.5	4	1.5
ADACS	1	0.693	0.3	2.4	0.06
ADACS	1	0.007	0.1	0.2	0
ADACS	1	0.35			
ADACS	1	0.049	0.09	1	0
C&DH	1	0.03968	0.85	1.75	.85
C&DH	1	0.036	1	1.5	0.5
Power	1	0.225			
Power	0.039432	1.028			
	1.039432				
Structures	1	0.439			
Structures					
Structures					
Structures					
Telecomm	1	0.03	1	7.5	0.225

B. Modes

Throughout the duration of the mission, the spacecraft will be constantly cycling through different modes. These different modes represent the main function of the spacecraft at different points in time. There are seven modes in total, which our spacecraft will cycle through and they are: Initialization, De-tumble, Sun-Point, Science, Eclipse, Downlink and Fail mode. Each of these modes have different durations and will be activated continuously. After launch, the spacecraft will first initialize. The next step is to de-tumble and initiate attitude control. After, the spacecraft will cycle throughout its various modes of science, downlink and eclipse throughout the mission lifetime. Table 29 lists the different modes, their duration, and power draw.

Table 29. Satellite mode durations and power draw.

Modes	Duration [min]	Power [W]
Initialization	30.00	1.50
De-tumble	15.00	10.90
Sun-point	10.00	12.50
Science		7.10
Eclipse	37.00	2.60
Downlink	15.00	8.70
Fail Mode	93.00	2.50

The figures below display the power usage through each mode of the mission. The different modes require various levels of functionality from each component or subsystem. Power draw by each subsystem through the de-tumble, science and downlink modes of the mission are displayed as well. It is easy to observe how particular subsystems draw more power during different modes. For example, the attitude determination and control uses more power during the de-tumble mode, payload during the science mode, and telecom during the downlink mode. The payload requires the most power during the science mode and the telecommunications subsystem requires the most power during the downlink mode.

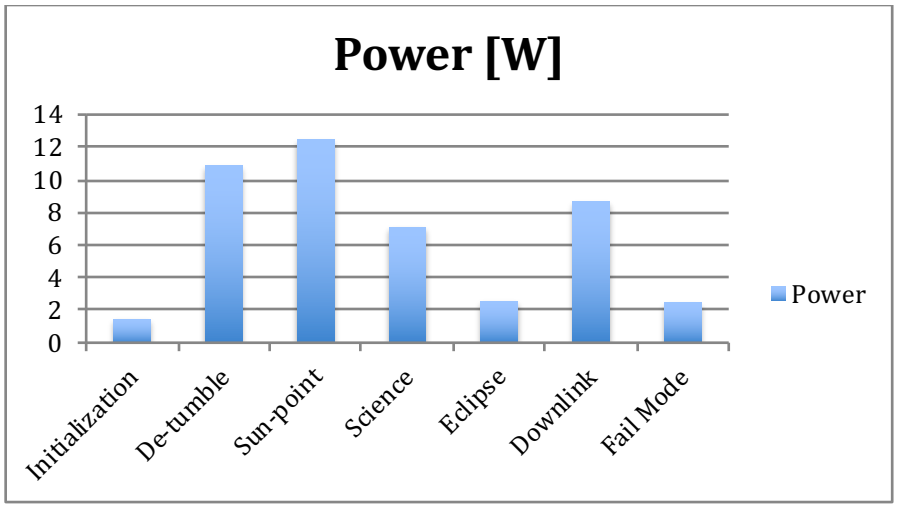

Figure 30. Mode power draw in Watts.

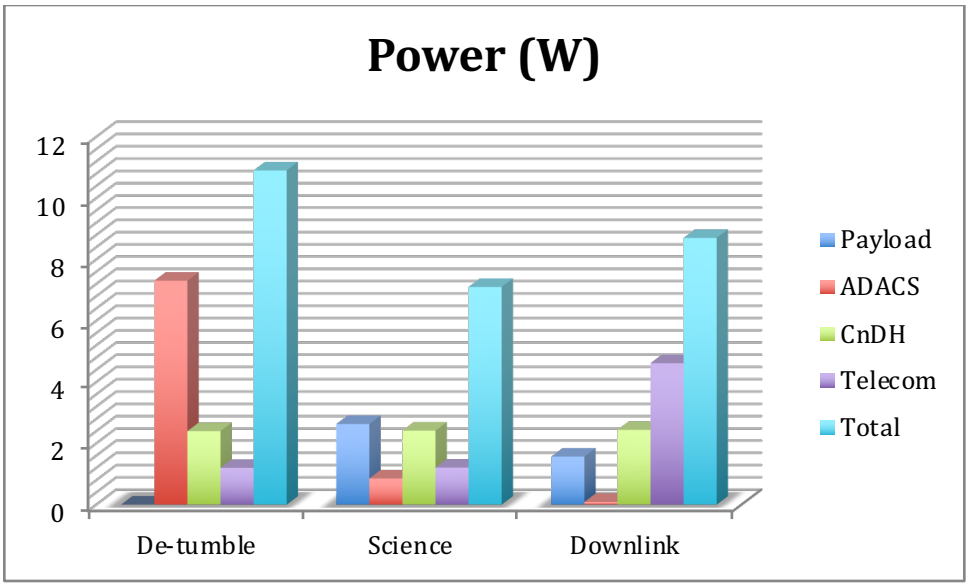

Figure 31. Power draw per component.

C. Power Draw by Component

Figure 32 displays the power consumption by each component during the three different levels of operation. Each component has average, peak and standby power levels. It is essential that the power consumption not exceed the available power

provided by the generation and storage systems. For proper sizing, a 10% margin was added to the total power consumption.

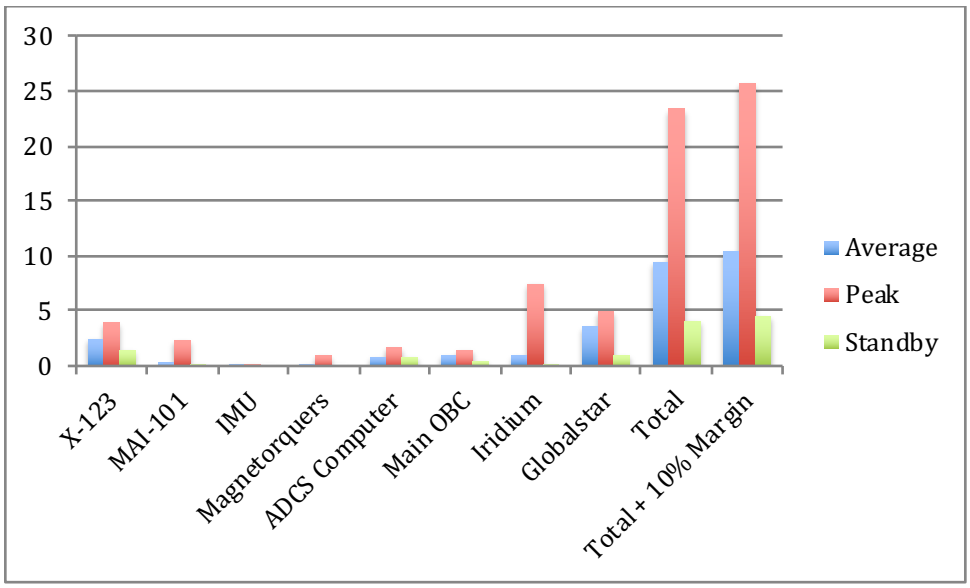

Figure 32. Power consumption by component during average, peak and standby levels.

D. Duty Cycle

Duty-cycles describe the percentage that a signal is active in a particular system. Establishing the duty-cycle of each component and-or subsystem is an important step in establishing an adequate power budget. Based upon the modes designated by the systems engineer, we can begin determine the rate of power consumption relative to the power storage component. From the mode duration specified in Table 29, the duration percent of each orbit is determined. Initialization will take 30% of an orbit de-tumble will take 16% and so on. The next column describes the percent of an hour, which each mode will take to complete. From the percent-hour values, along with the power draw values from Table 29, we can then determine the watt-hours of each mode. Watt-hours are a measurement unit, which define the rate of power consumption. For example, Initialization takes a half hour to complete and draws 1.5 W. Multiplying by hour

percentage gives a Watt-hour rate of .75. As the battery, and energy storage components in general, are defined in watt-hours, we can begin to determine if our battery selection is adequate.

Table 30. Power mode Wh consumption and Duty-cycle

Modes	Duration-%-Orbit	%-Hour	Wh	Duty Cycle
Initialization	32.35	0.50	0.75	NAN
De-tumble	16.17	0.25	2.73	NAN
Sun-point	10.78	0.17	2.08	0.11
Science	NAN	NAN	NAN	NAN
Eclipse	39.90	0.62	1.60	0.41
Downlink	16.17	0.25	2.18	0.17
Fail Mode	100.28	1.55	3.88	NAN
		Total	13.21	
		Available	13.43	

This process is completed for each mode. The science mode component designation is defined, however there is no specified duration for the science mode. Science mode initiates and continues to run until the completion of that orbit. The total watt-hour consumption is the sum of all the modes. With an undefined science mode, the total is $13.21Wh$ with $13.43Wh$ still available. The available watt-hours is determined subtracting of the total watt-hour consumption from the rate of the BP-930 battery. Found in the BP-930 data sheet, the battery capacity is $3700\ mAh$. The watt-hour capacity of the battery can be found by multiplying the battery capacity in mAh by the battery voltage $7.2V$. This gives a total of $26.64Wh$.

As the Science mode is not technically defined, we can calculate for scenarios that may take place. As the science mode is made to run the remained of the orbit, we know the minimum and maximum duration for the Science mode. Table 31 displays the results

of the science mode simulation in order to observe power total power draw for different scenarios.

Table 31. Science Mode simulation.

Mode	Min	% orbit	% Hour	Wh	Total	Available
Science	0.00	0.00	0.00	0.00	13.21	13.43
	2.00	2.17	0.03	0.24	13.45	13.19
	12.00	13.04	0.20	1.42	14.63	12.01
	22.00	23.91	0.37	2.60	15.82	10.83
	32.00	34.78	0.53	3.79	17.00	9.64
	42.00	45.65	0.70	4.97	18.18	8.46
	52.00	56.52	0.87	6.15	19.37	7.28
	62.00	67.39	1.03	7.34	20.55	6.09
	72.00	78.26	1.20	8.52	21.73	4.91
	82.00	89.13	1.37	9.70	22.92	3.73
	92.00	100.00	1.53	10.89	24.10	2.54
	102.00	110.87	1.70	12.07	25.28	1.36
	112.00	121.74	1.87	13.25	26.47	0.18
	122.00	132.61	2.03	14.44	27.65	-1.01

Starting with a duration of 0 minutes, the watt-hour rate is calculated and subtracted from available capacity of the battery including the subtracted capacity from the other components. This will give worst-case scenario in the case that components are on at the same time. At 92 minutes of Science, there is still an available capacity of 2.54Wh. At 122 minutes of Science mode duration, the available capacity is negative, indicating that the battery capacity has been exceeded. The capacity is still positive at 112 minutes. The capacity is exceeded between 112 and 122 minutes.

The column on the far right of Table 30 defines the duty cycle. As each cycle is equivalent to one orbit, we take the percentage the per orbit duration as the length of each pulse and the period is equal to one orbit. As initialization and de-tumble are both modes

that should occur once, after launch, they do not have a periodic functionality and their duty cycles can't be calculated.

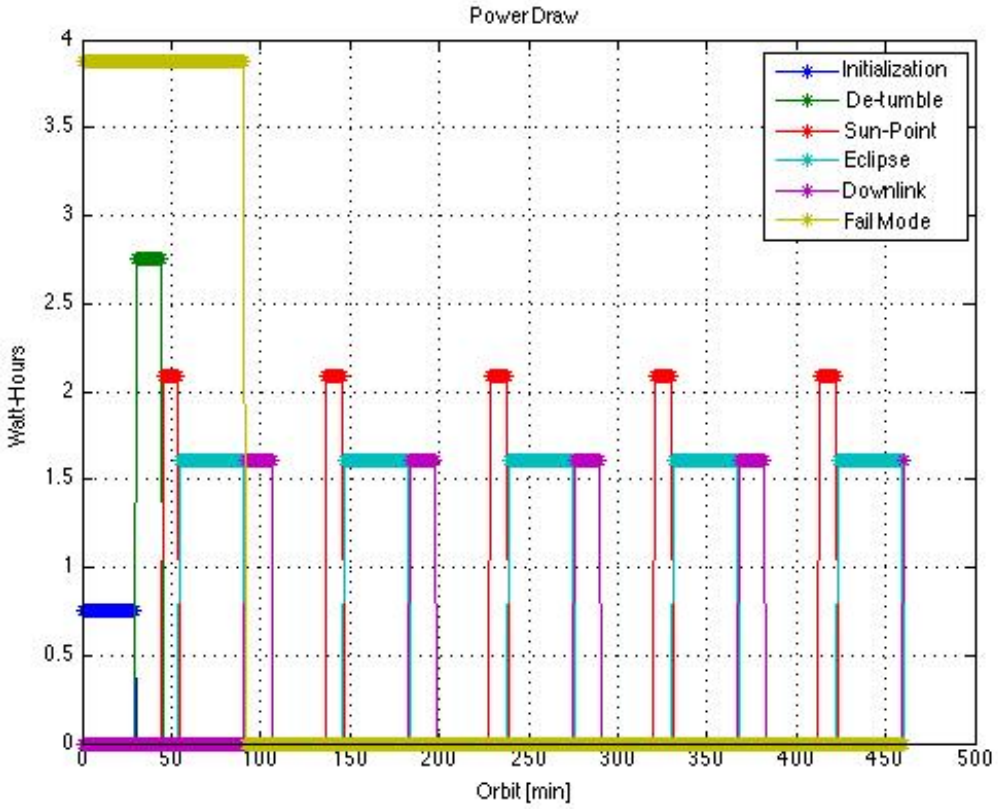

Figure 33. Combined pulse generation of each mode.

Figure 33 displays the super imposed graphs of each of the satellite operation modes for 5 orbits. Listed in the legend is initialization mode, de-tumble, sun-point, eclipse, downlink and fail mode. This gives a visual representation of the results found in Table 30. Initialization and fail mode represent the two extremes between the different pulse cycles. While Fail mode only draws 2.5W, it has the longest duration and thus has the highest peak. The next highest peaks are De-tumble, then sun-point and downlink.

The duty satellite mode pulses were plotted separately displayed in Figure 34. The individual plots represent the modes in the same order as mentioned before

excluding Science-mode as it has no defined duration. The duty cycles are calculated and listed above each plot.

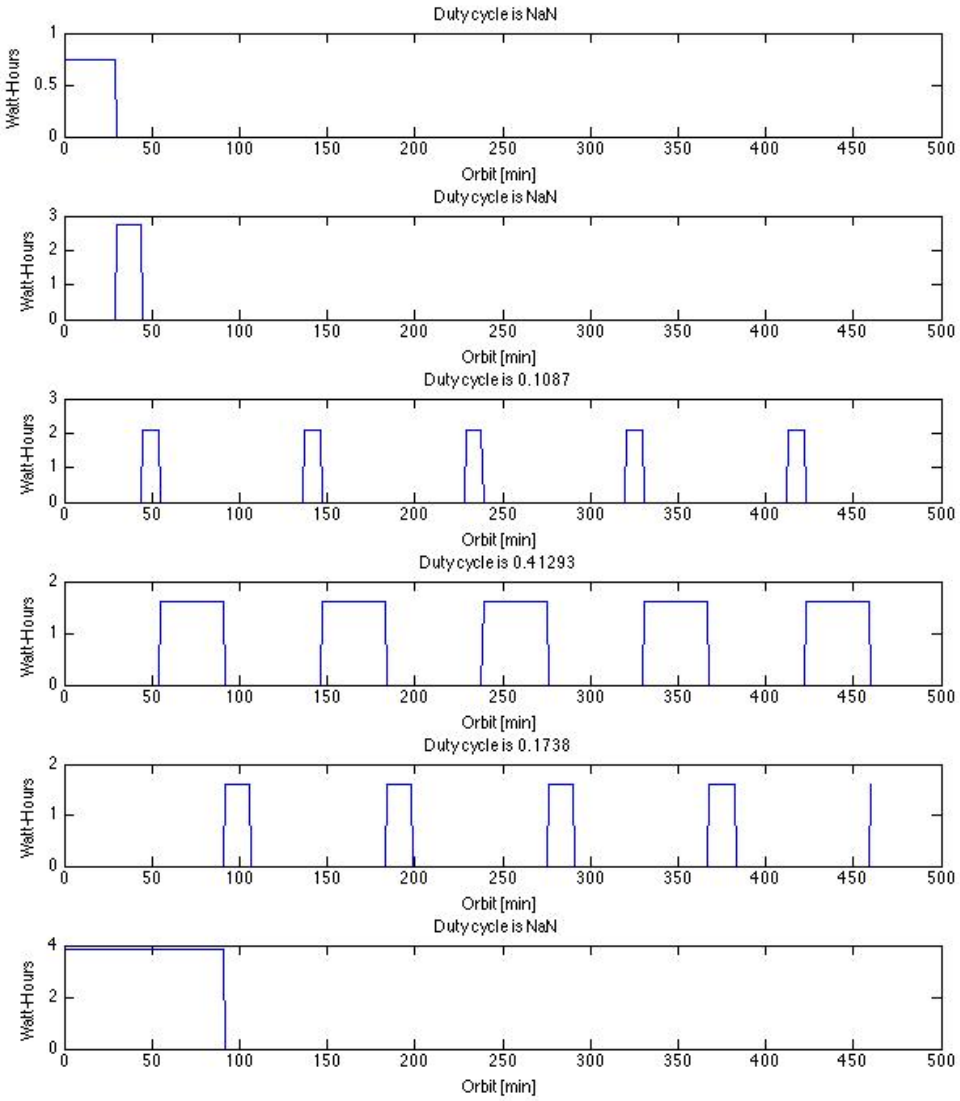

Figure 34. Duty cycle of each mode.

E. Depth of Discharge

In order for the battery cells to sustain optimal functionality, it is essential that the cells are not discharged passed their maximum discharge. Throughout out the duration of

the mission, the spacecraft will cycle through various operational modes explained above. As can be seen in the figure below, the battery charge cycle remains level and operational well above the line of maximum discharge. Overtime, constant charging and discharging will eventually lead to cell degradation. However, for a short mission lifetime (<1 year), the mission can be achieved without threat of cell degradation. Constant charge below the maximum discharge will result in a negative sloping trend, at which point the cells will not be able to properly function for the required mission.

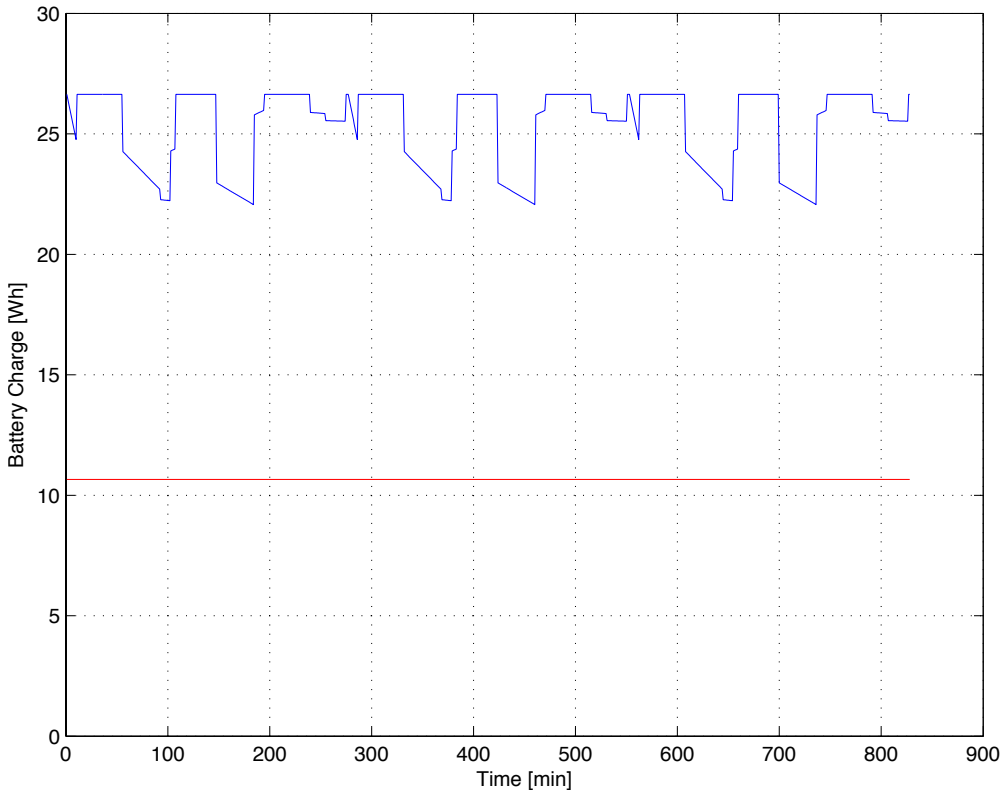

Figure 35. Battery discharge from component usage through mission duration

Figure 35 displays a simulation of battery discharge through cycles of various modes. The maximum height corresponds to the maximum Watt-hour capacity specified by the battery. The times when the discharge levels out is when the satellite is generating power and facing the sun. The power modes switch from sun-point, eclipse, to science,

to downlink, to power generation. Discharge remains above near 60% discharge limit throughout the simulated mission cycles. This indicates that the battery is sufficient to store power and properly provide power for the spacecraft while avoiding over discharging.

IX. Deployment Mechanism

The design of the solar panel deployment is critical to the overall functionality of the spacecraft. Sizing and fitting for power requirements is only part of the process. As actuating mechanisms, damping, release mechanisms and articulating are just as important and dependent on the spacecraft's mission requirements. The mechanism must provide enough force to successfully deploy the solar panels. As the solar array area is dependent upon 6U's of area not including the main body of the spacecraft, the deployment of the solar panels is essential for operating functionality for the mission. The design will consist of a classical loaded torsion spring. Figure 36 displays a general torsion spring diagram.

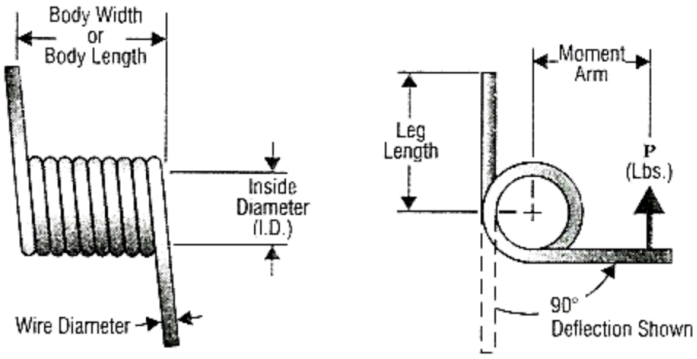

Figure 36. General torsion spring diagram [18].

The potential energy of a torsional spring where κ is the torsion-spring constant measured in [Nm/rad] can be expressed through the equation:

$$U = \frac{1}{2}\kappa\theta^2 \tag{32}$$

Where κ is based on the spring index, $\frac{D}{d}$, and typical values can be found in Table 32. After finding the spring index, the correct value for κ can be found through interpolation.

Table 32. Spring index and spring constant values.

Index, D/d	6	8	10
κ	1.15	1.11	1.08

The torque or moment formula and the equation for bending stress can be expressed as:

$$M = \frac{Ed^4T}{10.8N_tD} \tag{33}$$

$$S = \frac{32Mk}{\pi d^3} \tag{34}$$

Where, D is the mean coil diameter, d is the diameter of the round wire, Nt is the number of coils, E is the elastic modulus, and T is the deflection or revolutions of the spring. The body length in deflected position is expressed as:

$$L_t = d(N_t + 1 + T) \tag{35}$$

Where T can be expressed as:

$$T = \frac{Final\ Postition}{360} \tag{36}$$

The stretched length of the spring can be expressed as:

$$\frac{l}{n} = ((D_i + d)\pi)\text{^}2 + d\text{^}2) \tag{37}$$

The stress concentration factor is expressed as:

$$K_i = \frac{4C^2 - C - 1}{4C(C-1)} \tag{38}$$

where C is the spring index denoted as the spring diameter divided by the wire diameter. The moment of inertia is denoted as:

$$I = \frac{\pi d^3 y}{32} \tag{39}$$

The angular spring rate can be expressed as:

$$k_a = \frac{M}{\theta} = \frac{Ed^4}{64Dn} \tag{40}$$

The frequency is calculated through the equation:

$$\omega = \sqrt{\frac{2U}{J}} \tag{41}$$

The time for deployment can be calculated through the equation:

$$t = \frac{\pi}{2\omega} \tag{42}$$

Table 33 and Table 34 display results from the iteration process used to calculate values for the torsion spring via equations 33 through 42. An assumption for moment first needs to be made. The moment was varied from .5 to 13Nmm by increments of .5Nmm. The spring should be designed such that it is strong enough to deploy the panel, so the moment is then assumed to be 110 percent of the original value. The next step is to calculate a wire diameter sufficient to carry the load. A minimal tensile strength of 365,000MPa, mid range for typical spring material, is assumed and a trial value of 75 percent of that is used to solve for the size of the wire. The maximum allowable tensile strength is then looked up for that wire size. If the allowable stress is within 95 percent of the design stress, then the wire diameter size is deemed sufficient. If not, then a new diameter is calculated using the previously looked up allowable stress. After calculating a sufficient wire diameter, the body length is then calculated. The time for the spring to deploy can be calculated after determining frequency, mass moment of inertia, potential energy, and spring rate.

Table 33. Iteration process for torsion spring design.

M1	M2	S1 psi	S1 mPa	S2 psi	S2 Mpa	d in	d mm	Scalc_PSI	Scalc_mPA	Sufficient
0.50	0.55	365000.00	2516.59	273750.00	1887.44	0.03	0.14	290000.00	1999.48	Suff.
1.00	1.10	365000.00	2516.59	273750.00	1887.44	0.03	0.18	277000.00	1909.85	Suff.
1.50	1.65	365000.00	2516.59	273750.00	1887.44	0.04	0.21	273000.00	1882.27	Suff.
2.00	2.20	365000.00	2516.59	273750.00	1887.44	0.04	0.23	263000.00	1813.32	Suff.
2.50	2.75	365000.00	2516.59	273750.00	1887.44	0.05	0.25	267000.00	1840.90	Suff.
3.00	3.30	365000.00	2516.59	273750.00	1887.44	0.05	0.26	263000.00	1813.32	Suff.
3.50	3.85	365000.00	2516.59	273750.00	1887.44	0.05	0.27	261000.00	1799.53	Suff.
4.00	4.40	365000.00	2516.59	273750.00	1887.44	0.05	0.29	261000.00	1799.53	Suff.
4.50	4.95	365000.00	2516.59	273750.00	1887.44	0.06	0.30	260000.00	1792.64	Insuff.
5.00	5.50	260000.00	1792.64	195000.00	1344.48	0.07	0.35	255000.00	1758.16	Suff.
5.50	6.05	365000.00	2516.59	273750.00	1887.44	0.06	0.32	258000.00	1778.85	Insuff.
6.00	6.60	258000.00	1778.85	193500.00	1334.14	0.07	0.37	250000.00	1723.69	Suff.
6.50	7.15	365000.00	2516.59	273750.00	1887.44	0.06	0.34	256000.00	1765.06	Insuff.
7.00	7.70	256000.00	1765.06	192000.00	1323.79	0.07	0.39	250000.00	1723.69	Suff.
7.50	8.25	365000.00	2516.59	273750.00	1887.44	0.07	0.35	254000.00	1751.27	Insuff.
8.00	8.80	254000.00	1751.27	190500.00	1313.45	0.08	0.41	250000.00	1723.69	Suff.
8.50	9.35	365000.00	2516.59	273750.00	1887.44	0.07	0.37	250000.00	1723.69	Insuff.
9.00	9.90	250000.00	1723.69	187500.00	1292.77	0.08	0.43	245000.00	1689.22	Suff.
9.50	10.45	365000.00	2516.59	273750.00	1887.44	0.07	0.38	250000.00	1723.69	Insuff.
10.00	11.00	250000.00	1723.69	187500.00	1292.77	0.08	0.44	245000.00	1689.22	Suff.
10.50	11.55	365000.00	2516.59	273750.00	1887.44	0.08	0.40	250000.00	1723.69	Insuff.
11.00	12.10	250000.00	1723.69	187500.00	1292.77	0.09	0.46	245000.00	1689.22	Suff.
11.50	12.65	365000.00	2516.59	273750.00	1887.44	0.08	0.41	250000.00	1723.69	Insuff.
12.00	13.20	250000.00	1723.69	187500.00	1292.77	0.09	0.47	255000.00	1758.16	Suff.
12.50	13.75	365000.00	2516.59	273750.00	1887.44	0.08	0.42	255000.00	1758.16	Insuff.
13.00	14.30	255000.00	1758.16	191250.00	1318.62	0.09	0.48	255000.00	1758.16	Suff.

Table 34. Iteration process for torsion spring design.

M1	Lt	Index	K	U	MMI	Omega	t
5.00E-01	6.39E-01	2.23E+01	8.64E-01	1.07E+00	2.33E-02	9.56E+00	1.64E-01
1.00E+00	9.56E-01	1.77E+01	9.44E-01	1.16E+00	4.66E-02	7.07E+00	2.22E-01
1.50E+00	1.22E+00	1.54E+01	9.83E-01	1.21E+00	6.99E-02	5.89E+00	2.67E-01
2.00E+00	1.44E+00	1.40E+01	1.01E+00	1.24E+00	9.32E-02	5.16E+00	3.04E-01
2.50E+00	1.65E+00	1.30E+01	1.03E+00	1.27E+00	1.17E-01	4.66E+00	3.37E-01
3.00E+00	1.84E+00	1.23E+01	1.04E+00	1.28E+00	1.40E-01	4.28E+00	3.67E-01
3.50E+00	2.03E+00	1.16E+01	1.05E+00	1.29E+00	1.63E-01	3.98E+00	3.94E-01
4.00E+00	2.20E+00	1.11E+01	1.06E+00	1.31E+00	1.86E-01	3.74E+00	4.20E-01
4.50E+00	2.36E+00	1.07E+01	1.07E+00	1.32E+00	2.10E-01	3.54E+00	4.44E-01
5.00E+00	4.19E+00	9.23E+00	1.09E+00	1.35E+00	3.27E-01	2.87E+00	5.47E-01
5.50E+00	2.67E+00	1.00E+01	1.08E+00	1.33E+00	2.56E-01	3.22E+00	4.88E-01
6.00E+00	4.76E+00	8.66E+00	1.10E+00	1.36E+00	3.96E-01	2.62E+00	5.99E-01
6.50E+00	2.96E+00	9.47E+00	1.09E+00	1.34E+00	3.03E-01	2.98E+00	5.28E-01
7.00E+00	5.31E+00	8.21E+00	1.11E+00	1.37E+00	4.65E-01	2.43E+00	6.48E-01
7.50E+00	3.24E+00	9.03E+00	1.10E+00	1.35E+00	3.50E-01	2.78E+00	5.65E-01
8.00E+00	5.85E+00	7.83E+00	1.12E+00	1.38E+00	5.36E-01	2.27E+00	6.93E-01
8.50E+00	3.50E+00	8.66E+00	1.10E+00	1.36E+00	3.96E-01	2.62E+00	6.00E-01
9.00E+00	6.47E+00	7.49E+00	1.12E+00	1.38E+00	6.13E-01	2.13E+00	7.39E-01
9.50E+00	3.75E+00	8.34E+00	1.11E+00	1.37E+00	4.43E-01	2.48E+00	6.32E-01
1.00E+01	6.92E+00	7.23E+00	1.13E+00	1.39E+00	6.81E-01	2.02E+00	7.77E-01
1.05E+01	3.99E+00	8.07E+00	1.11E+00	1.37E+00	4.90E-01	2.37E+00	6.63E-01
1.10E+01	7.35E+00	7.00E+00	1.13E+00	1.39E+00	7.49E-01	1.93E+00	8.14E-01
1.15E+01	4.23E+00	7.83E+00	1.12E+00	1.38E+00	5.36E-01	2.27E+00	6.93E-01
1.20E+01	7.77E+00	6.80E+00	1.13E+00	1.40E+00	8.17E-01	1.85E+00	8.49E-01
1.25E+01	4.45E+00	7.62E+00	1.12E+00	1.38E+00	5.83E-01	2.18E+00	7.21E-01
1.30E+01	7.93E+00	6.67E+00	1.14E+00	1.40E+00	8.68E-01	1.80E+00	8.74E-01

Optimal spring design results are displayed in Table 35. With an assumption of M = 5 Nmm for the moment of the spring, the following parameters were calculated. These values should provide for a design with enough strength to properly deploy the panels to an angle of 90 degrees.

Table 35. Optimal spring design results.

theta [deg]	90
d [mm]	0.35
D [mm]	3.20
Nt	10.83
Lt [mm]	4.19
t [s]	0.55

Table 36 displays calculations for torque sufficient to overcome aluminum to steel friction for the panel to deploy. The coefficient of friction is held constant at .45. The radius is increased from 1 to 21mm. Assuming an applied force of 1N, the torque required to rotate the mechanism are calculated using the following equation:

$$T = \mu r F \tag{43}$$

It is a linear relationship and the values for torque vary accordingly. A torque of over 5Nmm is satisfied with a radius of 7mm. This is the preliminary radius that will be used for the design of the spring. The current spring design wire diameter is well sufficient to sustain the calculated load.

Table 36. Sufficient Torque.

mu	r	F	T
0.45	1	1	0.45
0.45	2	1	0.9
0.45	3	1	1.35
0.45	4	1	1.8
0.45	5	1	2.25
0.45	6	1	2.7
0.45	7	1	3.15
0.45	8	1	3.6
0.45	9	1	4.05
0.45	10	1	4.5
0.45	11	1	4.95
0.45	12	1	5.4
0.45	13	1	5.85
0.45	14	1	6.3
0.45	15	1	6.75
0.45	16	1	7.2
0.45	17	1	7.65
0.45	18	1	8.1
0.45	19	1	8.55
0.45	20	1	9
0.45	21	1	9.45

The design will consist of more than just one spring. For each panel, two in total, there will be two separate spring mechanisms. Each spring mechanism will consist of an axel, two springs, two washers, one socket and one lever. The common material for all components to be used, besides the torsions springs, is Aluminum 6061 alloy. Aluminum 6061 is specified by the cubesat design standard as the main material used for the structure and rails of the cubesat. The material for the torsion spring itself was chosen for its high resistance to corrosion. The total list of components for the deployment mechanism is listed in Table 37.

Table 37. Deployment mechanism component list.

Component	Material	Quantity
Torsion Spring	1.4310 V2A Stainless Steel	8
Levers	Aluminum Alloy 6061	4
washers	Aluminum Alloy 6062	8
axel	Aluminum Alloy 6063	4
socket	Aluminum Alloy 6064	4

Further work to be done for the deployment mechanism includes development of a CAD model and fitting bars for the mechanism to be placed on. Figure 37 and Figure 38 display rough CAD drawings of the cubesat, which display the solar panel deployment mechanism and placement. In Figure 37, the circles surround where the deployment mechanisms will be located on the cubesat body. The P-Pod rails will need to be modified for the accommodation of these devices. A burn wire circuit will be used to activate the mechanism. It will consist of a Nichrome resistance heating wire [19]. When applied with a constant current, the wire will heat up and cut through a tie down cable and deploy the solar panels. Each spring will require its own cable making four burn circuits in total. The circuit design is still in development. The panels will deploy to a 90 degree position so the front faces of the panels will be parallel with the front face of the cubesat as seen in Figure 38. This will allow for maximum exposure to the sun and power generation from the solar cells when in sunlight.

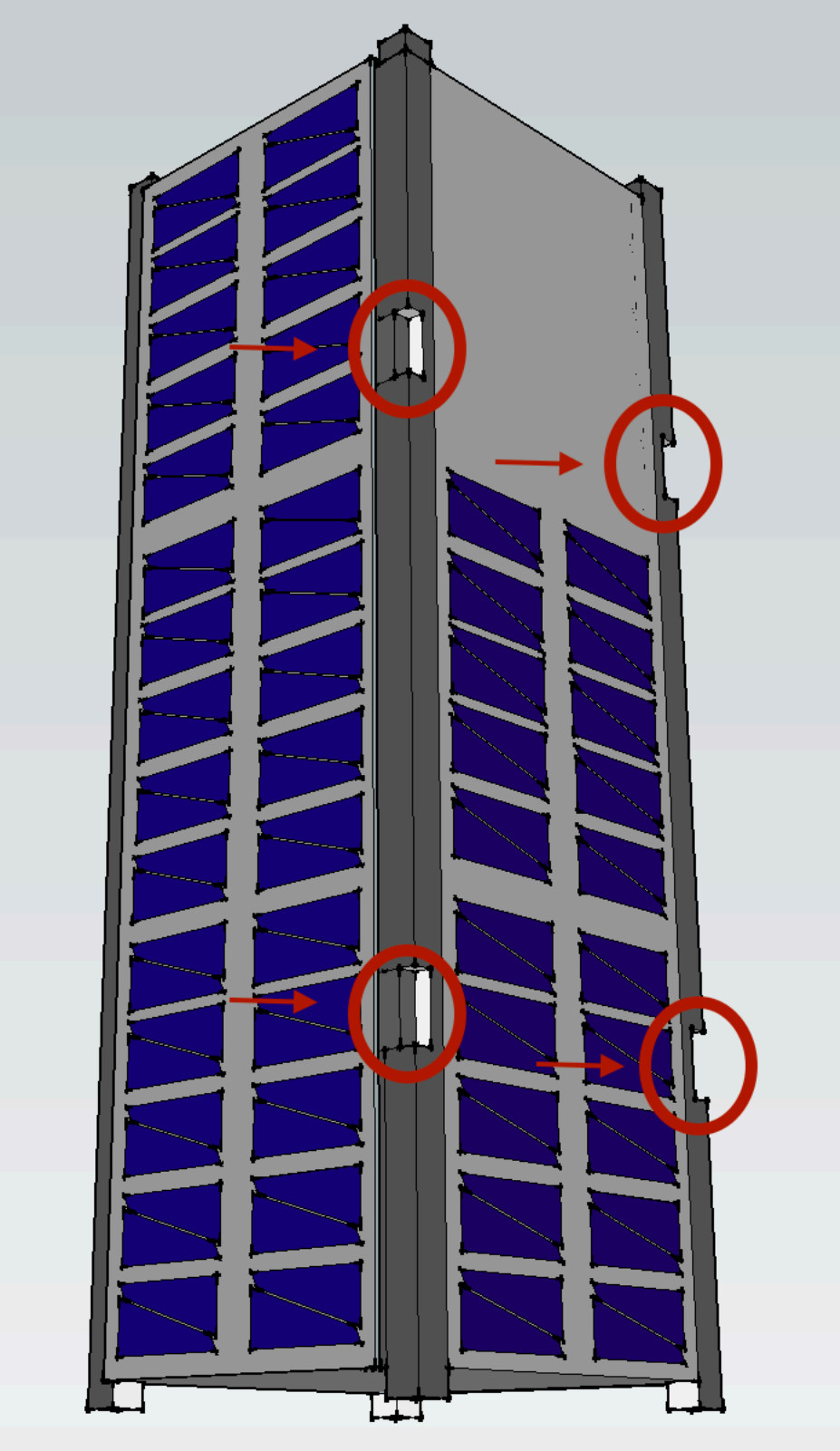

Figure 37. 3U cubesat with deployment mechanism indicators.

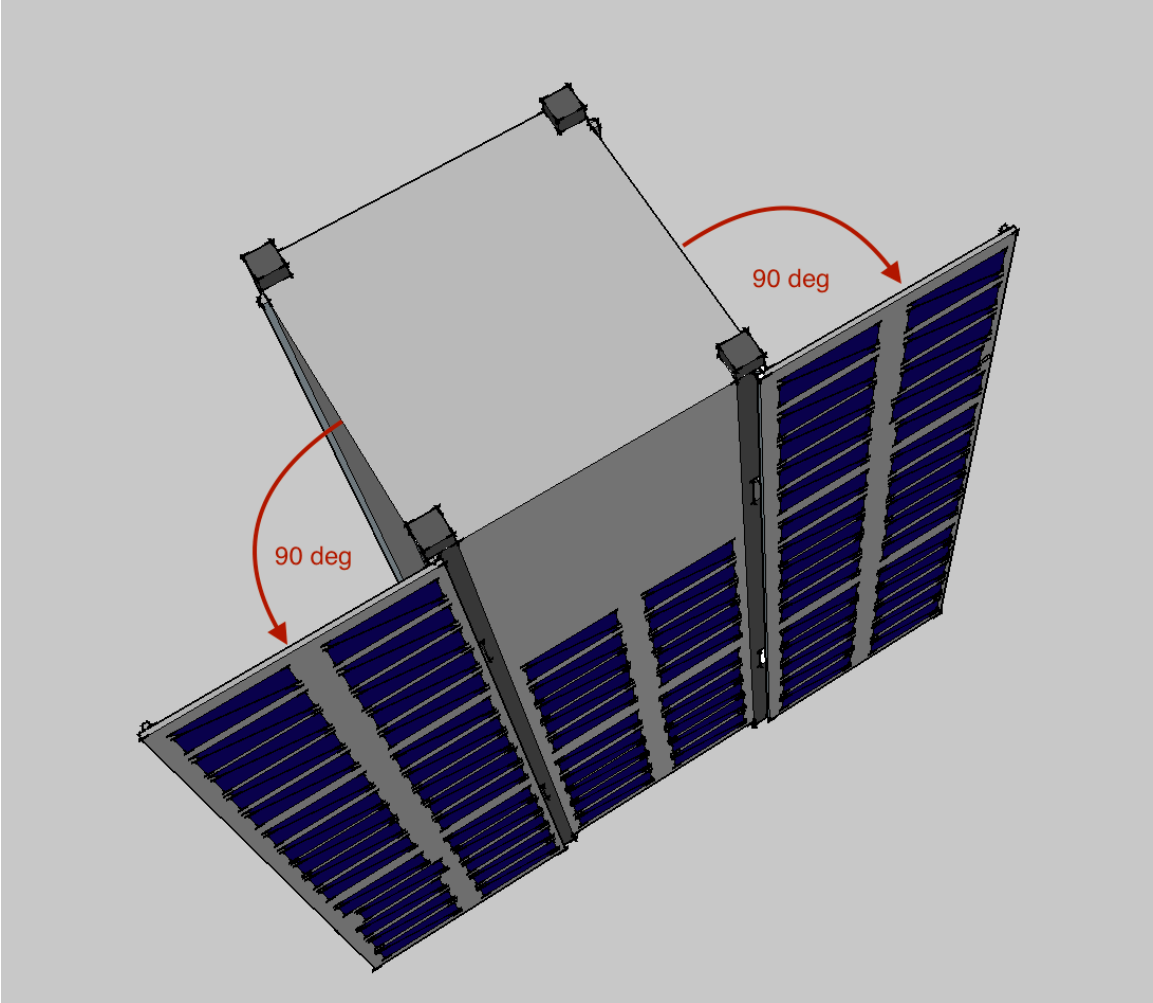

Figure 38. 3U cubesat demonstrating deployment mechanism.

X. PCB Design

A. Electrical diagram

An electrical diagram was made showing the layout of the solar panels. In section 6, it was discussed that the each 1U panel will consist of 10 strings, each having two solar cells connected in series. Each 3U deployable panel consists of 30 strings while the body mounted solar panel consists of 20 strings. Figure 39 displays the layout of the 3 panels. On the left are the two 3U solar panels while on the right is the 2U panel. A blocking

diode was at the end of each string to prevent reverse current from the batteries or other strings. Reverse current can occur when there is a difference in voltage potential between the cells. The diodes only allow current to flow in one direction, therefore placing them at the end of each string will prevent current from flowing back to the solar cells.

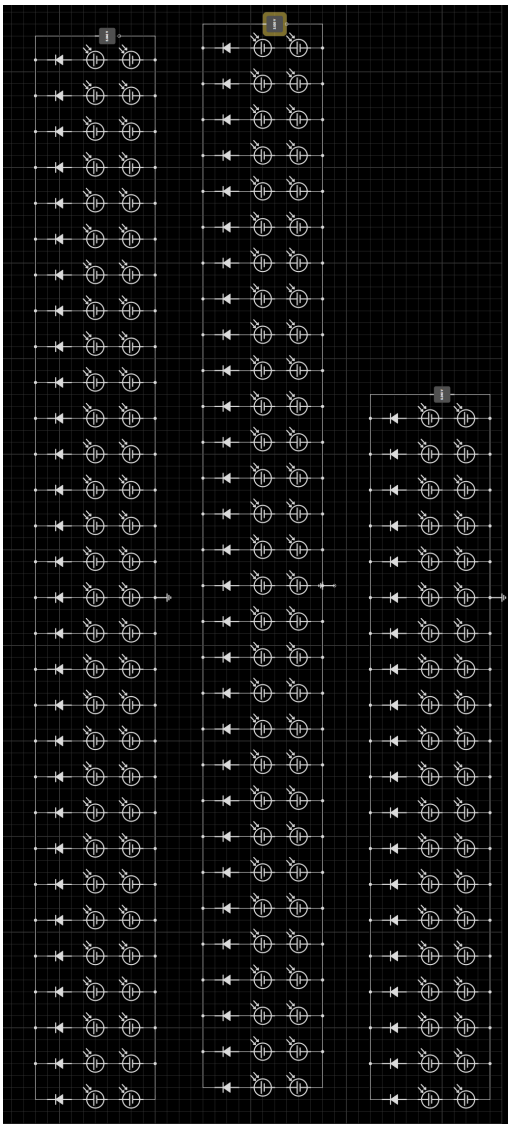

Figure 39. Electrical layout of the solar panels.

B. PCB Design

PCB (Printed Circuit Board) design is an essential step in completing the design of the power system. It provides the team the ability to create their own layout for the

electrical components that fits their specific mission and needs. After determining the layout of the cells, the next step was finding sufficient PCB design software. Out of the available software, DipTrace was chosen based off recommendations from other students and colleagues.

For extra caution, bypass diodes were added between the solar cells and ground pours. While the addition of bypass diodes was not completely necessary, it was added for redundant assurance to prevent unwanted current from flowing into and damaging the solar cells.

Typically, the first step in PCB design begins with creating an electrical schematic and then converting that schematic into a PCB. However, solar cells were not available within the component library. This initially presented a problem with beginning the design since the solar cells are the main components. Bypassing the schematic design and starting with designing the board avoided this problem. First, outlines of the solar cells were created for visual representation and aid. The solar cell outlines were designed based off dimensions given in the TASC data sheet. In addition to the solar cells polygon outlines being created, pads were added to the output of each solar cell to allow for electrical connection once implemented. A trace was then routed between the outputs of the solar cells to allow for a series connection between each solar cell pair. Blocking and bypass diodes were then added to the design from the component library. A general-purpose diode was chosen for both the blocking and bypass diodes that could withstand at least 5.04V and 62mA. Dio_1306 was chosen from the DipTrace library. Vias were then inserted at each end of the diodes to allow for electrical connection to the ground pours on the bottom layer and power bus on the top layer. The board outline was then created

with dimensions 8.3cmx30cm to accommodate for space taken up by the PPOD rails. The solar cell outline was copy and pasted thirty times over to account for the thirty strings of solar cells for the 3U panel. Copper pours were then added to the bottom layer to serve as a ground for the design. A bus trace was added to the top layer to allow for the parallel connections of the strings. Once all the connections were manually routed, an electrical connection test was run to make sure everything was connected properly. Figure 40 displays the interface of the PCB design software layout with the completed solar panel. The component list is on the left hand side of the window. The routing tools are on the top of the window and the layer selection is on the right hand side of the window. The solar cell outlines are visible on the top layer of the design. All the traces on the top layer are highlighted in red while the bottom layer traces are in pink. The silk screens denoted in green represent the labels for the blocking and bypass diodes. Figure 41 through Figure 43 display the final designs of the 3U solar panel. Figure 41 is the top layer of the solar panel. The bus trace, diodes and solar cell outlines can be seen on this layer. Figure 42 is the bottom layer of the 3U solar panel displaying connecting routes between the solar cell strings along with the copper pours. Figure 43 displays a combined view of the solar panel with transparent bottom and top layers. Figure 44, Figure 45, and Figure 46 are 3D images of the printed circuit boards. Figure 44 and Figure 45 give alternate views of the top layer of the board to show its profile. The diodes can be seen in black along with the power bus along the center of the longitudinal axis. Figure 46 shows the bottom layer of the board. All the vias are apparent in this view to show where the routing alternates between the top and bottom layer of the board. The same images of the 2U solar panel design can be found in the Figure 48, Figure 49

and Figure 50. The 2U solar panel is 10 cm smaller along the vertical axis. The next step is to get the PCB boards printed and mailed. Two versions of the 3U design will be printed to accommodate for both 3U panels.

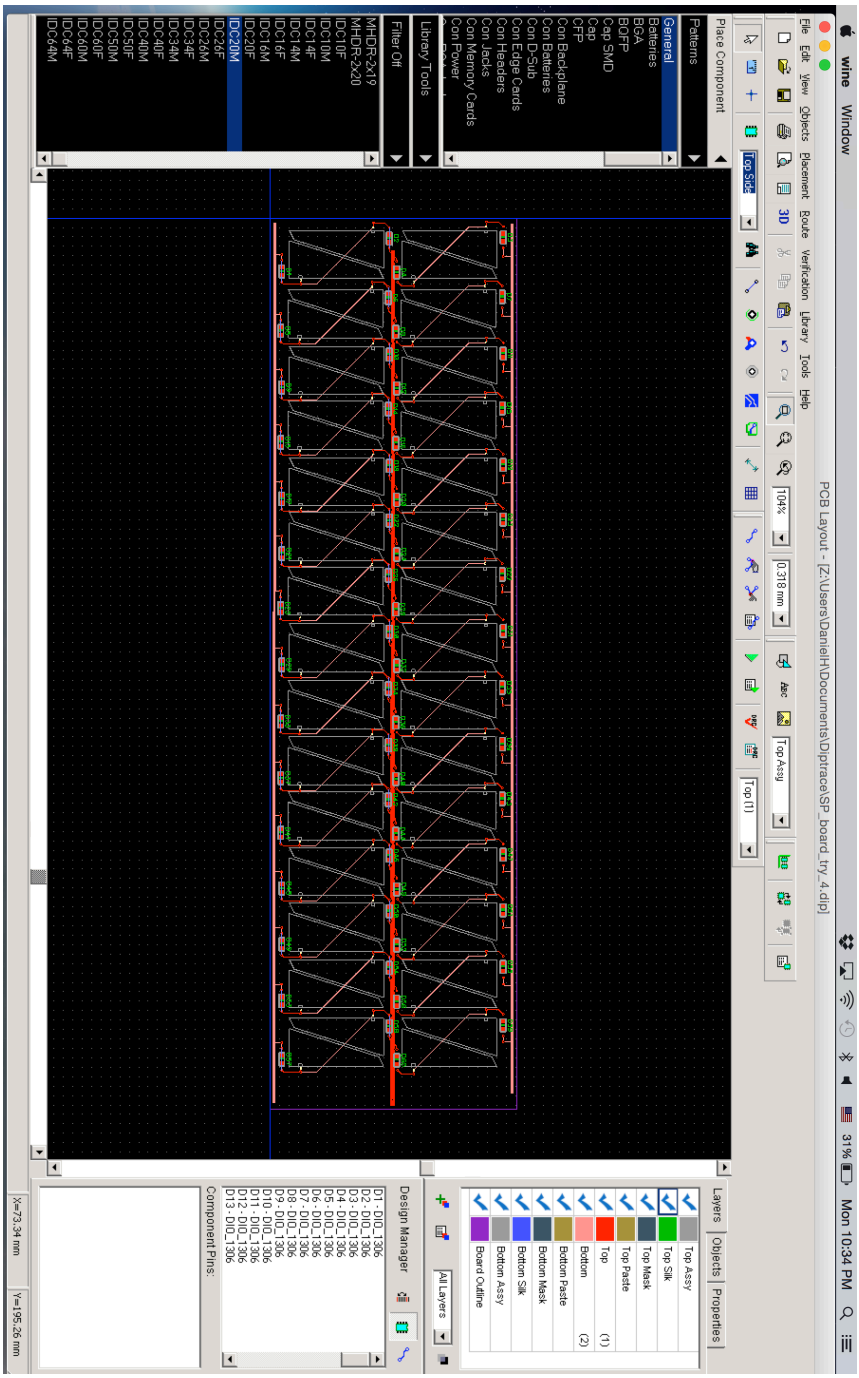

Figure 40. DipTrace interface and Solar Panel PCB layout.

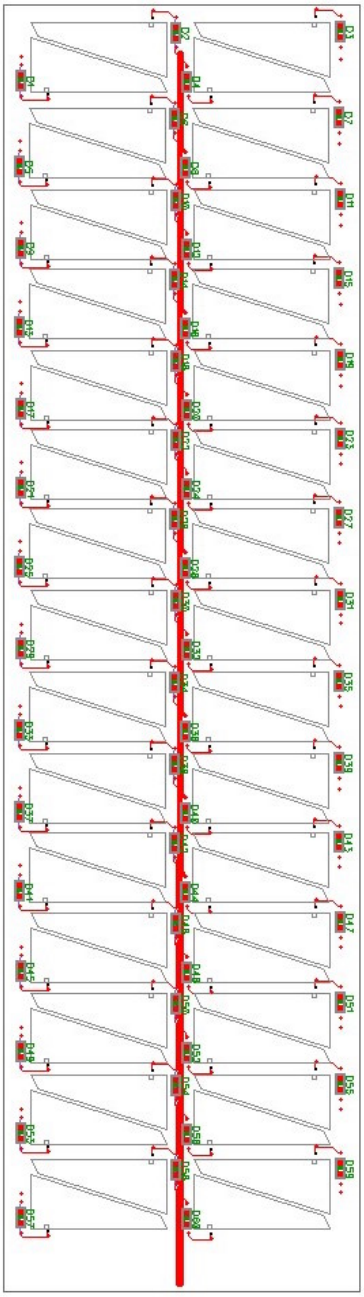

Figure 41. Top layer of 3U solar panel.

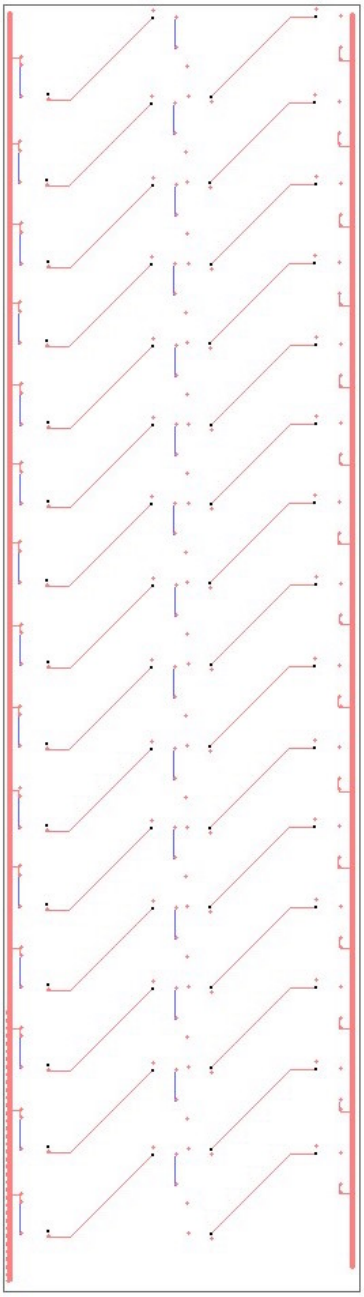

Figure 42. Bottom layer of 3U solar panel.

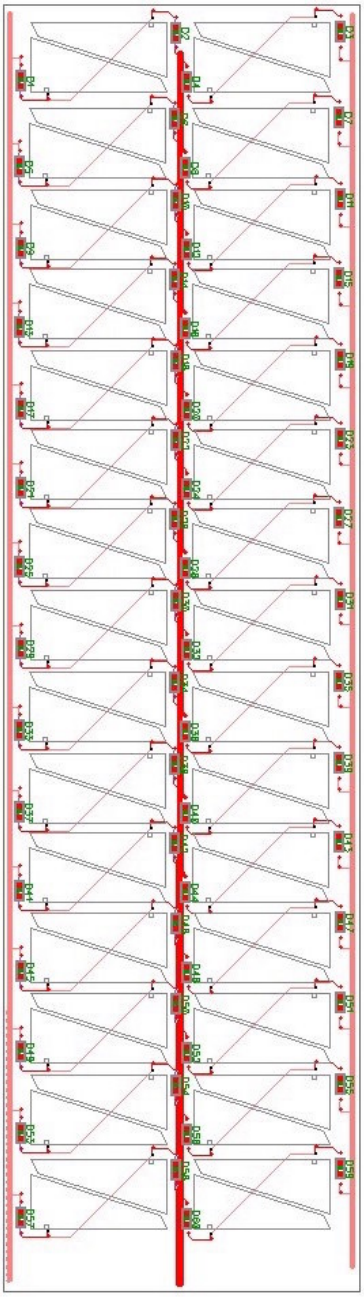

Figure 43. Combined image of both layers of 3U solar panel.

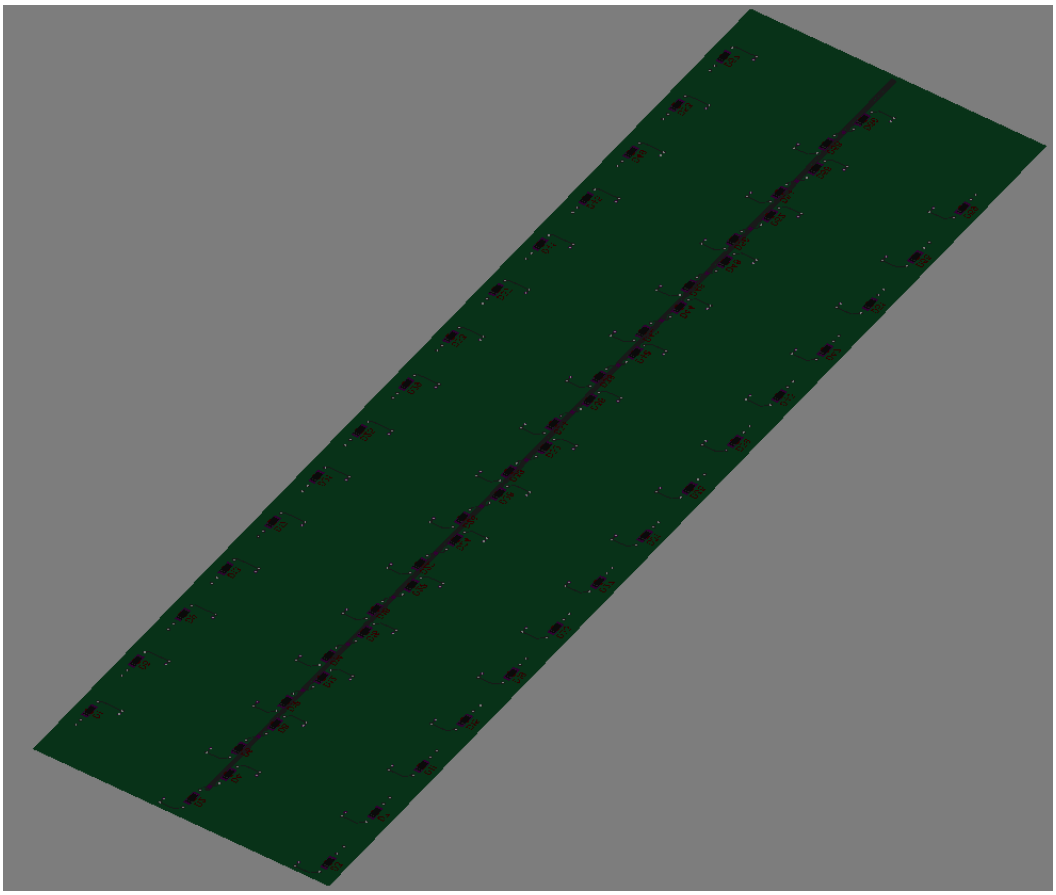

Figure 44. 3D view for 3U solar panel.

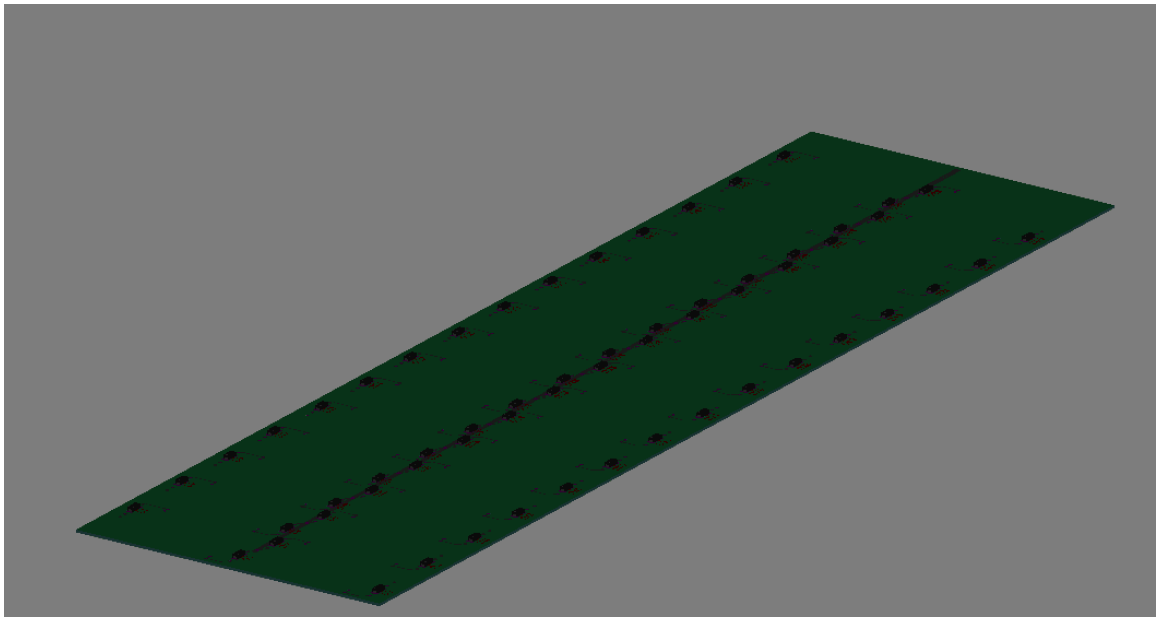

Figure 45. Alternate 3D view of 3U solar panel.

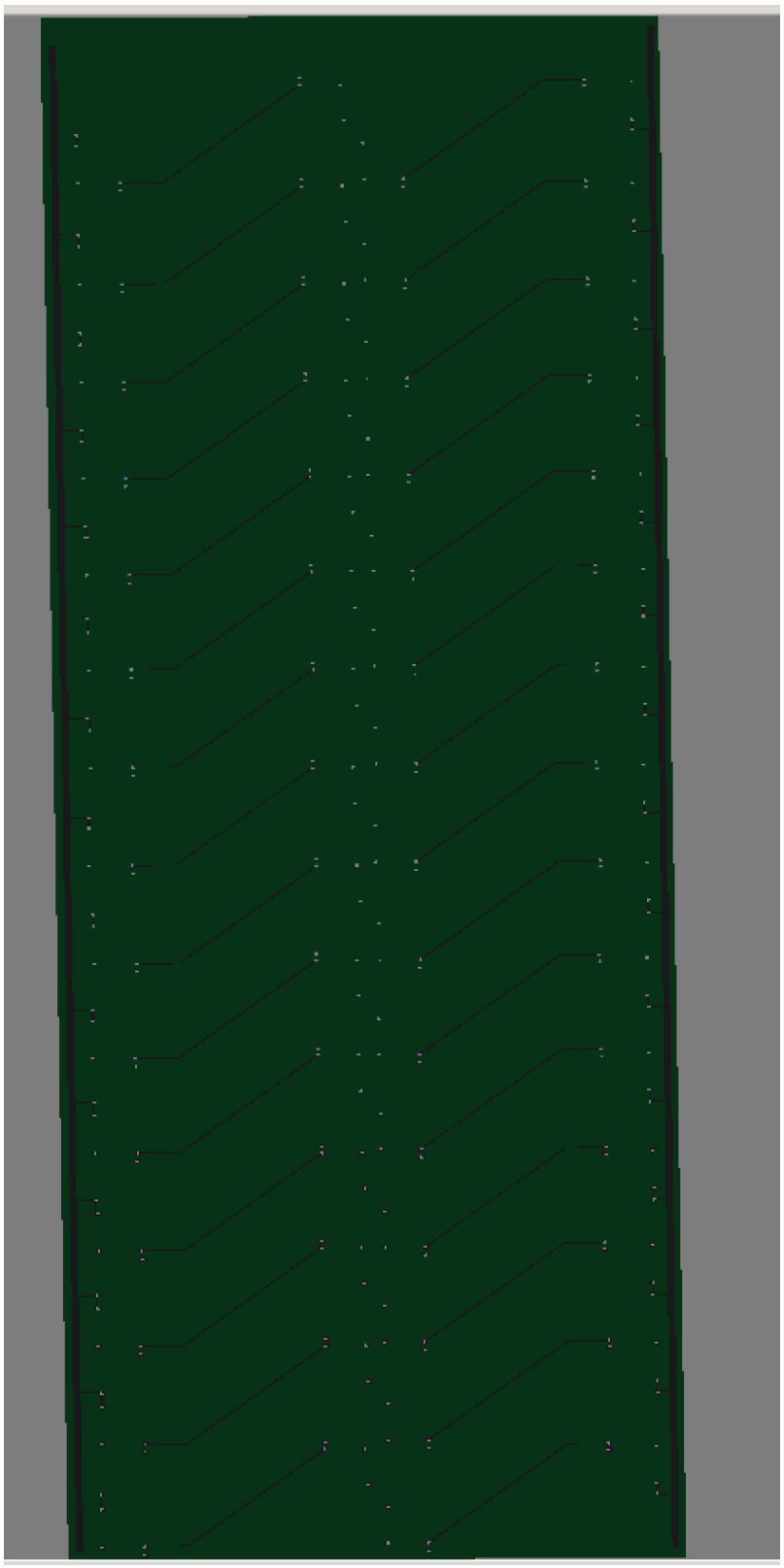

Figure 46. 3D view of bottom layer of 3U solar panel.

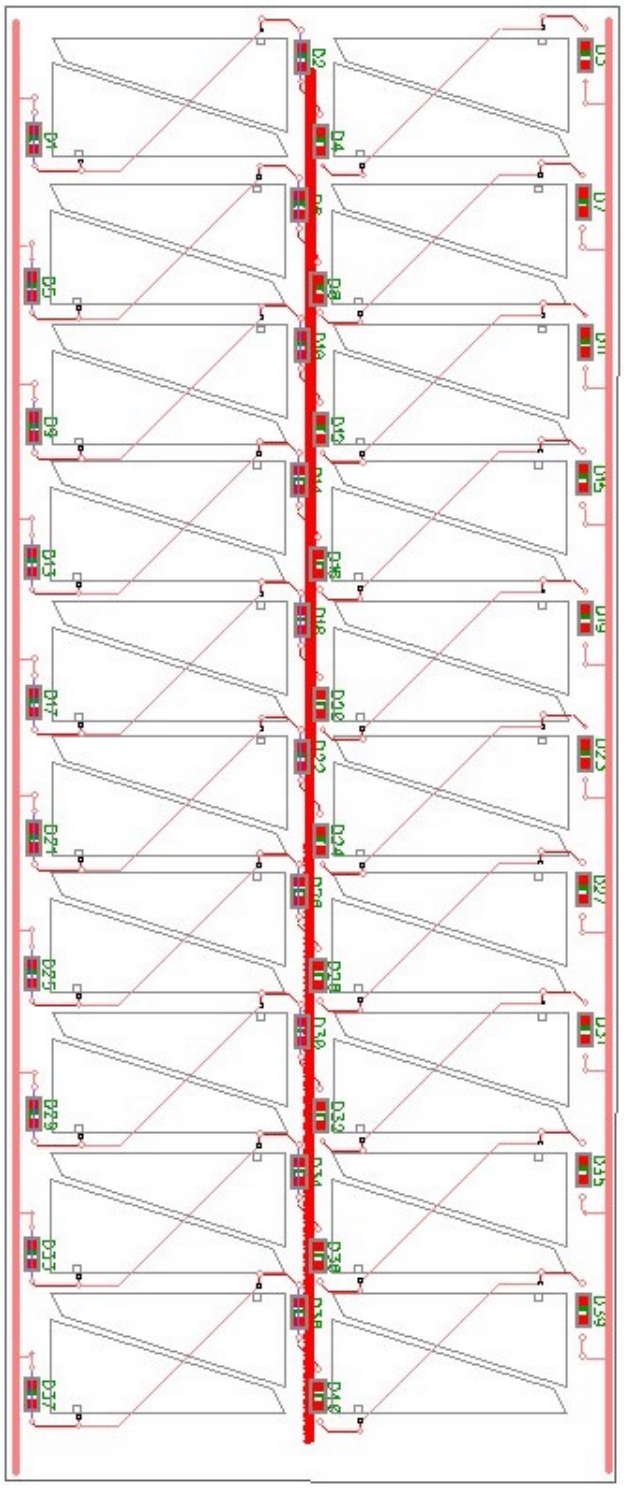

Figure 47. 2U solar panel top layer contrast.

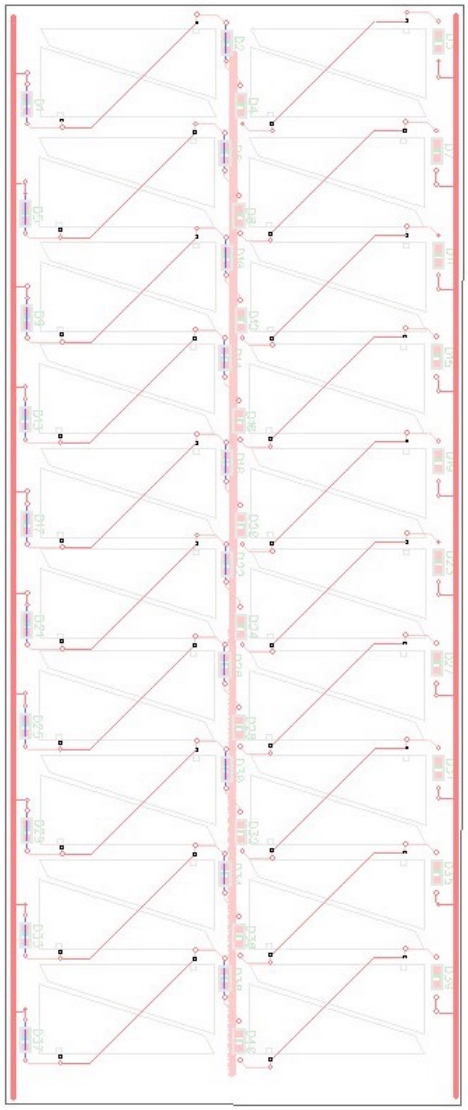

Figure 48. 2U solar panel bottom layer contrast.

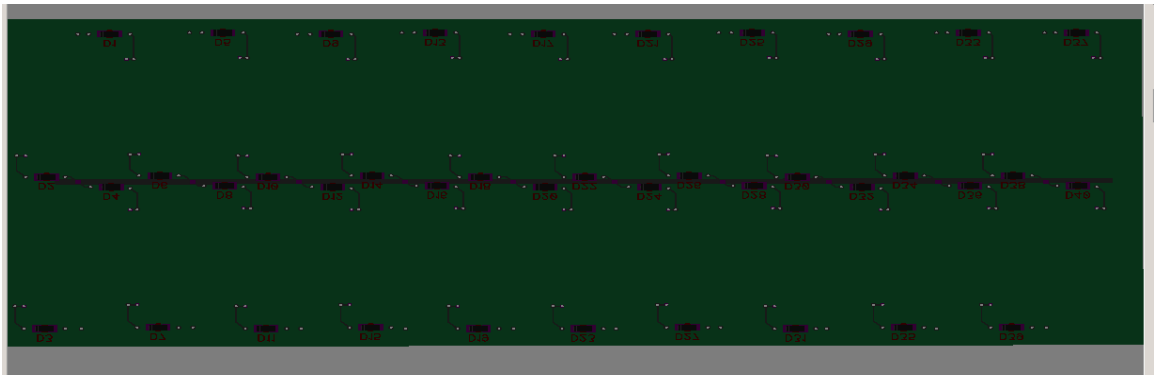

Figure 49. 2U PCB board top layer.

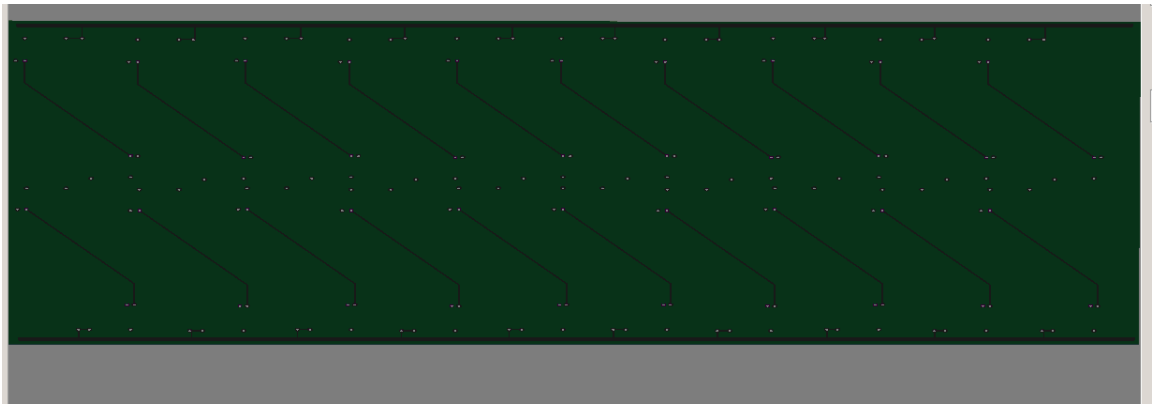

Figure 50. 2U PCB board bottom layer.

XI. Solar Cell Comparisons

Currently, alternative solar cells are being used on the TechEdSat. These cells have a lower efficiency than the TASC solar cells. The current cell efficiency is 18.5% while the TASC cells are rated at an efficiency of 27%. In order to compare the difference in output of the two cells, equations 26 and 27 were used to graph the power to angle of incidence relation of both types of cells. The TASC cells are plotted in blue, while the current cells being used are plotted in green and red. With the same effective area being used, it is obvious to see that the TASC cells will generate more power. However, the advantage the current cells are thought to have more effective area. The geometry of the cells allow for more cells to be placed on the faces of the cubesat. The

red curve displays the current cells with an additional 50% of effective area. From this configuration, more power can be produced. At zero incidence, 13.3W is output with the TASC cells, where the current cells output with 50% more area is 13.67W. The average difference in power between the two configurations is 2.89W.

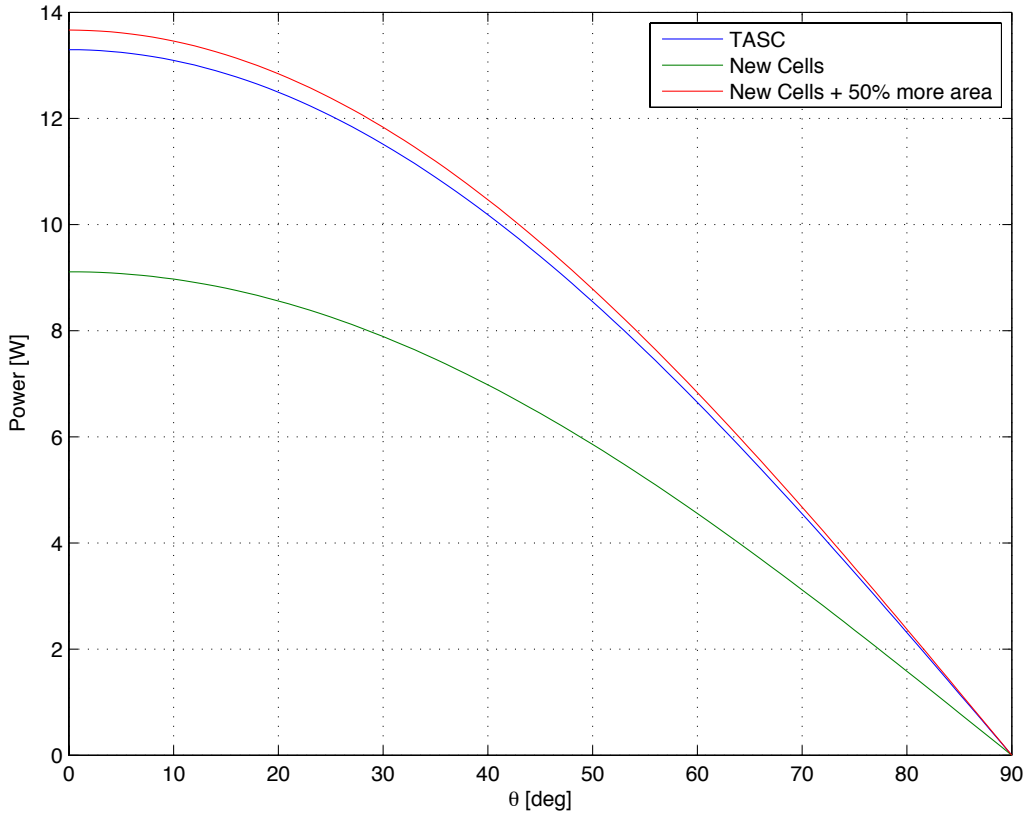

Figure 51. Solar cell power generation comparison.

XII. Communications Subsystem

A. Background

The communications subsystem is an essential part of the spacecraft's design as the required data rate can drive the power system design. It is desirable to optimize data rate while minimizing hardware, power and price. The data rate then determines the frequency spectrum over, which the information is sent. Transmitters are responsible for

modulating the signal to send to the antenna. Ka band transmitters are commonly used for scientific missions and can provide higher data rates than other alternative bands.

B. Near Earth and Deep Space analysis

Initial sizing of the communications subsystem can be accomplished by first calculating the receiver power density P_r through the equation:

$$P_r = \frac{P_t G_t G_r}{\left(\frac{4\pi d^{\frac{1}{n}}}{\lambda}\right)^2} \tag{44}$$

Where G_t is the transmit antenna gain, G_r is the receiver antenna gain, P_t is the transmitted power, d is the distance from the receiver, n is the exponent for environmental conditions and λ is the wavelength of the signal [16]. For free space propagation, n is assumed to be 2. In decibel form, equation 44 can be expressed as:

$$P_r(dB) = -20\log\left(\frac{4\pi}{\lambda}\right) - 10nlog(d) + G_t + G_r + P_t \tag{45}$$

The path loss, L_{PATH}, which expresses the loss in power between transmission and reception, can be expressed as:

$$L_{PATH} = \frac{P_R}{P_T} \quad , \qquad L_{PATH}(dB) = P_R - P_T \tag{46), (47}$$

Using the previous equations, we can begin to design a downlink analysis for a communication system based off of varying parameters. Table 38 through Table 42 provides calculations of downlink analysis for near Earth communication systems. A 1watt transmitter is assumed for Table 38, a 2watt transmitter is assumed for Table 39 and so on through Table 42. For each table, the frequency is kept constant at 1620Mhz. For each table, the distance from the transmitter to the receiver is varied from 160km to 2200 km to account for the varying distances that fall within low Earth orbit. Values for

transmission gain and receiver gain are held constant and were assumed based off of examples from the SMAD communications design model. All of these calculations assume free space propagation, which neglects other propagation effects. Table 43 displays calculations for deep space mission communication systems. For this analysis, transmitter power is held constant at 100watts and the distance is held constant at 2.5AU. Frequency is then varied from 2110Mhz to 32300Mhz to account for different deep space networks that use the S, X and Ka frequency bands [20].

Table 38. Near Earth downlink analysis with 1Watt transmitter.

Freq.	WvLngth	Dist.	Trns. Gain	Rec. Gain	Trns. Pwr	Trns. Pwr	Rec. Pwr	Rec. Pwr	Path loss	Path Loss
f	lambda	d	Gt	Gr	Pt [dBm]	Pt [Watts]	Pr[dBm]	Pr [Watts]	Lpath [Watts]	Lpath [dB]
2200000000	0.136363636	2560000	-4	45	30	1	-96.45502511	2.26203E-13	2.26203E-13	-126.4550251
1620000000	0.185185185	160000	-4	45	30	1	-69.71447213	1.06795E-10	1.06795E-10	-99.71447213
1620000000	0.185185185	200000	-4	45	30	1	-71.65267239	6.83491E-11	6.83491E-11	-101.6526724
1620000000	0.185185185	300000	-4	45	30	1	-75.17449757	3.03774E-11	3.03774E-11	-105.1744976
1620000000	0.185185185	400000	-4	45	30	1	-77.673272 3	1.70873E-11	1.70873E-11	-107.6732723
1620000000	0.185185185	500000	-4	45	30	1	-79.61147256	1.09359E-11	1.09359E-11	-109.6114726
1620000000	0.185185185	600000	-4	45	30	1	-81.19509748	7.59434E-12	7.59434E-12	-111.1950975
1620000000	0.185185185	700000	-4	45	30	1	-82.53403328	5.57952E-12	5.57952E-12	-112.5340333
1620000000	0.185185185	800000	-4	45	30	1	-83.69387222	4.27182E-12	4.27182E-12	-113.6938722
1620000000	0.185185185	900000	-4	45	30	1	-84.71692267	3.37526E-12	3.37526E-12	-114.7169227
1620000000	0.185185185	1000000	-4	45	30	1	-85.63207248	2.73396E-12	2.73396E-12	-115.6320725
1620000000	0.185185185	1200000	-4	45	30	1	-87.2156974	1.89859E-12	1.89859E-12	-117.2156974
1620000000	0.185185185	1400000	-4	45	30	1	-88.55463319	1.39488E-12	1.39488E-12	-118.5546332
1620000000	0.185185185	1600000	-4	45	30	1	-89.71447213	1.06795E-12	1.06795E-12	-119.7144721
1620000000	0.185185185	1800000	-4	45	30	1	-90.73752258	8.43816E-13	8.43816E-13	-120.7375226
1620000000	0.185185185	2000000	-4	45	30	1	-91.65267239	6.83491E-13	6.83491E-13	-121.6526724
1620000000	0.185185185	2200000	-4	45	30	1	-92.48052609	5.64869E-13	5.64869E-13	-122.4805261

Table 39. Near Earth downlink analysis with 2 Watt transmitter.

Freq.	WvLngth	Dist.	Trns. Gain	Rec. Gain	Trns. Pwr	Trns. Pwr	Rec. Pwr	Rec. Pwr	Path loss	Path Loss
f	lambda	d	Gt	Gr	Pt [dBm]	Pt [Watts]	Pr[dBm]	Pr [Watts]	Lpath [Watts]	Lpath [dB]
2200000000	0.136363636	2560000	-4	45	33.01029996	2	-93.44472515	4.52405E-13	2.26203E-13	-126.4550251
1620000000	0.185185185	160000	-4	45	33.01029996	2	-66.70417217	2.13591E-10	1.06795E-10	-99.71447213
1620000000	0.185185185	200000	-4	45	33.01029996	2	-68.64237243	1.36698E-10	6.83491E-11	-101.6526724
1620000000	0.185185185	300000	-4	45	33.01029996	2	-72.16419761	6.07548E-11	3.03774E-11	-105.1744976
1620000000	0.185185185	400000	-4	45	33.01029996	2	-74.66297235	3.41745E-11	1.70873E-11	-107.6732723
1620000000	0.185185185	500000	-4	45	33.01029996	2	-76.60117261	2.18717E-11	1.09359E-11	-109.6114726
1620000000	0.185185185	600000	-4	45	33.01029996	2	-78.18479753	1.51887E-11	7.59434E-12	-111.1950975
1620000000	0.185185185	700000	-4	45	33.01029996	2	-79.52373332	1.1159E-11	5.57952E-12	-112.5340333
1620000000	0.185185185	800000	-4	45	33.01029996	2	-80.68357226	8.54364E-12	4.27182E-12	-113.6938722
1620000000	0.185185185	900000	-4	45	33.01029996	2	-81.70662271	6.75053E-12	3.37526E-12	-114.7169227
1620000000	0.185185185	1000000	-4	45	33.01029996	2	-82.62177252	5.46793E-12	2.73396E-12	-115.6320725
1620000000	0.185185185	1200000	-4	45	33.01029996	2	-84.20539744	3.79717E-12	1.89859E-12	-117.2156974
1620000000	0.185185185	1400000	-4	45	33.01029996	2	-85.54433323	2.78976E-12	1.39488E-12	-118.5546332
1620000000	0.185185185	1600000	-4	45	33.01029996	2	-86.70417217	2.13591E-12	1.06795E-12	-119.7144721
1620000000	0.185185185	1800000	-4	45	33.01029996	2	-87.72722262	1.68763E-12	8.43816E-13	-120.7375226
1620000000	0.185185185	2000000	-4	45	33.01029996	2	-88.64237243	1.36698E-12	6.83491E-13	-121.6526724
1620000000	0.185185185	2200000	-4	45	33.01029996	2	-89.47022614	1.12974E-12	5.64869E-13	-122.4805261

Table 40. Near Earth downlink analysis with 3 Watt transmitter.

Freq.	WvLngth	Dist.	Trns. Gain	Rec. Gain	Trns. Pwr	Trns. Pwr	Rec. Pwr	Rec. Pwr	Path loss	Path Loss
f	lambda	d	Gt	Gr	Pt [dBm]	Pt [Watts]	Pr[dBm]	Pr [Watts]	Lpath [Watts]	Lpath [dB]
2200000000	0.136363636	2560000	-4	45	34.77121255	3	-91.68381256	6.78608E-13	2.26203E-13	-126.4550251
1620000000	0.185185185	160000	-4	45	34.77121255	3	-64.94325958	3.20386E-10	1.06795E-10	-99.71447213
1620000000	0.185185185	200000	-4	45	34.77121255	3	-66.88145984	2.05047E-10	6.83491E-11	-101.6526724
1620000000	0.185185185	300000	-4	45	34.77121255	3	-70.40328502	9.11321E-11	3.03774E-11	-105.1744976
1620000000	0.185185185	400000	-4	45	34.77121255	3	-72.90205976	5.12618E-11	1.70873E-11	-107.6732723
1620000000	0.185185185	500000	-4	45	34.77121255	3	-74.84026002	3.28076E-11	1.09359E-11	-109.6114726
1620000000	0.185185185	600000	-4	45	34.77121255	3	-76.42388494	2.2783E-11	7.59434E-12	-111.1950975
1620000000	0.185185185	700000	-4	45	34.77121255	3	-77.76282073	1.67386E-11	5.57952E-12	-112.5340333
1620000000	0.185185185	800000	-4	45	34.77121255	3	-78.92265967	1.28155E-11	4.27182E-12	-113.6938722
1620000000	0.185185185	900000	-4	45	34.77121255	3	-79.94571012	1.01258E-11	3.37526E-12	-114.7169227
1620000000	0.185185185	1000000	-4	45	34.77121255	3	-80.86085993	8.20189E-12	2.73396E-12	-115.6320725
1620000000	0.185185185	1200000	-4	45	34.77121255	3	-82.44448485	5.69576E-12	1.89859E-12	-117.2156974
1620000000	0.185185185	1400000	-4	45	34.77121255	3	-83.78342064	4.18464E-12	1.39488E-12	-118.5546332
1620000000	0.185185185	1600000	-4	45	34.77121255	3	-84.94325958	3.20386E-12	1.06795E-12	-119.7144721
1620000000	0.185185185	1800000	-4	45	34.77121255	3	-85.96631003	2.53145E-12	8.43816E-13	-120.7375226
1620000000	0.185185185	2000000	-4	45	34.77121255	3	-86.88145984	2.05047E-12	6.83491E-13	-121.6526724
1620000000	0.185185185	2200000	-4	45	34.77121255	3	-87.70931355	1.69461E-12	5.64869E-13	-122.4805261

Table 41. Near Earth downlink analysis with 4 Watt transmitter.

Freq.	WvLngth	Dist.	Trns. Gain	Rec. Gain	Trns. Pwr	Trns. Pwr	Rec. Pwr	Rec. Pwr	Path loss	Path Loss
f	lambda	d	Gt	Gr	Pt [dBm]	Pt [Watts]	Pr[dBm]	Pr [Watts]	Lpath [Watts]	Lpath [dB]
2200000000	0.136363636	2560000	-4	45	36.02059991	4	-90.4344252	9.0481E-13	2.26203E-13	-126.4550251
1620000000	0.185185185	160000	-4	45	36.02059991	4	-63.69387222	4.27182E-10	1.06795E-10	-99.71447213
1620000000	0.185185185	200000	-4	45	36.02059991	4	-65.63207248	2.73396E-10	6.83491E-11	-101.6526724
1620000000	0.185185185	300000	-4	45	36.02059991	4	-69.15389766	1.2151E-10	3.03774E-11	-105.1744976
1620000000	0.185185185	400000	-4	45	36.02059991	4	-71.65267239	6.83491E-11	1.70873E-11	-107.6732723
1620000000	0.185185185	500000	-4	45	36.02059991	4	-73.59087265	4.37434E-11	1.09359E-11	-109.6114726
1620000000	0.185185185	600000	-4	45	36.02059991	4	-75.17449757	3.03774E-11	7.59434E-12	-111.1950975
1620000000	0.185185185	700000	-4	45	36.02059991	4	-76.51343336	2.23181E-11	5.57952E-12	-112.5340333
1620000000	0.185185185	800000	-4	45	36.02059991	4	-77.6732723	1.70873E-11	4.27182E-12	-113.6938722
1620000000	0.185185185	900000	-4	45	36.02059991	4	-78.69632275	1.35011E-11	3.37526E-12	-114.7169227
1620000000	0.185185185	1000000	-4	45	36.02059991	4	-79.61147256	1.09359E-11	2.73396E-12	-115.6320725
1620000000	0.185185185	1200000	-4	45	36.02059991	4	-81.19509748	7.59434E-12	1.89859E-12	-117.2156974
1620000000	0.185185185	1400000	-4	45	36.02059991	4	-82.53403328	5.57952E-12	1.39488E-12	-118.5546332
1620000000	0.185185185	1600000	-4	45	36.02059991	4	-83.69387222	4.27182E-12	1.06795E-12	-119.7144721
1620000000	0.185185185	1800000	-4	45	36.02059991	4	-84.71692267	3.37526E-12	8.43816E-13	-120.7375226
1620000000	0.185185185	2000000	-4	45	36.02059991	4	-85.63207248	2.73396E-12	6.83491E-13	-121.6526724
1620000000	0.185185185	2200000	-4	45	36.02059991	4	-86.45992618	2.25947E-12	5.64869E-13	-122.4805261

Table 42. Near Earth downlink analysis with 5 Watt transmitter.

Freq.	WvLngth	Dist.	Trns. Gain	Rec. Gain	Trns. Pwr	Trns. Pwr	Rec. Pwr	Rec. Pwr	Path loss	Path Loss
f	lambda	d	Gt	Gr	Pt [dBm]	Pt [Watts]	Pr[dBm]	Pr [Watts]	Lpath [Watts]	Lpath [dB]
2200000000	0.136363636	2560000	-4	45	36.98970004	5	-89.46532507	1.13101E-12	2.26203E-13	-126.4550251
1620000000	0.185185185	160000	-4	45	36.98970004	5	-62.72477209	5.33977E-10	1.06795E-10	-99.71447213
1620000000	0.185185185	200000	-4	45	36.98970004	5	-64.66297235	3.41745E-10	6.83491E-11	-101.6526724
1620000000	0.185185185	300000	-4	45	36.98970004	5	-68.18479753	1.51887E-10	3.03774E-11	-105.1744976
1620000000	0.185185185	400000	-4	45	36.98970004	5	-70.68357226	8.54364E-11	1.70873E-11	-107.6732723
1620000000	0.185185185	500000	-4	45	36.98970004	5	-72.62177252	5.46793E-11	1.09359E-11	-109.6114726
1620000000	0.185185185	600000	-4	45	36.98970004	5	-74.20539744	3.79717E-11	7.59434E-12	-111.1950975
1620000000	0.185185185	700000	-4	45	36.98970004	5	-75.54433323	2.78976E-11	5.57952E-12	-112.5340333
1620000000	0.185185185	800000	-4	45	36.98970004	5	-76.70417217	2.13591E-11	4.27182E-12	-113.6938722
1620000000	0.185185185	900000	-4	45	36.98970004	5	-77.72722262	1.68763E-11	3.37526E-12	-114.7169227
1620000000	0.185185185	1000000	-4	45	36.98970004	5	-78.64237243	1.36698E-11	2.73396E-12	-115.6320725
1620000000	0.185185185	1200000	-4	45	36.98970004	5	-80.22599735	9.49293E-12	1.89859E-12	-117.2156974
1620000000	0.185185185	1400000	-4	45	36.98970004	5	-81.56493315	6.9744E-12	1.39488E-12	-118.5546332
1620000000	0.185185185	1600000	-4	45	36.98970004	5	-82.72477209	5.33977E-12	1.06795E-12	-119.7144721
1620000000	0.185185185	1800000	-4	45	36.98970004	5	-83.74782254	4.21908E-12	8.43816E-13	-120.7375226
1620000000	0.185185185	2000000	-4	45	36.98970004	5	-84.66297235	3.41745E-12	6.83491E-13	-121.6526724
1620000000	0.185185185	2200000	-4	45	36.98970004	5	-85.49082605	2.82434E-12	5.64869E-13	-122.4805261

Table 43. Deep Space downlink analysis with varying frequencies.

Freq.	WvLngth	Dist.	Trns. Gain	Rec. Gain	Trns. Pwr	Trns. Pwr	Rec. Pwr	Rec. Pwr	Path loss	Path Loss
f	lambda	d	Gt	Gr	Pt [dBm]	Pt [Watts]	Pr[dBm]	Pr [Watts]	Lpath [Watts]	Lpath [dB]
2110000000	0.142180095	3.74E+11	46	68.2	50	100	-106.1848533	2.40721E-14	2.40721E-16	-156.1848533
2120000000	0.141509434	3.74E+11	46	68.2	50	100	-106.2259214	2.38456E-14	2.38456E-16	-156.2259214
2290000000	0.131004367	3.74E+11	46	68.2	50	100	-106.8959139	2.04366E-14	2.04366E-16	-156.8959139
2300000000	0.130434783	3.74E+11	46	68.2	50	100	-106.933761	2.02593E-14	2.02593E-16	-156.933761
7145000000	0.041987404	3.74E+11	46	68.2	50	100	-116.7792489	2.0993E-15	2.0993E-17	-166.7792489
7190000000	0.041724618	3.74E+11	46	68.2	50	100	-116.833782	2.07311E-15	2.07311E-17	-166.833782
8400000000	0.035714286	3.74E+11	46	68.2	50	100	-118.18479	1.51887E-15	1.51887E-17	-168.18479
8450000000	0.035502959	3.74E+11	46	68.2	50	100	-118.2363384	1.50095E-15	1.50095E-17	-168.2363384
34200000000	0.0087719	3.74E+11	46	68.2	50	100	-130.3797264	9.16278E-17	9.16278E-19	-180.3797264
34700000000	0.008645533	3.74E+11	46	68.2	50	100	-130.5057937	8.90063E-17	8.90063E-19	-180.5057937
31800000000	0.009433962	3.74E+11	46	68.2	50	100	-129.7477466	1.0598E-16	1.0598E-18	-179.7477466
23200000000	0.012931034	3.74E+11	46	68.2	50	100	-127.0089639	1.99115E-16	1.99115E-18	-177.0089639

C. Iridium

The communication subsystem will implement the Iridium 9602 transceiver and take advantage of the Iridium network. The Iridium 9602 transceiver was chosen for its flight heritage in the TechEdSat series as well for its ability to meet data transmission requirements. It is a two-way short burst data transceiver whose packets can fit all the required data generated in a 20-minute window. It can also provide multi-orbital information. The iridium constellation consists of 66 satellites flying in 6 different orbital planes with 11 satellites in each plane. The satellites' orbits allow for optimum

exposure among satellites. Specifications for the Iridium can be found in Table 44 and Table 45.

Table 44. Iridium 9602 specifications.

Transmit/Receive Frequency	1616 – 1625.5 MHz
Transmit Power	1.6W
Message size	Tx 340 bytes, Rx 270 Bytes
Latency	~20 sec
External Power Source	5 +/- .5 VDC
Transmit	190mA – 1.5A
Standby	45-195 mA
Operating Temp	-40 – 85C

Table 45. Iridium 9602 specifications.

Parameter	Value
Receiver sensitivity	-117dB,
Max Cable loss permitted	2dB
Link Margin – Downlink	13dB
Link Margin - Uplink	7dB

Taking the communications transmit power into consideration, we can begin to construct a duty cycle for the Iridium transceiver. From Table 44, we see that the transmit power is 1.6W. The planned downlink time per day requirement was roughly 10 minutes per day. Using this knowledge the information in Table 44, and the same method used in the power budget section, the duty cycle for the iridium transceiver can be constructed. Figure 52 displays the duty cycle for the Iridium transceiver. At 1.6W and 10 minutes per day, it accounts for 1.33Whr. The duty cycle is .00833 for bi-hourly use. This allows for sufficient energy use as well as sufficient data transmission.

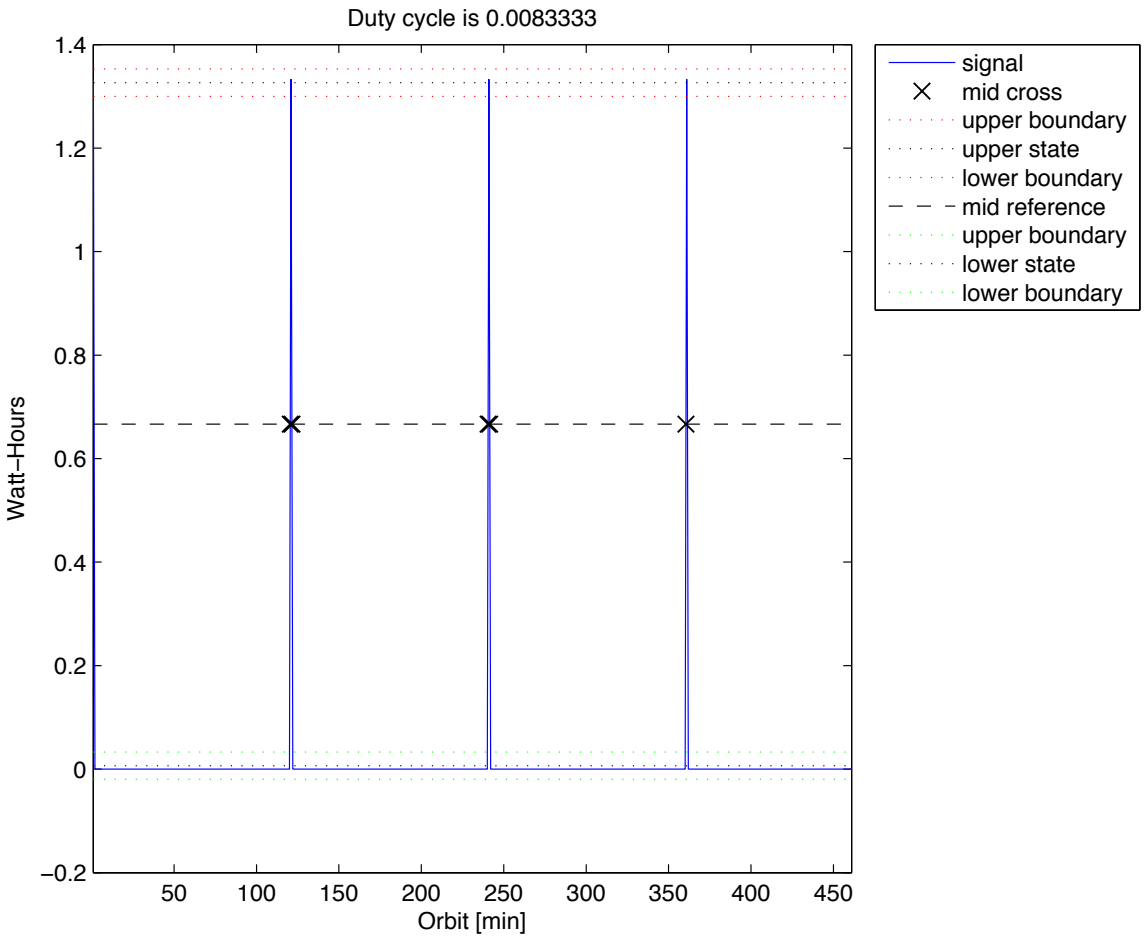

Figure 52. Iridium transceiver duty cycle.

XIII. Conclusion

All of the presented work contributes to the development of a power subsystem that will support a 3U cubesat for solar observation in LEO. Simulation of power mode cycling, power budget and duty cycle analysis verifies that the current design choices provide for optimum functionality of the cubesat bus throughout the mission lifespan. While the final list of components has yet to be determined, it is deemed feasible to build a low cost cubesat to meet the mission requirements. Once the final materials are determined, a full electrical wiring diagram can be made. Thermal effects of the solar cells can be determined through experimentation and use of a ceramic heater and

thermocouple. The overall materials for the burn wire circuit and release mechanism have been decided upon, but the design of the circuit is still in development. The current deployment mechanism can be approved upon through the design of a damping mechanism to prevent structural failure of the solar panels. Finite Element Analysis (FEA) and lab testing can also be performed to analyze the integrity of the solar panels. The PCBs need to be printed and ordered for experimental testing. The solar panels will then be tested to ensure that the cells meet the specifications provided by the manufacturer's datasheets as well as to observe their functionality with the rest of the spacecraft bus.

References

[1] Hapgood, Mike. "Space Weather: Its Impact On Earth and Implications For Business." Lloyd's. RAL Space, 2010. Web. 22 Feb. 2015. <http://www.lloyds.com/~/media/lloyds/reports/360/360%20space%20weather/7311_lloyds_360_space%20weather_03.pdf>.

[2] Kai-Rang, W., Jun, L., Lian-Guang, L., "A Statistical Study on the Geomagnetically Induced Current Events Driven by Earth-directed Full-Halo Coronal Mass Ejections," *Chinese Astronomy and Astrophysics,* Vol. 36, No. 3, 2012, pp. 261-281.

[3] Mansour, Nagi, and Jeremie Meurisse. "The Potential of CubeSats for Space Weather Applications." (2014): n. pag. Research Gate. Web. 2 Feb. 2015. <http://www.researchgate.net/profile/Meurisse_Jeremie/publication/266852705_The_potential_of_CubeSats_for_space_weather_applications/links/543d47250cf25d6b1ad74a50.pdf.>.

[4] Wertz, J.R., and Larson, W.J., "Space mission analysis and design," Space technology library, Kluwer Academic, Dordrecht, Netherlands; Boston, 1991, pp. 811.

[5] Erlank, A., Steyn., "Arcminute Attitude Estimation for CubeSats with a Novel Nano Star Tracker," International Federation of Automatic Control, Stellenbosch University, South Africa, 2014.

[6] Brown, C.D., and ebrary, I., "Elements of spacecraft design," *AIAA education series,* American Institute of Aeronautics and Astronautics, Inc., Reston, Va., 2002, pp. 606.

[7] Viscio, M.A., Viola, N., Corpino, S., "Interplanetary CubeSats system for space weather evaluations and technology demonstration," *Acta Astronautica,* Vol. 104, No. 2, 2014, pp. 516-525.

[8] "Small Spacecraft Technology State of the Art." Spacecraft 47.2 (2014): 150-58. Nasa.gov. Mission Design Division Staff, July 2014. Web. Feb. 2015. <http://www.nasa.gov/sites/default/files/files/Small_Spacecraft_Technology_State_of_the_Art_2014.pdf>.

[9] "BCT." BCT. Blue Canyon Technology, 2013. Web. 26 Feb. 2015. <http://bluecanyontech.com/all_products/cubesats/>.

[10] C. Passerone, M. Tranchero, S. Speretta, L. Reyneri, C. Sansoe, D. Del Corso, Design solutions for a university Nano-satellite, in: Proceed- ings of the Aerospace Conference, 2008 IEEE, vol. no., 1–8 March 2008, pp. 1, 13.

[11] "TechEdSat Nano-Satellite Series. Technologies for Passive Reentry, Future Sample Return and Mars Missions". National Aeronautics and Space Administration. Ames Research Center. 8-1-2013.

<http://ntrs.nasa.gov/archive/nasa/casi.ntrs.nasa.gov/20140013242.pdf>.

[12] Curtis, H., "Orbital Mechanics for Engineering Students," Aerospace Engineering, Elsevier Science, Burlington, 2009, pp. 740.

[13] Seeber, G., and ebrary, I., "Satellite geodesy," Walter de Gruyter, Berlin; New York, 2003, pp. 589.

[14] Patrick Hoehn, *Design, Construction and Validation of an articulated solar panel for CubeSats*, ISSN: 1653- 0187-ISRN:LTU-PB-EX—10/075-SE, 2011

[15] Patel, Mukund R. *Spacecraft Power Systems*. Boca Raton: CRC, 2005. Print.

[16] Clark, C., and Mazarias, L., "Power System Challenges For Small Satellite Missions," Clyde Space Ltd., 6.01 Kelvon Campus, Scotland, 2006.

[17] Villalva, Marcelo, Gazoli, Jonas. Filho, Ruppert, "Comprehensive Approach to Modeling and simulation of Photovoltaic Arrays," *IEEE Transactions on Power Elctronics*, Vol. 24, No. 5, 2009, 1198-1208.

[18] "Torsion Springs." (n.d.): n. pag. *Springs and Things*. Web. 10 Oct. 2015.

[19] "Nichrome 60 (NiCr) Resistance Wire." *Nichrome 60 (NiCr) Resistance Wire*. N.p., n.d. Web. 1 Nov. 2015. <https://www.heatersplus.com/nichrome.html>.

[20] "Radio Frequencies for Space Communication." *Radio Frequencies for Space Communication*. N.p., n.d. Web. 1 Dec. 2015. <http://www.spaceacademy.net.au/spacelink/radiospace.htm>.

[21] Ali, A., Mughal, M.R., Ali, H., "Innovative power management, attitude determination and control tile for CubeSat standard NanoSatellites," *Acta Astronautica,* Vol. 96, No. 0, 2014, pp. 116-127.

[22] Ian, Poole. "Radio Waves and the Ionosphere." Nature 154.3909 (1944): 413. Staines TW18 2PW, Nov. 1999. Web. 2 Feb. 2015.

[23] Navarathinam, N., Lee, R., and Chesser, H., "Characterization of Lithium-Polymer batteries for CubeSat applications," *Acta Astronautica,* Vol. 68, No. 11–12, 2011, pp. 1752-1760.

[24] Xie, Ning. "A Miniaturized Micro-Digital Sun Sensor by Means of Low-Power Low-Noise CMOS Imager." IEEE SENSORS JOURNAL 14.1 (2014): n. pag. IEEE Xplore. IEEE. Web. Feb. 2015. <http://ieeexplore.ieee.org/stamp/stamp.jsp?arnumber=6588567>.

[25] CubeSat Design Specification Rev. 12,The CubeSat Program, Cal Poly SLO

[26] Leroy, Thibaut (2011). Simple solar cell and panel model (http://www.mathworks.com/matlabcentral/fileexchange/31305-simple-solar-cell-and-panel-model), MATLAB Central File Exchange. Retrieved June, 2015.

[27] "Specification for Safety of Power-driven Industrial Brushes." *Information about Processing Stainless Steel (INOX)* (n.d.): 8+. PFERD. Web. 10 Oct. 2015. <http://www.pferd.com/images/Prospekt_Inox_Total_72dpi_en.pdf>.

[28] United States, "Code of federal regulations," National Archives and Records Administration, Washington, D.C., 199u,

Appendix A – TASC Solar Cell Datasheet

Spectrolab

Photovoltaic Products www.spectrolab.com

Triangular Advanced Solar Cells (TASC)

Product Description & Applications

- Designed for high power terrestrial applications, where space is at a premium.
- Two solar cells can be arranged within an approximate rectangular area of 0.611 x 1.254 inches (1.55 x 3.18 cm) with a cell gap of 0.018 inches (0.46 mm). See picture.
- Each solar cell is ideally matched to charge a single 1.2 V battery cell (eg. Ni-MH, NiCad, etc.). Cells can be wired in parallel for increased current. Two solar cells in series can charge one 3.6V Li-ion battery cell.
- A major advantage using these solar cells compared to silicon cells is that they deliver greater than 4 times higher voltage. Therefore, only one of Spectrolab's multi-junction solar cells is required to generate the same voltage as 5 Si solar cells connected in series
- Compared to typical silicon cells, these solar cells are ***over twice as efficient*** and thus will deliver more than twice the power for the same area.
- Uses and applications: A variety of power-consuming electronic equipment can benefit from these cells, especially if the area available is small or the time required for charging is limited. For example, these cells help power devices used during business trips, emergency situations or for the outdoor activities.

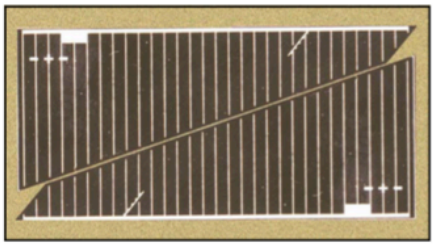

Not Actual Size

Typical Cell Electrical Parameters

1 Sun, AM1.5G (100.0 mW/cm²) 25°C

I_{sc}= 31 mA	I_{mp}= 28 mA
V_{oc}= 2.52 V	V_{mp}= 2.19 V
P_{mp}= 0.027 W/cm²	Cff= 80 %
Efficiency= 27 ± 3% Absolute	Temp. Coeff. V_{mp} = -6.2 mV/°C

Typical Cell I-V Curve (AM 1.5G)

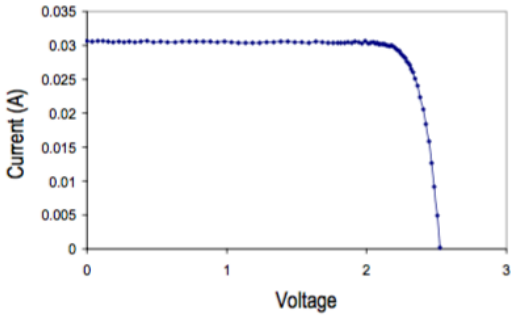

Product Description

Cell Type	Improved triple-junction gallium arsenide
Method of Cell Growth	Metal Organic Vapor Phase Epitaxy
Polarity	n/p
Thickness	190 µm (0.0075 in.)
Area	2.277 cm² (0.353 sq. in.)
Mass	0.234 g
Assembly Methods	Soldering, welding, metallized epoxy
Device Design	Monolithic, two terminal triple junction. n/p $GaInP_2$, GaAs, and Ge solar cells interconnected with two tunnel junctions.
Antireflective Coating	Multi-layer providing low reflectance over wavelength range 0.3 to 1.8µm.

ISO9001:2000 REGISTERED

SPECTROLAB

A BOEING COMPANY

The information contained on this sheet is for reference only. Actual specifications for delivered products may vary. 4/10/02

Spectrolab Inc. 12500 Gladstone Avenue, Sylmar, California 91342 USA • Phone: 818.365.4611 • Fax: 818.361.5102

Appendix B – Cubesat Specification Dimensions

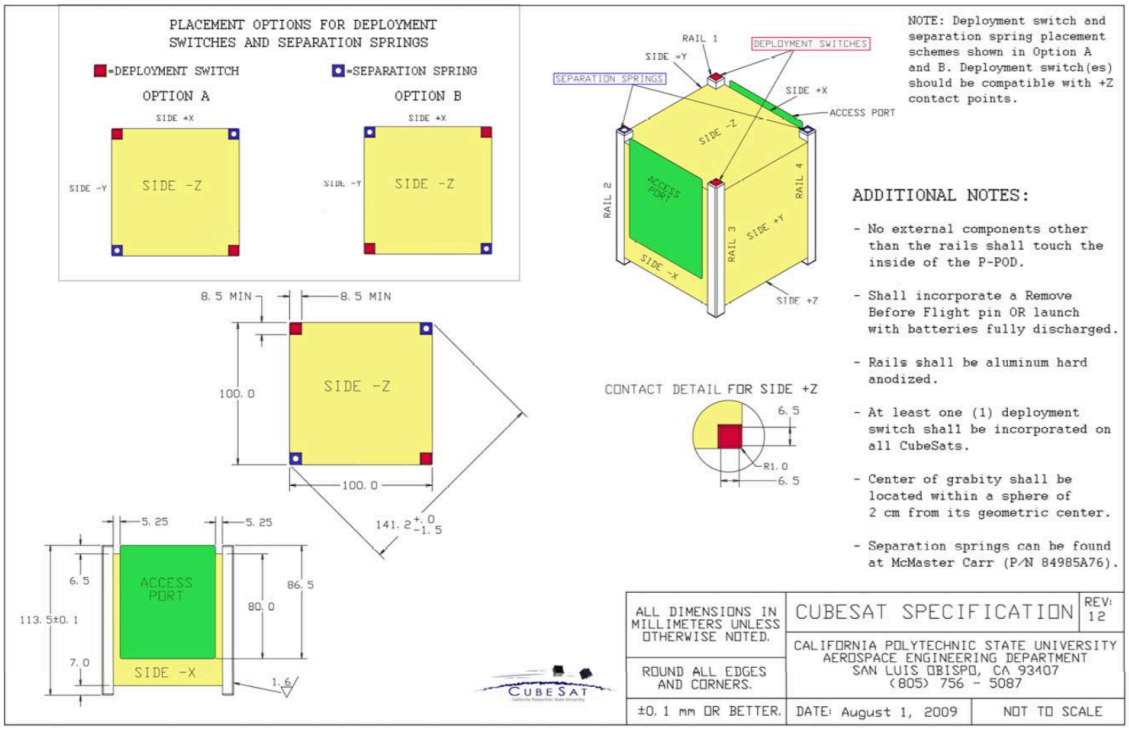

Appendix C – Cannon BP-930 Datasheet

CANON BP-930 Battery
· Exceed Original Specifications !

Battery Weight : 225g

Battery Chemistry : Li-ion

Voltage : 7.2V

Battery Capacity : 3700mAh

Battery Color : Black

Product Number : VCN004

Dimensions : 70.80x38.55x39.2

High capacity, Longer Record Ti

Appendix D – BP-930 Material Safety Datasheet

MATERIAL SAFETY DATA SHEET

MSDS#:BA0035-01-090218

SECTION 1 IDENTIFICATION OF THE SUBSTANCE/MIXTURE AND OF THE COMPANY/UNDERTAKING

Product Name:	Lithium Ion Battery
Product Code:	BP-930
Company Name:	Canon Inc.
Address:	30-2, Shimomaruko 3-Chome, Ohta-ku, Tokyo 146-8501, Japan
Use of the Product:	Battery for Video camera
Supplier:	
Address:	
Phone number:	

With regard to air transport, the International Civil Aviation Organization (ICAO) Packing Instruction 965 Part 1 complies with the Recommendation as is; further, the International Air Transport Association (IATA) adopts ICAO Packing Instruction 965 Part 1.
In addition, the regulations of the US Department of Transportation for land, sea and air transportation are based on the UN Recommendations.

SECTION 2 MATERIALS AND INGREDIENTS INFORMATION

IMPORT ANT NOTE:	The battery pack uses four US 18650S lithium-ion rechargeable cells and control circuit on the PWB.	
	The cells are connected in 2 parallel strings of 2 cells in series.	
	The battery pack should not be opened or burned since the following ingredients contained within the cells could be harmful under some circumstance if exposed or misused.	
	The cells contain neither metallic lithium nor lithium alloy.	
Cathode:	Lithium-Cobalt Dioxides	(active material)
	Polyvinyldiene Fluoride	(binder)
	Graphite	(conductive material)
Anode:	Graphite	(active material)
	Polyvinyldiene Fluoride	(binder)
Electrolyte:	Organic Solvent	(non-aqueous liquid)
	Lithium Salt	
Others:	Heavy metals such as Mercury, Cadmium, Lead, and Chromium are not used in the cells.	
Enclosure:	Plastic (PC)	

SECTION 3 FIRE HAZARD DATA

In case of fire, use CO_2 or dry chemical extinguishers.

Date of Issue: September 8, 2009 **Revised Date: -**

Ver. 2009/6/01

SECTION 4 HEALTH HAZARD DATA

Under normal condition of use, these chemicals are contained in sealed can. Risk of exposure occurs only if the cells are mechanically abused.

Inhalation:	Contents of an opened cell can cause respiratory irritation.
	Remove to fresh air immediately and call a doctor.
Skin Contact:	Contents of an opened cell can cause skin irritation.
	Wash skin with soap and water.
Eye Contact:	Contents of an opened cell can cause eye irritation.
	Immediately flush eyes thoroughly with water for at least 15 minutes. Seek medical attention.

SECTION 5 PRECAUTIONS FOR SAFE HANDLING AND USE

Storage:	Store within the recommended limit of -20 degrees C to 45 degrees C (-4 degrees F to 113 degrees F), well-ventilated area. Do not expose to high temperature (60 degrees C/140 degrees F). Since short circuit can cause burn hazard or safety vent to open, do not store with metal jewelry, metal covered tables, or metal belt.
Handling:	Do not disassemble, remodel, or solder. Do not short + and - terminals with a metal. Do not open the battery pack.
Charging:	Charge within the limits of 0 degrees C to 40 degrees C (32 degrees F to 104 degrees F) temperature. Charge with specified charger designed for this battery pack.
Discharging:	Discharge within the limits of -10 degrees C to 50 degrees C (14 degrees F to 122 degrees F) temperature.
Disposal:	Dispose in accordance with applicable federal, state and local regulation.
Caution:	Attach the cover to the battery pack to prevent short circuits. Do not disassemble. Do not incinerate. Do not expose to temperature above 140 degrees F.

SECTION 6 SPECIAL PROTECTION INFORMATION

Respiratory Protection:	Not necessary under normal use.
Ventilation:	Not necessary under normal use.
Eye Protection:	Not necessary under normal use.
Protective Gloves:	Not necessary under normal use.

Date of Issue: September 8, 2009 **Revised Date: -**

Ver. 2009/6/01

Appendix E – SMAD Model Spreadsheet

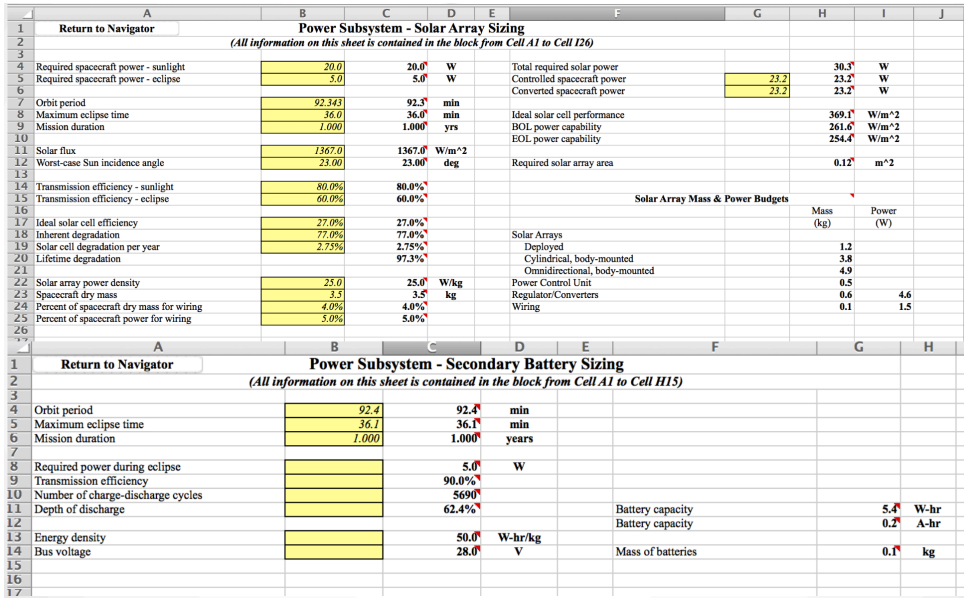

	A	B	C	D	E	F	G	H	I	J
1	Return to Navigator		Power Subsystem - Solar Array Sizing							
2			*(All information on this sheet is contained in the block from Cell A1 to Cell I26)*							
3										
4	Required spacecraft power - sunlight	*20.0*	20.0	W		Total required solar power		30.3	W	
5	Required spacecraft power - eclipse	*5.0*	5.0	W		Controlled spacecraft power	*23.2*	23.2	W	
6						Converted spacecraft power	*23.2*	23.2	W	
7	Orbit period	*92.343*	92.3	min						
8	Maximum eclipse time	*36.0*	36.0	min		Ideal solar cell performance		369.1	W/m^2	
9	Mission duration	*1.000*	1.000	yrs		BOL power capability		261.6	W/m^2	
10						EOL power capability		254.4	W/m^2	
11	Solar flux	*1367.0*	1367.0	W/m^2						
12	Worst-case Sun incidence angle	*23.00*	23.00	deg		Required solar array area		0.12	m^2	
13										
14	Transmission efficiency - sunlight	*80.0%*	80.0%							
15	Transmission efficiency - eclipse	*60.0%*	60.0%			Solar Array Mass & Power Budgets				
16								Mass	Power	
17	Ideal solar cell efficiency	*27.0%*	27.0%					(kg)	(W)	
18	Inherent degradation	*77.0%*	77.0%			Solar Arrays				
19	Solar cell degradation per year	*2.75%*	2.75%			Deployed		1.2		
20	Lifetime degradation		97.3%			Cylindrical, body-mounted		3.8		
21						Omnidirectional, body-mounted		4.9		
22	Solar array power density	*25.0*	25.0	W/kg		Power Control Unit		0.5		
23	Spacecraft dry mass	*3.5*	3.5	kg		Regulator/Converters		0.6	4.6	
24	Percent of spacecraft dry mass for wiring	*4.0%*	4.0%			Wiring		0.1	1.5	
25	Percent of spacecraft power for wiring	*5.0%*	5.0%							
26										

	A	B	C	D	E	F	G	H
1	Return to Navigator	Power Subsystem - Secondary Battery Sizing						
2		*(All information on this sheet is contained in the block from Cell A1 to Cell H15)*						
3								
4	Orbit period	*92.4*	92.4	min				
5	Maximum eclipse time	*36.1*	36.1	min				
6	Mission duration	*1.000*	1.000	years				
7								
8	Required power during eclipse		5.0	W				
9	Transmission efficiency		90.0%					
10	Number of charge-discharge cycles		5690					
11	Depth of discharge		62.4%			Battery capacity	5.4	W-hr
12						Battery capacity	0.2	A-hr
13	Energy density		50.0	W-hr/kg				
14	Bus voltage		28.0	V		Mass of batteries	0.1	kg
15								
16								
17								

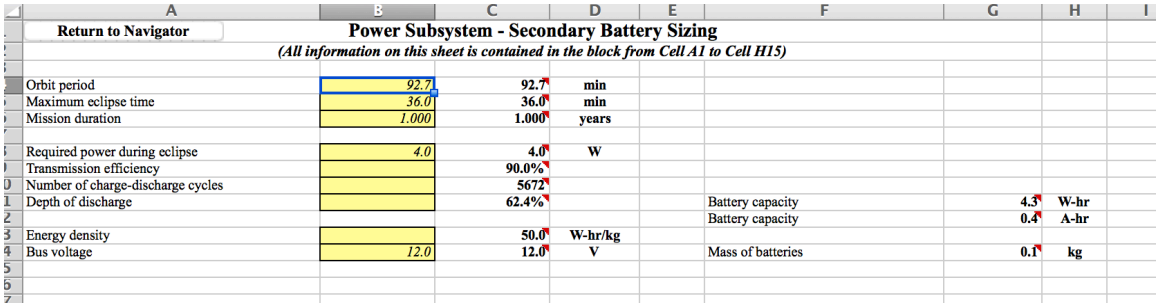

	A	B	C	D	E	F	G	H	I
	Return to Navigator	Power Subsystem - Secondary Battery Sizing							
		(All information on this sheet is contained in the block from Cell A1 to Cell H15)							
	Orbit period	*92.7*	92.7	min					
	Maximum eclipse time	*36.0*	36.0	min					
	Mission duration	*1.000*	1.000	years					
	Required power during eclipse	*4.0*	4.0	W					
	Transmission efficiency		90.0%						
	Number of charge-discharge cycles		5672						
	Depth of discharge		62.4%			Battery capacity	4.3	W-hr	
						Battery capacity	0.4	A-hr	
	Energy density		50.0	W-hr/kg					
	Bus voltage	*12.0*	12.0	V		Mass of batteries	0.1	kg	

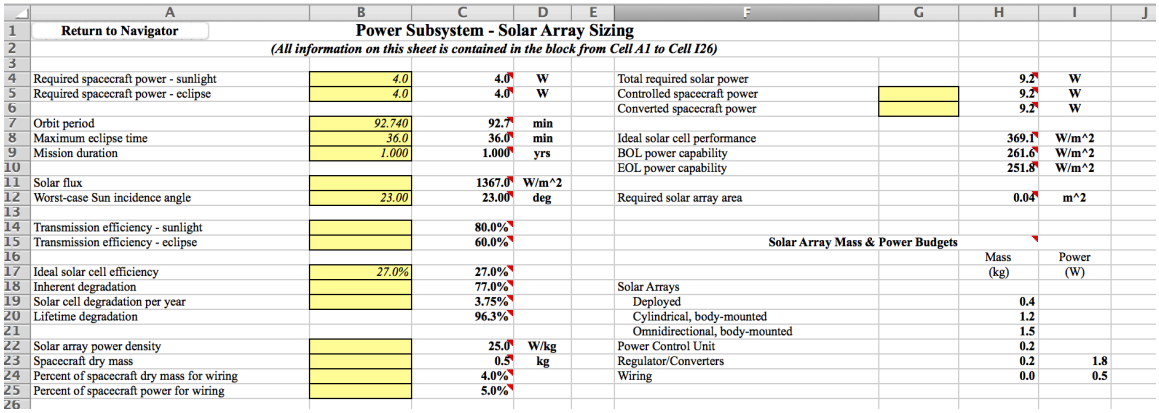

	A	B	C	D	E	F	G	H	I	J
1	Return to Navigator		Power Subsystem - Solar Array Sizing							
2			*(All information on this sheet is contained in the block from Cell A1 to Cell I26)*							
3										
4	Required spacecraft power - sunlight	*4.0*	4.0	W		Total required solar power		9.2	W	
5	Required spacecraft power - eclipse	*4.0*	4.0	W		Controlled spacecraft power		9.2	W	
6						Converted spacecraft power		9.2	W	
7	Orbit period	*92.740*	92.7	min						
8	Maximum eclipse time	*36.0*	36.0	min		Ideal solar cell performance		369.1	W/m^2	
9	Mission duration	*1.000*	1.000	yrs		BOL power capability		261.6	W/m^2	
10						EOL power capability		251.8	W/m^2	
11	Solar flux		1367.0	W/m^2						
12	Worst-case Sun incidence angle	*23.00*	23.00	deg		Required solar array area		0.04	m^2	
13										
14	Transmission efficiency - sunlight		80.0%							
15	Transmission efficiency - eclipse		60.0%			Solar Array Mass & Power Budgets				
16								Mass	Power	
17	Ideal solar cell efficiency	*27.0%*	27.0%					(kg)	(W)	
18	Inherent degradation		77.0%			Solar Arrays				
19	Solar cell degradation per year		3.75%			Deployed		0.4		
20	Lifetime degradation		96.3%			Cylindrical, body-mounted		1.2		
21						Omnidirectional, body-mounted		1.5		
22	Solar array power density		25.0	W/kg		Power Control Unit		0.2		
23	Spacecraft dry mass		0.5	kg		Regulator/Converters		0.2	1.8	
24	Percent of spacecraft dry mass for wiring		4.0%			Wiring		0.0	0.5	
25	Percent of spacecraft power for wiring		5.0%							
26										

Appendix F – CAD of proposed Cubesat

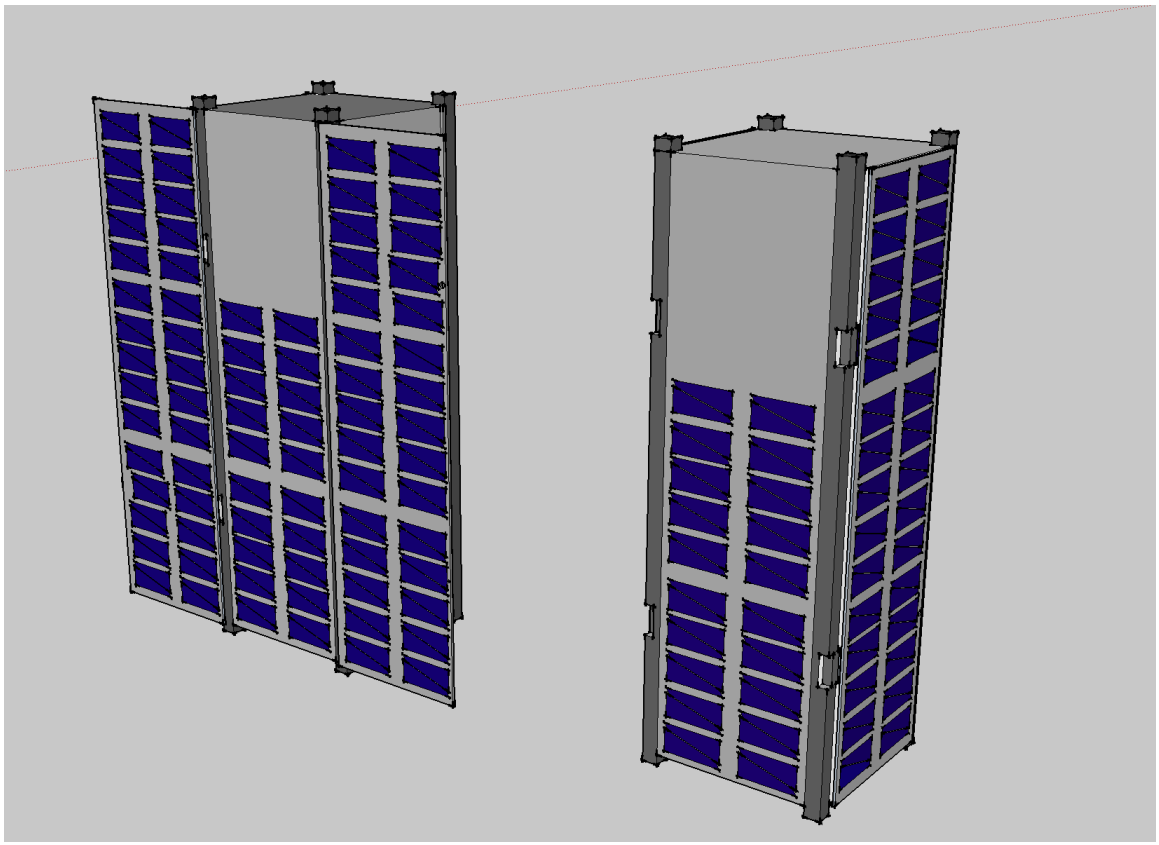

Appendix F – Solar Panel Diode Datasheet

MA2C029

Silicon epitaxial planar type

For reduced voltage and temperature compensation

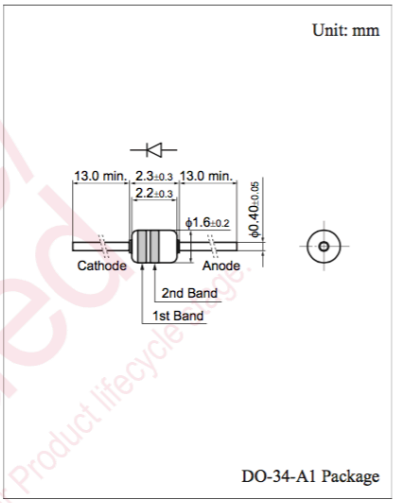

■ Features

- High reliability achieved through combination of a planar type chip and glass sealing structure
- Easy mounting because of employing DO-35 (DHD) envelope
- Extremely small reverse current I_R
- Large power dissipation P_D
- Wide forward voltage V_F range

■ Absolute Maximum Ratings $T_a = 25°C$

Parameter	Symbol	Rating	Unit
Reverse voltage	V_R	6	V
Forward current (Average)	$I_{F(AV)}$	50	mA
Power dissipation	P_D	150	mW
Junction temperature	T_j	150	°C
Storage temperature	T_{stg}	−55 to +150	°C

■ Electrical Characteristics $T_a = 25°C \pm 3°C$ *1

Parameter	Symbol	Conditions	Min	Typ	Max	Unit
Forward current	V_{F1}	$I_F = 1.5$ mA		2 *2		V
	V_{F2}	$I_F = 50$ mA			1.1	
Reverse current	I_R	$V_R = 6$ V			10	μA
Temperature coefficient of forward voltage *3	$-\Delta V_F/V_T$	$I_F = 1.5$ mA		2.0		mV/°C

Note) 1. Measuring methods are based on JAPANESE INDUSTRIAL STANDARD JIS C 7031 measuring methods for diodes.

2. *1: The temperature must be controlled 25°C for V_F mesurement. V_F value measured at other temperature must be adjusted to V_F (25°C)

*2:

Type	V_F (V)
MA2C0290A	0.56 to 0.61
MA2C0290A1	0.56 to 0.59
MA2C0290A2	0.58 to 0.61
MA2C0290B	0.59 to 0.64
MA2C0290B1	0.59 to 0.62
MA2C0290B2	0.61 to 0.64

*3: $T_j = 25°C$ to 150°C

■ Cathode Indication

Type No.	MA2C0290A	MA2C0290A1	MA2C0290A2	MA2C0290B	MA2C0290B1	MA2C0290B2
1st band color	Red	Red	Red	Blue	Blue	Blue
2nd band color	—	Blue	Yellow	—	Blue	Yellow

Appendix H – STK Orbit Data

Table 46. STK Orbit Data.

stk = [0	-1647.783258	-4951.68809	-4337.677417	-1647.783258	-4951.68809	-4337.677417	;
1	-1258.904788	-4887.303474	-4536.245256	-1258.904788	-4887.303474	-4536.245256	;
2	-863.635644	-4804.047902	-4713.966782	-863.635644	-4804.047902	-4713.966782	;
3	-463.617072	-4702.354337	-4870.029496	-463.617072	-4702.354337	-4870.029496	;
4	-60.51531	-4582.724663	-5003.720137	-60.51531	-4582.724663	-5003.720137	;
5	343.985292	-4445.727133	-5114.427768	343.985292	-4445.727133	-5114.427768	;
6	748.189222	-4291.993604	-5201.646421	748.189222	-4291.993604	-5201.646421	;
7	1150.396807	-4122.216576	-5264.977279	1150.396807	-4122.216576	-5264.977279	;
8	1548.911247	-3937.146049	-5304.130391	1548.911247	-3937.146049	-5304.130391	;
9	1942.045649	-3737.58621	-5318.925934	1942.045649	-3737.58621	-5318.925934	;
10	2328.130048	-3524.391974	-5309.294997	2328.130048	-3524.391974	-5309.294997	;
11	2705.518387	-3298.46537	-5275.279903	2705.518387	-3298.46537	-5275.279903	;
12	3072.595437	-3060.751803	-5217.034054	3072.595437	-3060.751803	-5217.034054	;
13	3427.783635	-2812.236198	-5134.821315	3427.783635	-2812.236198	-5134.821315	;
14	3769.549814	-2553.939035	-5029.014923	3769.549814	-2553.939035	-5029.014923	;
15	4096.411806	-2286.912279	-4900.095924	4096.411806	-2286.912279	-4900.095924	;
16	4406.94489	-2012.235234	-4748.65115	4406.94489	-2012.235234	-4748.65115	;
17	4699.788057	-1731.010317	-4575.370725	4699.788057	-1731.010317	-4575.370725	;
18	4973.650077	-1444.358763	-4381.045111	4973.650077	-1444.358763	-4381.045111	;
19	5227.315325	-1153.416284	-4166.561703	5227.315325	-1153.416284	-4166.561703	;
20	5459.64935	-859.328687	-3932.900973	5459.64935	-859.328687	-3932.900973	;
21	5669.604151	-563.247463	-3681.13217	5669.604151	-563.247463	-3681.13217	;
22	5856.22314	-266.325365	-3412.408608	5856.22314	-266.325365	-3412.408608	;
23	6018.645748	30.28801	-3127.962521	6018.645748	30.28801	-3127.962521	;
24	6156.11166	325.450618	-2829.099547	6156.11166	325.450618	-2829.099547	;
25	6267.96464	618.032336	-2517.192816	6267.96464	618.032336	-2517.192816	;
26	6353.655927	906.919267	-2193.676699	6353.655927	906.919267	-2193.676699	;
27	6412.747172	1191.01798	-1860.040233	6412.747172	1191.01798	-1860.040233	;
28	6444.91289	1469.259652	-1517.820246	6444.91289	1469.259652	-1517.820246	;
29	6449.942417	1740.604101	-1168.594223	6449.942417	1740.604101	-1168.594223	;
30	6427.741335	2004.043697	-813.972947	6427.741335	2004.043697	-813.972947	;

31	6378.33238	2258.607107	-455.59295	6378.33238	2258.607107	-455.59295	;
32	6301.855786	2503.362892	-95.108817	6301.855786	2503.362892	-95.108817	;
33	6198.569088	2737.422901	265.814616	6198.569088	2737.422901	265.814616	;
34	6068.846369	2959.945476	625.510131	6068.846369	2959.945476	625.510131	;
35	5913.176947	3170.138427	982.316004	5913.176947	3170.138427	982.316004	;
36	5732.163523	3367.261791	1334.583875	5732.163523	3367.261791	1334.583875	;
37	5526.519779	3550.63033	1680.686529	5526.519779	3550.63033	1680.686529	;
38	5297.067463	3719.61579	2019.025575	5297.067463	3719.61579	2019.025575	;
39	5044.732956	3873.648889	2348.038969	5044.732956	3873.648889	2348.038969	;
40	4770.543357	4012.221039	2666.20834	4770.543357	4012.221039	2666.20834	;
41	4475.622105	4134.885803	2972.066085	4475.622105	4134.885803	2972.066085	;
42	4161.18416	4241.260067	3264.202187	4161.18416	4241.260067	3264.202187	;
43	3828.530778	4331.024951	3541.270743	3828.530778	4331.024951	3541.270743	;
44	3479.043907	4403.926444	3801.996147	3479.043907	4403.926444	3801.996147	;
45	3114.180233	4459.775774	4045.178921	3114.180233	4459.775774	4045.178921	;
46	2735.464916	4498.449516	4269.701161	2735.464916	4498.449516	4269.701161	;
47	2344.485038	4519.889456	4474.53157	2344.485038	4519.889456	4474.53157	;
48	1942.882803	4524.102195	4658.730084	1942.882803	4524.102195	4658.730084	;
49	1532.348521	4511.158536	4821.452042	1532.348521	4511.158536	4821.452042	;
50	1114.613398	4481.192631	4961.95192	1114.613398	4481.192631	4961.95192	;
51	691.442182	4434.400922	5079.586599	691.442182	4434.400922	5079.586599	;
52	264.625674	4371.040875	5173.818161	264.625674	4371.040875	5173.818161	;
53	-164.026855	4291.429516	5244.216221	-164.026855	4291.429516	5244.216221	;
54	-592.695314	4195.941792	5290.459769	-592.695314	4195.941792	5290.459769	;
55	-1019.556484	4085.008748	5312.338537	-1019.556484	4085.008748	5312.338537	;
56	-1442.791723	3959.115548	5309.753884	-1442.791723	3959.115548	5309.753884	;
57	-1860.594664	3818.799334	5282.719192	-1860.594664	3818.799334	5282.719192	;
58	-2271.178866	3664.646942	5231.359779	-2271.178866	3664.646942	5231.359779	;
59	-2672.785414	3497.292474	5155.912331	-2672.785414	3497.292474	5155.912331	;
60	-3063.690413	3317.414743	5056.723847	-3063.690413	3317.414743	5056.723847	;
61	-3442.212382	3125.734592	4934.25011	-3442.212382	3125.734592	4934.25011	;
62	-3806.719494	2923.012091	4789.053676	-3806.719494	2923.012091	4789.053676	;
63	-4155.636646	2710.043628	4621.801397	-4155.636646	2710.043628	4621.801397	;
64	-4487.452337	2487.658896	4433.261469	-4487.452337	2487.658896	4433.261469	;

65	-4800.725305	2256.717777	4224.300031	-4800.725305	2256.717777	4224.300031	;
66	-5094.09092	2018.107148	3995.877305	-5094.09092	2018.107148	3995.877305	;
67	-5366.267275	1772.737593	3749.043306	-5366.267275	1772.737593	3749.043306	;
68	-5616.06097	1521.540057	3484.933119	-5616.06097	1521.540057	3484.933119	;
69	-5842.372537	1265.462423	3204.761768	-5842.372537	1265.462423	3204.761768	;
70	-6044.201486	1005.466051	2909.818704	-6044.201486	1005.466051	2909.818704	;
71	-6220.650952	742.522264	2601.461907	-6220.650952	742.522264	2601.461907	;
72	-6370.931889	477.608817	2281.111662	-6370.931889	477.608817	2281.111662	;
73	-6494.36681	211.70634	1950.244	-6494.36681	211.70634	1950.244	;
74	-6590.393034	-54.205211	1610.383867	-6590.393034	-54.205211	1610.383867	;
75	-6658.565422	-319.150099	1263.098034	-6658.565422	-319.150099	1263.098034	;
76	-6698.558579	-582.160318	909.987779	-6698.558579	-582.160318	909.987779	;
77	-6710.168512	-842.279065	552.681406	-6710.168512	-842.279065	552.681406	;
78	-6693.313726	-1098.56415	192.826608	-6693.313726	-1098.56415	192.826608	;
79	-6648.035755	-1350.091338	-167.917268	-6648.035755	-1350.091338	-167.917268	;
80	-6574.499111	-1595.9576	-527.887004	-6574.499111	-1595.9576	-527.887004	;
81	-6472.990666	-1835.284259	-885.423326	-6472.990666	-1835.284259	-885.423326	;
82	-6343.918465	-2067.220026	-1238.878677	-6343.918465	-2067.220026	-1238.878677	;
83	-6187.809965	-2290.943899	-1586.624931	-6187.809965	-2290.943899	-1586.624931	;
84	-6005.309739	-2505.667931	-1927.06099	-6005.309739	-2505.667931	-1927.06099	;
85	-5797.176628	-2710.639834	-2258.620232	-5797.176628	-2710.639834	-2258.620232	;
86	-5564.280388	-2905.145437	-2579.777768	-5564.280388	-2905.145437	-2579.777768	;
87	-5307.597833	-3088.510965	-2889.057476	-5307.597833	-3088.510965	-2889.057476	;
88	-5028.208518	-3260.10515	-3185.038771	-5028.208518	-3260.10515	-3185.038771	;
89	-4727.289964	-3419.341165	-3466.363084	-4727.289964	-3419.341165	-3466.363084	;
90	-4406.112484	-3565.678373	-3731.740023	-4406.112484	-3565.678373	-3731.740023	;
91	-4066.033611	-3698.623896	-3979.953187	-4066.033611	-3698.623896	-3979.953187	;
92	-3708.492181	-3817.734001	-4209.86561	-3708.492181	-3817.734001	-4209.86561	;
93	-3335.002089	-3922.615302	-4420.42482	-3335.002089	-3922.615302	-4420.42482	;
94	-2947.145755	-4012.925787	-4610.667489	-2947.145755	-4012.925787	-4610.667489	;
95	-2546.567333	-4088.375661	-4779.723665	-2546.567333	-4088.375661	-4779.723665	;
96	-2134.965688	-4148.728021	-4926.820576	-2134.965688	-4148.728021	-4926.820576	;
97	-1714.087175	-4193.79936	-5051.285985	-1714.087175	-4193.79936	-5051.285985	;
98	-1285.71825	-4223.459902	-5152.551104	-1285.71825	-4223.459902	-5152.551104	;

99	-851.677937	-4237.63378	-5230.153048	-851.677937	-4237.63378	-5230.153048	;
100	-413.810186	-4236.299052	-5283.736832	-413.810186	-4236.299052	-5283.736832	;
101	26.023863	-4219.487566	-5313.056902	26.023863	-4219.487566	-5313.056902	;
102	465.953673	-4187.284676	-5317.978204	465.953673	-4187.284676	-5317.978204	;
103	904.107141	-4139.828804	-5298.476781	904.107141	-4139.828804	-5298.476781	;
104	1338.618441	-4077.310865	-5254.639904	1338.618441	-4077.310865	-5254.639904	;
105	1767.635853	-3999.973542	-5186.665731	1767.635853	-3999.973542	-5186.665731	;
106	2189.32955	-3908.110425	-5094.862495	2189.32955	-3908.110425	-5094.862495	;
107	2601.899328	-3802.064998	-4979.647228	2601.899328	-3802.064998	-4979.647228	;
108	3003.582242	-3682.229501	-4841.544006	3003.582242	-3682.229501	-4841.544006	;
109	3392.660119	-3549.043634	-4681.181743	3392.660119	-3549.043634	-4681.181743	;
110	3767.466933	-3402.993133	-4499.291502	3767.466933	-3402.993133	-4499.291502	;
111	4126.396004	-3244.608197	-4296.703367	4126.396004	-3244.608197	-4296.703367	;
112	4467.906988	-3074.461777	-4074.342846	4467.906988	-3074.461777	-4074.342846	;
113	4790.53263	-2893.167724	-3833.226841	4790.53263	-2893.167724	-3833.226841	;
114	5092.885257	-2701.3788	-3574.459177	5092.885257	-2701.3788	-3574.459177	;
115	5373.662962	-2499.784541	-3299.225715	5373.662962	-2499.784541	-3299.225715	;
116	5631.655453	-2289.109004	-3008.789052	5631.655453	-2289.109004	-3008.789052	;
117	5865.749541	-2070.108358	-2704.482845	5865.749541	-2070.108358	-2704.482845	;
118	6074.934228	-1843.568374	-2387.70576	6074.934228	-1843.568374	-2387.70576	;
119	6258.305358	-1610.30177	-2059.915082	6258.305358	-1610.30177	-2059.915082	;
120	6415.069811	-1371.145463	-1722.620019	6415.069811	-1371.145463	-1722.620019	;
121	6544.549211	-1126.957704	-1377.374717	6544.549211	-1126.957704	-1377.374717	;
122	6646.183116	-878.615122	-1025.77103	6646.183116	-878.615122	-1025.77103	;
123	6719.531666	-627.009685	-669.43108	6719.531666	-627.009685	-669.43108	;
124	6764.277684	-373.045586	-309.999642	6764.277684	-373.045586	-309.999642	;
125	6780.228194	-117.636076	50.863596	6780.228194	-117.636076	50.863596	;
126	6767.315362	138.299753	411.491872	6767.315362	138.299753	411.491872	;
127	6725.596837	393.840214	770.219228	6725.596837	393.840214	770.219228	;
128	6655.255508	648.064282	1125.388384	6655.255508	648.064282	1125.388384	;
129	6556.59865	900.054861	1475.358581	6556.59865	900.054861	1475.358581	;
130	6430.0565	1148.902028	1818.513326	6430.0565	1148.902028	1818.513326	;
131	6276.180242	1393.706252	2153.268015	6276.180242	1393.706252	2153.268015	;
132	6095.639432	1633.581571	2478.077377	6095.639432	1633.581571	2478.077377	;

133	5889.218878	1867.658708	2791.442714	5889.218878	1867.658708	2791.442714	;
134	5657.814996	2095.088126	3091.918887	5657.814996	2095.088126	3091.918887	;
135	5402.431666	2315.042996	3378.121025	5402.431666	2315.042996	3378.121025	;
136	5124.175611	2526.722075	3648.730911	5124.175611	2526.722075	3648.730911	;
137	4824.25134	2729.35249	3902.503033	4824.25134	2729.35249	3902.503033	;
138	4503.955677	2922.192406	4138.270253	4503.955677	2922.192406	4138.270253	;
139	4164.671906	3104.533582	4354.949097	4164.671906	3104.533582	4354.949097	;
140	3807.863575	3275.703809	4551.544624	3807.863575	3275.703809	4551.544624	;
141	3435.067982	3435.069217	4727.154863	3435.067982	3435.069217	4727.154863	;
142	3047.889384	3582.036453	4880.974818	3047.889384	3582.036453	4880.974818	;
143	2647.991958	3716.054731	5012.300007	2647.991958	3716.054731	5012.300007	;
144	2237.09254	3836.617738	5120.529542	2237.09254	3836.617738	5120.529542	;
145	1816.953192	3943.265406	5205.16874	1816.953192	3943.265406	5205.16874	;
146	1389.373602	4035.585549	5265.831254	1389.373602	4035.585549	5265.831254	;
147	956.183369	4113.215344	5302.240726	956.183369	4113.215344	5302.240726	;
148	519.234191	4175.842684	5314.231959	519.234191	4175.842684	5314.231959	;
149	80.391979	4223.207376	5301.751601	80.391979	4223.207376	5301.751601	;
150	-358.471061	4255.102188	5264.858348	-358.471061	4255.102188	5264.858348	;
151	-795.484363	4271.373754	5203.722662	-795.484363	4271.373754	5203.722662	;
152	-1228.786926	4271.923315	5118.626006	-1228.786926	4271.923315	5118.626006	;
153	-1656.535186	4256.707309	5009.959594	-1656.535186	4256.707309	5009.959594	;
154	-2076.910837	4225.737792	4878.222671	-2076.910837	4225.737792	4878.222671	;
155	-2488.128542	4179.082694	4724.020309	-2488.128542	4179.082694	4724.020309	;
156	-2888.443527	4116.865908	4548.060737	-2888.443527	4116.865908	4548.060737	;
157	-3276.159021	4039.267193	4351.152208	-3276.159021	4039.267193	4351.152208	;
158	-3649.633512	3946.521905	4134.19941	-3649.633512	3946.521905	4134.19941	;
159	-4007.287788	3838.920529	3898.199432	-4007.287788	3838.920529	3898.199432	;
160	-4347.611733	3716.808037	3644.237291	-4347.611733	3716.808037	3644.237291	;
161	-4669.170853	3580.583033	3373.481052	-4669.170853	3580.583033	3373.481052	;
162	-4970.612482	3430.696712	3087.176531	-4970.612482	3430.696712	3087.176531	;
163	-5250.671658	3267.651617	2786.641626	-5250.671658	3267.651617	2786.641626	;
164	-5508.176619	3092.000188	2473.26029	-5508.176619	3092.000188	2473.26029	;
165	-5742.053902	2904.343123	2148.476158	-5742.053902	2904.343123	2148.476158	;
166	-5951.333012	2705.32753	1813.785886	-5951.333012	2705.32753	1813.785886	;

167	-6135.150624	2495.644883	1470.732199	-6135.150624	2495.644883	1470.732199	;
168	-6292.754309	2276.028797	1120.896712	-6292.754309	2276.028797	1120.896712	;
169	-6423.505747	2047.252612	765.892541	-6423.505747	2047.252612	765.892541	;
170	-6526.883422	1810.126799	407.35675	-6526.883422	1810.126799	407.35675	;
171	-6602.484762	1565.496205	46.942674	-6602.484762	1565.496205	46.942674	;
172	-6650.027733	1314.237142	-313.687841	-6650.027733	1314.237142	-313.687841	;
173	-6669.351867	1057.25433	-672.872244	-6669.351867	1057.25433	-672.872244	;
174	-6660.418718	795.477712	-1028.955073	-6660.418718	795.477712	-1028.955073	;
175	-6623.311754	529.859154	-1380.295719	-6623.311754	529.859154	-1380.295719	;
176	-6558.235675	261.369047	-1725.276089	-6558.235675	261.369047	-1725.276089	;
177	-6465.515184	-9.007183	-2062.308151	-6465.515184	-9.007183	-2062.308151	;
178	-6345.593202	-280.272624	-2389.84131	-6345.593202	-280.272624	-2389.84131	;
179	-6199.028557	-551.422489	-2706.369578	-6199.028557	-551.422489	-2706.369578	;
180	-6026.493158	-821.44776	-3010.438503	-6026.493158	-821.44776	-3010.438503	;
181	-5828.768678	-1089.338856	-3300.651826	-5828.768678	-1089.338856	-3300.651826	;
182	-5606.742769	-1354.089308	-3575.677837	-5606.742769	-1354.089308	-3575.677837	;
183	-5361.404831	-1614.699431	-3834.255395	-5361.404831	-1614.699431	-3834.255395	;
184	-5093.84138	-1870.179976	-4075.199594	-5093.84138	-1870.179976	-4075.199594	;
185	-4805.231012	-2119.555745	-4297.407058	-4805.231012	-2119.555745	-4297.407058	;
186	-4496.839023	-2361.869174	-4499.860832	-4496.839023	-2361.869174	-4499.860832	;
187	-4170.011702	-2596.183856	-4681.634868	-4170.011702	-2596.183856	-4681.634868	;
188	-3826.170321	-2821.588	-4841.89808	-3826.170321	-2821.588	-4841.89808	;
189	-3466.804864	-3037.197825	-4979.917973	-3466.804864	-3037.197825	-4979.917973	;
190	-3093.467516	-3242.160872	-5095.063818	-3093.467516	-3242.160872	-5095.063818	;
191	-2707.765937	-3435.659223	-5186.80938	-2707.765937	-3435.659223	-5186.80938	;
192	-2311.356361	-3616.912634	-5254.73519	-2311.356361	-3616.912634	-5254.73519	;
193	-1905.936531	-3785.181561	-5298.530352	-1905.936531	-3785.181561	-5298.530352	;
194	-1493.238505	-3939.770075	-5317.993888	-1493.238505	-3939.770075	-5317.993888	;
195	-1075.021359	-4080.028672	-5313.035616	-1075.021359	-4080.028672	-5313.035616	;
196	-653.063798	-4205.35694	-5283.676562	-653.063798	-4205.35694	-5283.676562	;
197	-229.156721	-4315.206116	-5230.048895	-229.156721	-4315.206116	-5230.048895	;
198	194.904263	-4409.081483	-5152.395399	194.904263	-4409.081483	-5152.395399	;
199	617.32632	-4486.544633	-5051.068475	617.32632	-4486.544633	-5051.068475	;
200	1036.326869	-4547.215558	-4926.52867	1036.326869	-4547.215558	-4926.52867	;

201	1450.141024	-4590.774584	-4779.342736	1450.141024	-4590.774584	-4779.342736	;
202	1857.028973	-4616.964109	-4610.181233	1857.028973	-4616.964109	-4610.181233	;
203	2255.283266	-4625.590166	-4419.815662	2255.283266	-4625.590166	-4419.815662	;
204	2643.235992	-4616.523765	-4209.115142	2643.235992	-4616.523765	-4209.115142	;
205	3019.265815	-4589.702032	-3979.042645	3019.265815	-4589.702032	-3979.042645	;
206	3381.804828	-4545.129116	-3730.650778	3381.804828	-4545.129116	-3730.650778	;
207	3729.345216	-4482.876848	-3465.077147	3729.345216	-4482.876848	-3465.077147	;
208	4060.445677	-4403.085165	-3183.539301	4060.445677	-4403.085165	-3183.539301	;
209	4373.73758	-4305.962258	-2887.329277	4373.73758	-4305.962258	-2887.329277	;
210	4667.930829	-4191.784454	-2577.807767	4667.930829	-4191.784454	-2577.807767	;
211	4941.819399	-4060.895826	-2256.397931	4941.819399	-4060.895826	-2256.397931	;
212	5194.286504	-3913.707507	-1924.578879	5194.286504	-3913.707507	-1924.578879	;
213	5424.309387	-3750.696722	-1583.878851	5424.309387	-3750.696722	-1583.878851	;
214	5630.963688	-3572.405528	-1235.868133	5630.963688	-3572.405528	-1235.868133	;
215	5813.427362	-3379.439254	-882.151734	5813.427362	-3379.439254	-882.151734	;
216	5970.984137	-3172.464661	-524.361873	5970.984137	-3172.464661	-524.361873	;
217	6103.026474	-2952.207806	-164.150305	6103.026474	-2952.207806	-164.150305	;
218	6209.058024	-2719.451637	196.819462	6209.058024	-2719.451637	196.819462	;
219	6288.695554	-2475.033308	556.880028	6288.695554	-2475.033308	556.880028	;
220	6341.670346	-2219.841234	914.367981	6341.670346	-2219.841234	914.367981	;
221	6367.829047	-1954.811914	1267.631767	6367.829047	-1954.811914	1267.631767	;
222	6367.133981	-1680.926499	1615.039498	6367.133981	-1680.926499	1615.039498	;
223	6339.662906	-1399.207169	1954.986653	6339.662906	-1399.207169	1954.986653	;
224	6285.608244	-1110.713293	2285.903632	6285.608244	-1110.713293	2285.903632	;
225	6205.275773	-816.537425	2606.263125	6205.275773	-816.537425	2606.263125	;
226	6099.082806	-517.801136	2914.587252	6099.082806	-517.801136	2914.587252	;
227	5967.555863	-215.650703	3209.454444	5967.555863	-215.650703	3209.454444	;
228	5811.327866	88.747308	3489.506021	5811.327866	88.747308	3489.506021	;
229	5631.134874	394.210567	3753.45245	5631.134874	394.210567	3753.45245	;
230	5427.812379	699.545573	4000.079242	5427.812379	699.545573	4000.079242	;
231	5202.291191	1003.552318	4228.252474	5202.291191	1003.552318	4228.252474	;
232	4955.592947	1305.02897	4436.923906	4955.592947	1305.02897	4436.923906	;
233	4688.825251	1602.776595	4625.135681	4688.825251	1602.776595	4625.135681	;
234	4403.176508	1895.603867	4792.024589	4403.176508	1895.603867	4792.024589	;

235	4099.910439	2182.331778	4936.825882	4099.910439	2182.331778	4936.825882	;
236	3780.360346	2461.798305	5058.876631	3780.360346	2461.798305	5058.876631	;
237	3445.923122	2732.863038	5157.618616	3445.923122	2732.863038	5157.618616	;
238	3098.053057	2994.411758	5232.600744	3098.053057	2994.411758	5232.600744	;
239	2738.255454	3245.360923	5283.480986	2738.255454	3245.360923	5283.480986	;
240	2368.080088	3484.662088	5310.027836	2368.080088	3484.662088	5310.027836	;
241	1989.114523	3711.306213	5312.121285	1989.114523	3711.306213	5312.121285	;
242	1602.977325	3924.327863	5289.753312	1602.977325	3924.327863	5289.753312	;
243	1211.31119	4122.809282	5243.02789	1211.31119	4122.809282	5243.02789	;
244	815.775999	4305.884329	5172.160506	815.775999	4305.884329	5172.160506	;
245	418.041846	4472.742259	5077.477203	418.041846	4472.742259	5077.477203	;
246	19.782041	4622.631339	4959.413137	19.782041	4622.631339	4959.413137	;
247	-377.333881	4754.862278	4818.51066	-377.333881	4754.862278	4818.51066	;
248	-771.647113	4868.811464	4655.416927	-771.647113	4868.811464	4655.416927	;
249	-1161.516477	4963.923981	4470.881041	-1161.516477	4963.923981	4470.881041	;
250	-1545.325251	5039.716403	4265.750729	-1545.325251	5039.716403	4265.750729	;
251	-1921.487881	5095.779337	4040.968574	-1921.487881	5095.779337	4040.968574	;
252	-2288.456564	5131.779704	3797.567803	-2288.456564	5131.779704	3797.567803	;
253	-2644.727678	5147.462739	3536.667643	-2644.727678	5147.462739	3536.667643	;
254	-2988.848013	5142.653699	3259.468275	-2988.848013	5142.653699	3259.468275	;
255	-3319.420794	5117.259254	2967.245381	-3319.420794	5117.259254	2967.245381	;
256	-3635.111462	5071.268563	2661.344328	-3635.111462	5071.268563	2661.344328	;
257	-3934.653177	5004.754001	2343.173996	-3934.653177	5004.754001	2343.173996	;
258	-4216.852025	4917.871545	2014.200288	-4216.852025	4917.871545	2014.200288	;
259	-4480.591896	4810.860801	1675.939344	-4480.591896	4810.860801	1675.939344	;
260	-4724.839011	4684.044661	1329.950495	-4724.839011	4684.044661	1329.950495	;
261	-4948.646069	4537.828598	977.828994	-4948.646069	4537.828598	977.828994	;
262	-5151.155995	4372.699583	621.198558	-5151.155995	4372.699583	621.198558	;
263	-5331.605269	4189.224634	261.703755	-5331.605269	4189.224634	261.703755	;
264	-5489.326813	3988.048999	-98.997706	-5489.326813	3988.048999	-98.997706	;
265	-5623.752429	3769.893973	-459.242761	-5623.752429	3769.893973	-459.242761	;
266	-5734.41477	3535.554369	-817.3708	-5734.41477	3535.554369	-817.3708	;
267	-5820.948843	3285.895639	-1171.731447	-5820.948843	3285.895639	-1171.731447	;
268	-5883.093028	3021.850681	-1520.692294	-5883.093028	3021.850681	-1520.692294	;

269	-5920.68962	2744.416321	-1862.646518	-5920.68962	2744.416321	-1862.646518	;
270	-5933.684902	2454.649514	-2196.020364	-5933.684902	2454.649514	-2196.020364	;
271	-5922.128736	2153.663261	-2519.280439	-5922.128736	2153.663261	-2519.280439	;
272	-5886.173699	1842.622281	-2830.940791	-5886.173699	1842.622281	-2830.940791	;
273	-5826.073769	1522.738453	-3129.56973	-5826.073769	1522.738453	-3129.56973	;
274	-5742.182571	1195.266043	-3413.796368	-5742.182571	1195.266043	-3413.796368	;
275	-5634.951211	861.496754	-3682.31684	-5634.951211	861.496754	-3682.31684	;
276	-5504.925704	522.754608	-3933.900186	-5504.925704	522.754608	-3933.900186	;
277	-5352.744025	180.390696	-4167.393867	-5352.744025	180.390696	-4167.393867	;
278	-5179.132808	-164.222197	-4381.728901	-5179.132808	-164.222197	-4381.728901	;
279	-4984.903704	-509.695052	-4575.924587	-4984.903704	-509.695052	-4575.924587	;
280	-4770.949431	-854.628157	-4749.092823	-4770.949431	-854.628157	-4749.092823	;
281	-4538.239537	-1197.616698	-4900.44199	-4538.239537	-1197.616698	-4900.44199	;
282	-4287.8159	-1537.256381	-5029.280393	-4287.8159	-1537.256381	-5029.280393	;
283	-4020.78798	-1872.149074	-5135.019262	-4020.78798	-1872.149074	-5135.019262	;
284	-3738.327864	-2200.908443	-5217.175293	-3738.327864	-2200.908443	-5217.175293	;
285	-3441.665102	-2522.165562	-5275.372732	-3441.665102	-2522.165562	-5275.372732	;
286	-3132.081376	-2834.574501	-5309.344997	-3132.081376	-2834.574501	-5309.344997	;
287	-2810.905006	-3136.817838	-5318.935837	-2810.905006	-3136.817838	-5318.935837	;
288	-2479.505325	-3427.612121	-5304.100015	-2479.505325	-3427.612121	-5304.100015	;
289	-2139.286935	-3705.713231	-5264.903533	-2139.286935	-3705.713231	-5264.903533	;
290	-1791.683857	-3969.921643	-5201.523379	-1791.683857	-3969.921643	-5201.523379	;
291	-1438.153614	-4219.087564	-5114.246808	-1438.153614	-4219.087564	-5114.246808	;
292	-1080.171235	-4452.115939	-5003.470153	-1080.171235	-4452.115939	-5003.470153	;
293	-719.223225	-4667.971287	-4869.697164	-719.223225	-4667.971287	-4869.697164	;
294	-356.801501	-4865.682366	-4713.536884	-356.801501	-4865.682366	-4713.536884	;
295	5.602671	-5044.34664	-4535.701057	5.602671	-5044.34664	-4535.701057	;
296	366.504739	-5203.134519	-4337.001084	366.504739	-5203.134519	-4337.001084	;
297	724.432887	-5341.293365	-4118.344512	724.432887	-5341.293365	-4118.344512	;
298	1077.934001	-5458.151228	-3880.73109	1077.934001	-5458.151228	-3880.73109	;
299	1425.579573	-5553.1203	-3625.248379	1425.579573	-5553.1203	-3625.248379	;
300	1765.971485	-5625.700053	-3353.066945	1765.971485	-5625.700053	-3353.066945	;
301	2097.747688	-5675.480046	-3065.435138	2097.747688	-5675.480046	-3065.435138	;
302	2419.587721	-5702.142385	-2763.673486	2419.587721	-5702.142385	-2763.673486	;

303	2730.218057	-5705.463797	-2449.16871	2730.218057	-5705.463797	-2449.16871	;
304	3028.417254	-5685.317321	-2123.367404	3028.417254	-5685.317321	-2123.367404	;
305	3313.020876	-5641.673573	-1787.769389	3313.020876	-5641.673573	-1787.769389	;
306	3582.92616	-5574.601605	-1443.920784	3582.92616	-5574.601605	-1443.920784	;
307	3837.096414	-5484.2693	-1093.40682	3837.096414	-5484.2693	-1093.40682	;
308	4074.565104	-5370.943342	-737.844434	4074.565104	-5370.943342	-737.844434	;
309	4294.439631	-5234.988709	-378.874688	4294.439631	-5234.988709	-378.874688	;
310	4495.904752	-5076.867721	-18.155047	4495.904752	-5076.867721	-18.155047	;
311	4678.225646	-4897.138625	342.648446	4678.225646	-4897.138625	342.648446	;
312	4840.750601	-4696.453721	701.869039	4840.750601	-4696.453721	701.869039	;
313	4982.913304	-4475.557043	1057.847157	4982.913304	-4475.557043	1057.847157	;
314	5104.234736	-4235.281602	1408.938251	5104.234736	-4235.281602	1408.938251	;
315	5204.324651	-3976.546203	1753.520563	5204.324651	-3976.546203	1753.520563	;
316	5282.882642	-3700.351859	2090.002782	5282.882642	-3700.351859	2090.002782	;
317	5339.698794	-3407.77781	2416.831521	5339.698794	-3407.77781	2416.831521	;
318	5374.653919	-3099.977185	2732.498601	5374.653919	-3099.977185	2732.498601	;
319	5387.719382	-2778.172313	3035.548094	5387.719382	-2778.172313	3035.548094	;
320	5378.956535	-2443.649726	3324.583076	5378.956535	-2443.649726	3324.583076	;
321	5348.515745	-2097.754867	3598.272091	5348.515745	-2097.754867	3598.272091	;
322	5296.635061	-1741.886537	3855.355258	5296.635061	-1741.886537	3855.355258	;
323	5223.638504	-1377.491115	4094.650023	5223.638504	-1377.491115	4094.650023	;
324	5129.934017	-1006.05656	4315.056519	5129.934017	-1006.05656	4315.056519	;
325	5016.011091	-629.106252	4515.562517	5016.011091	-629.106252	4515.562517	;
326	4882.43807	-248.192672	4695.24795	4882.43807	-248.192672	4695.24795	;
327	4729.859178	135.109035	4853.288998	4729.859178	135.109035	4853.288998	;
328	4558.991266	519.207593	4988.961719	4558.991266	519.207593	4988.961719	;
329	4370.620317	902.502198	5101.645218	4370.620317	902.502198	5101.645218	;
330	4165.597714	1283.389168	5190.824347	4165.597714	1283.389168	5190.824347	;
331	3944.8363	1660.26861	5256.091926	3944.8363	1660.26861	5256.091926	;
332	3709.306248	2031.551093	5297.150493	3709.306248	2031.551093	5297.150493	;
333	3460.030751	2395.664287	5313.813558	3460.030751	2395.664287	5313.813558	;
334	3198.081562	2751.059569	5306.006392	3198.081562	2751.059569	5306.006392	;
335	2924.574392	3096.218548	5273.766313	2924.574392	3096.218548	5273.766313	;
336	2640.664182	3429.65951	5217.242498	2640.664182	3429.65951	5217.242498	;

337	2347.540276	3749.943747	5136.695312	2347.540276	3749.943747	5136.695312	;
338	2046.421495	4055.681754	5032.495148	2046.421495	4055.681754	5032.495148	;
339	1738.551136	4345.539274	4905.120795	1738.551136	4345.539274	4905.120795	;
340	1425.19192	4618.243151	4755.15733	1425.19192	4618.243151	4755.15733	;
341	1107.620881	4872.586997	4583.29353	1107.620881	4872.586997	4583.29353	;
342	787.124241	5107.436613	4390.318832	787.124241	5107.436613	4390.318832	;
343	464.992262	5321.735176	4177.119827	464.992262	5321.735176	4177.119827	;
344	142.514113	5514.508125	3944.676307	142.514113	5514.508125	3944.676307	;
345	-179.027247	5684.867765	3694.056883	-179.027247	5684.867765	3694.056883	;
346	-498.36014	5832.017525	3426.41417	-498.36014	5832.017525	3426.41417	;
347	-814.229178	5955.255862	3142.979577	-814.229178	5955.255862	3142.979577	;
348	-1125.400192	6053.979796	2845.057702	-1125.400192	6053.979796	2845.057702	;
349	-1430.665059	6127.688021	2534.020373	-1430.665059	6127.688021	2534.020373	;
350	-1728.846403	6175.983606	2211.300339	-1728.846403	6175.983606	2211.300339	;
351	-2018.802156	6198.57624	1878.384661	-2018.802156	6198.57624	1878.384661	;
352	-2299.429951	6195.284012	1536.807811	-2299.429951	6195.284012	1536.807811	;
353	-2569.671326	6166.034712	1188.144538	-2569.671326	6166.034712	1188.144538	;
354	-2828.515726	6110.866631	834.002515	-2828.515726	6110.866631	834.002515	;
355	-3075.004279	6029.928869	476.01481	-3075.004279	6029.928869	476.01481	;
356	-3308.233319	5923.481121	115.832235	-3308.233319	5923.481121	115.832235	;
357	-3527.357659	5791.892954	-244.884402	-3527.357659	5791.892954	-244.884402	;
358	-3731.593578	5635.642583	-604.472099	-3731.593578	5635.642583	-604.472099	;
359	-3920.221524	5455.315121	-961.27346	-3920.221524	5455.315121	-961.27346	;
360	-4092.588509	5251.600354	-1313.644462	-4092.588509	5251.600354	-1313.644462	;
361	-4248.110202	5025.290014	-1659.962149	-4248.110202	5025.290014	-1659.962149	;
362	-4386.272698	4777.274591	-1998.632193	-4386.272698	4777.274591	-1998.632193	;
363	-4506.633966	4508.539691	-2328.096311	-4506.633966	4508.539691	-2328.096311	;
364	-4608.824981	4220.161964	-2646.839474	-4608.824981	4220.161964	-2646.839474	;
365	-4692.550525	3913.304633	-2953.396886	-4692.550525	3913.304633	-2953.396886	;
366	-4757.589677	3589.212627	-3246.360691	-4757.589677	3589.212627	-3246.360691	;
367	-4803.79598	3249.20738	-3524.386394	-4803.79598	3249.20738	-3524.386394	;
368	-4831.097312	2894.681289	-3786.198941	-4831.097312	2894.681289	-3786.198941	;
369	-4839.49545	2527.091887	-4030.598461	-4839.49545	2527.091887	-4030.598461	;
370	-4829.06535	2147.955742	-4256.465623	-4829.06535	2147.955742	-4256.465623	;

371	-4799.954153	1758.842121	-4462.766616	-4799.954153	1758.842121	-4462.766616	;
372	-4752.379924	1361.366451	-4648.557706	-4752.379924	1361.366451	-4648.557706	;
373	-4686.63014	957.183589	-4812.989378	-4686.63014	957.183589	-4812.989378	;
374	-4603.059949	547.98095	-4955.310043	-4603.059949	547.98095	-4955.310043	;
375	-4502.090194	135.471505	-5074.869306	-4502.090194	135.471505	-5074.869306	;
376	-4384.205234	-278.613323	-5171.120776	-4384.205234	-278.613323	-5171.120776	;
377	-4249.950571	-692.530827	-5243.624423	-4249.950571	-692.530827	-5243.624423	;
378	-4099.930287	-1104.53425	-5292.048482	-4099.930287	-1104.53425	-5292.048482	;
379	-3934.804312	-1512.88003	-5316.170881	-3934.804312	-1512.88003	-5316.170881	;
380	-3755.285533	-1915.835057	-5315.880209	-3755.285533	-1915.835057	-5315.880209	;
381	-3562.136753	-2311.683912	-5291.17622	-3562.136753	-2311.683912	-5291.17622	;
382	-3356.167514	-2698.736055	-5242.169856	-3356.167514	-2698.736055	-5242.169856	;
383	-3138.230783	-3075.332956	-5169.082812	-3138.230783	-3075.332956	-5169.082812	;
384	-2909.219532	-3439.855137	-5072.246626	-2909.219532	-3439.855137	-5072.246626	;
385	-2670.063193	-3790.729095	-4952.101297	-2670.063193	-3790.729095	-4952.101297	;
386	-2421.724025	-4126.434091	-4809.193438	-2421.724025	-4126.434091	-4809.193438	;
387	-2165.193381	-4445.50878	-4644.173963	-2165.193381	-4445.50878	-4644.173963	;
388	-1901.487895	-4746.557647	-4457.795312	-1901.487895	-4746.557647	-4457.795312	;
389	-1631.645593	-5028.257221	-4250.908215	-1631.645593	-5028.257221	-4250.908215	;
390	-1356.72195	-5289.362051	-4024.458008	-1356.72195	-5289.362051	-4024.458008	;
391	-1077.785882	-5528.710399	-3779.480507	-1077.785882	-5528.710399	-3779.480507	;
392	-795.915709	-5745.229636	-3517.097444	-795.915709	-5745.229636	-3517.097444	;
393	-512.195088	-5937.941287	-3238.511499	-512.195088	-5937.941287	-3238.511499	;
394	-227.708927	-6105.965727	-2945.000911	-227.708927	-6105.965727	-2945.000911	;
395	56.460692	-6248.526468	-2637.913724	56.460692	-6248.526468	-2637.913724	;
396	339.238579	-6364.954029	-2318.661658	339.238579	-6364.954029	-2318.661658	;
397	619.560464	-6454.689346	-1988.713659	619.560464	-6454.689346	-1988.713659	;
398	896.376986	-6517.286715	-1649.589131	896.376986	-6517.286715	-1649.589131];	